NASA/CR—2012-217654

Plasma Actuators for Turbomachinery Flow Control

Final Report

Richard B. Miles and Mikhail N. Shneider
Princeton University, Princeton, New Jersey

September 2012

NASA STI Program . . . in Profile

Since its founding, NASA has been dedicated to the advancement of aeronautics and space science. The NASA Scientific and Technical Information (STI) program plays a key part in helping NASA maintain this important role.

The NASA STI Program operates under the auspices of the Agency Chief Information Officer. It collects, organizes, provides for archiving, and disseminates NASA's STI. The NASA STI program provides access to the NASA Aeronautics and Space Database and its public interface, the NASA Technical Reports Server, thus providing one of the largest collections of aeronautical and space science STI in the world. Results are published in both non-NASA channels and by NASA in the NASA STI Report Series, which includes the following report types:

- TECHNICAL PUBLICATION. Reports of completed research or a major significant phase of research that present the results of NASA programs and include extensive data or theoretical analysis. Includes compilations of significant scientific and technical data and information deemed to be of continuing reference value. NASA counterpart of peer-reviewed formal professional papers but has less stringent limitations on manuscript length and extent of graphic presentations.

- TECHNICAL MEMORANDUM. Scientific and technical findings that are preliminary or of specialized interest, e.g., quick release reports, working papers, and bibliographies that contain minimal annotation. Does not contain extensive analysis.

- CONTRACTOR REPORT. Scientific and technical findings by NASA-sponsored contractors and grantees.

- CONFERENCE PUBLICATION. Collected papers from scientific and technical conferences, symposia, seminars, or other meetings sponsored or cosponsored by NASA.

- SPECIAL PUBLICATION. Scientific, technical, or historical information from NASA programs, projects, and missions, often concerned with subjects having substantial public interest.

- TECHNICAL TRANSLATION. English-language translations of foreign scientific and technical material pertinent to NASA's mission.

Specialized services also include creating custom thesauri, building customized databases, organizing and publishing research results.

For more information about the NASA STI program, see the following:

- Access the NASA STI program home page at *http://www.sti.nasa.gov*

- E-mail your question to *help@sti.nasa.gov*

- Fax your question to the NASA STI Information Desk at 443–757–5803

- Telephone the NASA STI Information Desk at 443–757–5802

- Write to:
  STI Information Desk
  NASA Center for AeroSpace Information (CASI)
  7115 Standard Drive
  Hanover, MD 21076–1320

NASA/CR—2012-217654

Plasma Actuators for Turbomachinery Flow Control

Final Report

Richard B. Miles and Mikhail N. Shneider
Princeton University, Princeton, New Jersey

Prepared under Cooperative Agreement No. NNX07AC02A

National Aeronautics and
Space Administration

Glenn Research Center
Cleveland, Ohio 44135

September 2012

Acknowledgments

The authors express their appreciation to David E. Ashpis of the NASA Glenn Research Center for serving as the Grant Technical Monitor. His support and deep involvement in the project, useful discussions, input, and suggestions contributed greatly to the project.

This work was sponsored by the Fundamental Aeronautics Program at the NASA Glenn Research Center.

Level of Review: This material has been technically reviewed by NASA technical management.

Available from

NASA Center for Aerospace Information
7115 Standard Drive
Hanover, MD 21076–1320

National Technical Information Service
5301 Shawnee Road
Alexandria, VA 22312

Available electronically at http://www.sti.nasa.gov

Plasma Actuators for Turbomachinery Flow Control
Final Report

Richard B. Miles and Mikhail N. Shneider
Princeton University
Princeton, New Jersey 08544

Summary

Work completed under this NASA Grant and Cooperative Agreement was focused on of the operation of surface dielectric barrier discharge devices driven by high voltage, nanosecond scale pulses plus constant or time varying applied bias voltages. The main interest was in momentum production and the range of voltages applied eliminated significant heating effects. The approach was experimental measurements and was supplemented by computational modeling. All the experiments were conducted at Princeton University. NASA funding supported mainly the experimental work while the computational work was supported by other sources. Most of the computational work was conducted at Princeton University and was completed at the Pennsylvania State University.

The project provided comprehensive understanding of the associated physical phenomena achieved by complementary measurements and modeling. Limitations on the performance of the devices for the generation of high velocity surface jets were established and various means for overcoming those limitations were proposed and tested. The major limitations included the maximum velocity limit of the jet due to electrical breakdown in air and across the dielectric, the occurrence of backward breakdown during the short pulse causing reverse thrust, the buildup of surface charge in the dielectric offsetting the forward driving potential of the bias voltage, and the interaction of the surface jet with the surface through viscous losses. It was also noted that the best performance occurred when the nanosecond pulse and the bias voltage were of opposite sign. Solutions include the development of partially conducting surface coatings to bleed off the surface charge, the development of a semiconductor diode inlaid surface material to suppress the backward breakdown. Extension to long discharge channels was studied and a new ozone imaging method developed for more quantitative determination of surface jet properties.

Details of the work are given in publications and a Ph.D. thesis. A list is provided below. Reprints of archival journal articles are attached in the Appendix. The dissertation is provided as Part II of this final report and is published separately as NASA/CR—2012-217655.

Research Personnel

Personnel supported under this Grant and Cooperative Agreement include

Graduate students:

Dmitry F. Opaits, Ph.D. completed September, 2010

Research Staff:

Dr. Mikhail N. Shneider (partial support)
Dr. Sohail Zaidi (partial support)

Subcontract (to Lockheed Martin Corporation):

Dr. Sergey Macheret (partial support)

Technical staff:

Mr. Philip Howard (partial support)

Faculty:

Prof. Richard B. Miles (partial summer)

The grant and cooperative agreement included a subcontract to Lockheed Martin Corporation for the partial support of Dr. Sergey Macheret who provided advice on the physics of the interaction of the dielectric barrier discharge with the surrounding air and on the modeling of those processes. He was initially at Princeton and a co-Principal Investigator on the proposal which was submitted in 2006, but left Princeton prior to the initiation of the award. He continued his participation through the subcontract.

Another graduate student who worked on the project while at Princeton University was Dr. Alexandre Likhanskii. His financial support came from other sources, but was he advised and guided by Princeton University faculty and research staff that were partially supported by this NASA grant. His work was completed at The Pennsylvania State University.

Publications

The results have been reported in numerous peer reviewed and conference manuscript publications, and are contained in a doctoral dissertation.

The archival journal papers are included in the Appendix of this report.

The conference papers have not been included in this report since the material presented in those papers is incorporated into the peer reviewed publications and the dissertations of Dr. Opaits and Dr. Likhanskii.

Doctoral Dissertations

1. Dmitry Florievich Opaits "Dielectric Barrier Discharge Plasma Actuator for Flow Control," Ph.D. Dissertation, Princeton University, September 2010.

   The Doctoral dissertation of Dr. Opaits is included as Part II of this report (published separately as NASA/CR—2012-217655).
2. Alexandre Likhanskii "Study of Plasma Phenomena at High Electric Fields in Applications for Active Flow Control and Ultra-Short Pulse Laser Drilling," Ph.D. Dissertation, The Pennsylvania State University, August 2009.

   The Doctoral dissertation of Dr. Likhanskii is available from The Pennsylvania State University.

List of Peer-Reviewed Archival Journal Publications

1. A. Likhanskii, M. Shneider, S. Macheret, R. Miles, Modeling of dielectric barrier discharge plasma actuators driven by repetitive nanosecond pulses, *Physics of Plasmas,* Vol. 14, 073501, 2007.

2. D.F. Opaits, A.V. Likhanskii, G. Neretti, S. Zaidi, M.N. Shneider, R.B. Miles and S.O. Macheret, "Experimental Investigation of Dielectric Barrier Discharge Plasma Actuators Driven by Repetitive High-Voltage Nanosecond Pulses with DC or Low Frequency Sinusoidal Bias," *Journal of Applied Physics*, Vol. 104, Issue 4, Article number 043304 (2008).

3. A. Likhanskii, M. Shneider, S. Macheret, R. Miles, "Modeling of dielectric barrier discharge plasma actuator in air*," Journal of Applied Physics*, Vol. 103, 053305, 2008.

4. D.F. Opaits, M.N. Shneider, R.B. Miles, "Surface Charge in Dielectric Barrier Discharge Plasma Actuators," *Physics of Plasmas*, Volume 15, Issue 7, Article Number: 073505 (July 2008).

5. D.F. Opaits, M.N. Shneider, R.B. Miles, "Electrodynamic effects in nanosecond-pulse sustained long dielectric-barrier-discharge plasma actuators," *Applied Physics Letters*, Volume 94, Issue 6, Article Number: 061503 (Feb 9, 2009).

6. R.B. Miles, D.F. Opaits, M.N. Shneider, S.H. Zaidi, and S.O. Macheret, Non-thermal atmospheric pressure plasmas for aeronautic applications, *Eur. Phys. J. Appl. Phys*. Vol. 47, 22802 (2009).

List of Conference Manuscripts

Conference manuscripts published under this Grant and Cooperative Agreement include

1. D.F. Opaits, G. Neretti, A.V. Likhanskii, S. Zaidi, M.N. Shneider, R.B. Miles, and S.O. Macheret, "Experimental Investigation of DBD Plasma Actuators Driven by Repetitive High Voltage Nanosecond Pulses with DC or Low Frequency Sinusoidal Bias," AIAA-2007-4532, 38th Plasma Dynamics and Lasers Conference, Miami, FL, 25-28 June 2007.

2. A.V. Likhanskii, M.N. Shneider, D.F. Opaits, R.B. Miles, and S.O. Macheret, "Numerical Modeling of DBD Plasma Actuators and the Induced Air Flow," AIAA-2007-4533, 38th Plasma Dynamics and Lasers Conference, Miami, FL, 25-28 June 2007.

3. D. Opaits, G. Neretti, S. Zaidi M. Shneider, and R.B. Miles, Princeton University, Princeton, NJ; A. Likhanskii, Penn State University, University Park, PA and S. Macheret, Lockheed Martin, Palmdale, CA "DBD Plasma Actuators Driven by a Combination of Low Frequency Bias Voltage and Nanosecond Pulses," AIAA-2008-1372, AIAA Aerospace Sciences Meeting, Reno, Nevada, Jan 7-10, 2008.

4. A. Likhanskii, V. Semak, M. Shneider, D. Opaits, R. Miles, S. Macheret, Parallel Code Development and Numerical Investigation of Surface Charge Build-Up in DBD Plasma Actuators, AIAA-2008-1380, 46th AIAA Aerospace Sciences Meeting and Exhibit, Reno, Nevada, Jan. 7-10, 2008.

5. A. Likhanskii, V. Semak, M. Shneider, D. Opaits, R. Miles, S. Macheret, Multiprocessor Modeling of DBD Plasma Actuator, AIAA-2008-4284 38th Fluid Dynamics Conference and Exhibit, Seattle, Washington, June 23-26, 2008.

6. R.B. Miles, D. Opaits, M.N. Shneider, S.H. Zaidi, "Non-Thermal Atmospheric Pressure Plasmas for Aeronautic Applications," HAKONE XI Oleron Island, September 7-12, 2008.

7. D. Opaits, M. Shneider, A. Likhanskii, S. Zaidi, Princeton University, Princeton, NJ; S. Macheret, and R. Miles, "Improving Thrust by Suppressing Charge Build- Up in Pulsed DBD Plasma Actuators," AIAA-2009-487, 47th AIAA Aerospace Sciences Meeting, Orlando, FL, Jan 5-9, 2009.

8. A. Likhanskii, V. Semak, D. Opaits, M. Shneider, R. Miles, S. Macheret, The role of the photoionization in the numerical modeling of the DBD plasma actuator, AIAA-2009-841, 47th AIAA Aerospace Sciences Meeting and Exhibit, Orlando, Florida, Jan. 5-8, 2009.

9. D. Opaits, A. Likhanskii, S. Zaidi, M. Shneider, S. Macheret, R. Miles, "Suppression of Dielectric Barrier Discharge Charge Build up Using a Partially Conducting Thin Film," AIAA-2009-4189, 39th AIAA Fluid Dynamics Conference, San Antonio, Texas, June 22-25, 2009.

10. A. Likhanskii, Tech-X, Boulder, CO; M. Shneider and D. Opaits, Princeton University, Princeton, NJ; S. Macheret, Lockheed Martin Corporation, Palmdale, CA; and R. Miles, Princeton University, Princeton, NJ, Limitations of the DBD effects on the external flow AIAA-2010-470, 48th AIAA Aerospace Sciences Meeting, Orlando, FL, Jan 4-7, 2010.

11. D. Opaits, S. Zaidi, R. Miles, and M. Shneider, Princeton University, Princeton, NJ; A. Likhanskii, Tech-X Corporation, Boulder, CO; M. Edwards, Princeton university, Princeton, NJ; S. Macheret, Lockheed Martin Corporation, Palmdale, CA, Surface plasma induced wall jets, AIAA-2010-469, 48th AIAA Aerospace Sciences Meeting, Orlando, FL, Jan 4-7, 2010.

12. R.B. Miles, "Limitations and Potential of flow Control with Dielectric Barrier Discharges" Lecture Series Notes for Von Karman Institute Lectures Flow Control Meeting, February 21-24, 2011.

Other Conference Proceedings

1. D. Opaits, S. Zaidi, M. Shneider, R. Miles, A. Likhanskii, S. Macheret, Parametric studies on thrust produced by pulsed DBD plasma actuators, American Physical Society, **61th Gaseous Electronics Conference**, Dallas, TX, October 13-17, 2008, abstract BAPS.2008.GEC.GW1.4.

2. A. Likhanskii, V. Semak, D. Opaits, M. Shneider, S. Macheret, Multiprocessor Modeling of Dielectric Barrier Discharge Plasma Actuator, American Physical Society, **61th Gaseous Electronics Conference**, Dallas, TX, October 13-17, 2008, abstract BAPS.2008.GEC.MWP1.94D.

3. D. Opaits, G. Neretti, S. Zaidi, M. Shneider, R. Miles, A. Likhanskii, S. Macheret, Schlieren observation of vortex flow structures in asymmetric dielectric barrier discharges, American Physical Society, **60th Gaseous Electronics Conference**, Arlington, VA, October 2-5, 2007, abstract BAPS.2007.GEC.SRP1.40.
4. A. Likhanskii, D. Opaits, M. Shneider, R. Miles, S. Macheret, Investigation of asymmetric dielectric barrier discharge plasma actuator, driven by repetitive nanosecond pulses, American Physical Society, **60th Gaseous Electronics Conference**, Arlington, VA, October 2-5, 2007, abstract BAPS.2007.GEC.LW2.7

Workshop Presentations

1. Mikhail Shneider, "State-of-the-art high-fidelity DBD plasma simulations," presentation at the AFOSR DBD Plasma Actuator Workshop, Gainesville, FL, 24-25, February 2010.

2. Dmitry Opaits, "DBD Actuator Developments," presentation at the AFOSR DBD Plasma Actuator Workshop, Gainesville, FL, 24-25 February 2010.

Each of these manuscripts had associated with it a presentation given by the lead author.

Appendix

Reprints of Publications

The appendix contains the following reprints of peer reviewed journal publications supported in full or in part by NASA Glenn Research Center Cooperative Agreement NNX07AC02A. Copyrighted papers are reprinted with permission of the publisher.

1. A. Likhanskii, M. Shneider, S. Macheret, R. Miles, "Modeling of dielectric barrier discharge plasma actuators driven by repetitive nanosecond pulses," Physics of Plasmas, Vol. 14, 073501, 2007.

2. D.F. Opaits, A.V. Likhanskii, G. Neretti, S. Zaidi, M.N. Shneider, R.B. Miles and S.O. Macheret, "Experimental Investigation of Dielectric Barrier Discharge Plasma Actuators Driven by Repetitive High-Voltage Nanosecond Pulses with DC or Low Frequency Sinusoidal Bias," *Journal of Applied Physics*, Vol. 104, Issue 4, Article number 043304 (2008).

3. Likhanskii, M. Shneider, S. Macheret, R. Miles, "Modeling of dielectric barrier discharge plasma actuator in air," Journal of Applied Physics, Vol. 103, 053305, 2008.

4. D.F. Opaits, M.N. Shneider, R.B. Miles, "Surface Charge in Dielectric Barrier Discharge Plasma Actuators," *Physics of Plasmas*, Volume 15, Issue 7, Article Number: 073505 (July 2008).

5. D.F. Opaits, M.N. Shneider, R.B. Miles, "Electrodynamic effects in nanosecond-pulse sustained long dielectric-barrier-discharge plasma actuators," *Applied Physics Letters,* Volume 94, Issue 6, Article Number: 061503 (February 9, 2009).

6. R.B. Miles, D.F. Opaits, M.N. Shneider, S.H. Zaidi, and S.O. Macheret, "Non-thermal atmospheric pressure plasmas for aeronautic applications," *Eur. Phys. J. Appl. Phys.*, Vol. 47, 22802 (2009).

PHYSICS OF PLASMAS **14**, 073501 (2007)

Modeling of dielectric barrier discharge plasma actuators driven by repetitive nanosecond pulses

Alexandre V. Likhanskii and Mikhail N. Shneider
Department of Mechanical and Aerospace Engineering, Princeton University, Princeton, New Jersey 08544, USA

Sergey O. Macheret
Lockheed Martin Skunk Works, 1011 Lockheed Way, Palmdale, California 93599, USA

Richard B. Miles
Department of Mechanical and Aerospace Engineering, Princeton University, Princeton, New Jersey 08544, USA

(Received 26 January 2007; accepted 3 May 2007; published online 9 July 2007)

A detailed physical model for an asymmetric dielectric barrier discharge (DBD) in air driven by repetitive nanosecond voltage pulses is developed. In particular, modeling of DBD with high voltage repetitive negative and positive nanosecond pulses combined with positive dc bias is carried out. Operation at high voltage is compared with operation at low voltage, highlighting the advantage of high voltages, however the effect of backward-directed breakdown in the case of negative pulses results in a decrease of the integral momentum transferred to the gas. The use of positive repetitive pulses with dc bias is demonstrated to be promising for DBD performance improvement. The effects of the voltage waveform not only on force magnitude, but also on the spatial profile of the force, are shown. The crucial role of background photoionization in numerical modeling of ionization waves (streamers) in DBD plasmas is demonstrated. © *2007 American Institute of Physics*.
[DOI: 10.1063/1.2744227]

I. INTRODUCTION

Asymmetric dielectric barrier discharge (DBD) plasma actuators are known to be effective in aerodynamic control (see Refs. 1–16). Experimental investigations showed the dramatic effect of DBD on the gas flow, resulting in flow separation control. Despite the plasma-induced flow complexity, there is an agreement that the major effect on the flow is due to the downstream force on the gas. The currently achieved performance of DBD plasma actuators is limited to relatively low gas velocities (of the order of 1–30 m/s). The prevention of flow separation at higher velocities needs stronger DBD effects on the gas, and optimization is required. A number of groups have explored different applied voltage shapes, such as sinusoidal or sawtooth voltage waveforms at frequencies 1–100 kHz and amplitudes 2–20 kV or repetitive pulses with full width at half-maximum (FWHM) from 4 to 400 ns at different repetition rates. The results showed that all the waveforms can prevent separation, but the strength of the DBD effect on the flow does depend on the voltage waveform.

Explanation of the experimental results and further optimization of plasma actuators has to rely on a firm foundation of modeling. Due to the vast difference of time scales that characterize plasma phenomena (ionization, recombination, evolution of electric field, etc.) and gas dynamics, the problem can be broken into hydrodynamic and plasma parts. The plasma part describes the local influence of the DBD actuator on the flow, and the hydrodynamic part uses the time-dependent distributed body force and heating terms from the plasma calculations to determine global flow field effects. The first attempt of the numerical modeling of plasma kinetics was made by Roy in Ref. 9. Notable results in hydrodynamic modeling of DBD have been obtained by Gaitonde *et al.* (see Ref. 14), however the plasma models used in his calculations were incomplete.

Our group has developed a comprehensive physically based numerical model (see Ref. 1), which includes relevant plasma kinetic phenomena. The results have shown that at low voltages (1.5–2 kV), a sinusoidal signal is not particularly effective in gas pushing due to the positive ion attraction to the upper electrode in the cathode half-cycle. Based on the analysis, a new voltage waveform, repetitive negative nanosecond pulses plus positive bias, has been proposed. In the present paper, we describe further development of the consistent, comprehensive, and physically based model, and computational exploration of DBD performance over a wide range of voltage amplitudes and waveforms.

II. PHYSICAL MODEL

The modeled configuration of the DBD plasma actuator is presented in Fig. 1. It consists of two electrodes separated by the dielectric. The geometrical sizes of the electrodes and the dielectric are different for different numerical experiments and vary from 1.5 mm to 1 cm for electrode lengths and from 100 to 300 μm for dielectric thickness. The relative dielectric permittivity is chosen to be equal to 5. The electrodes are considered to be infinitely thin. This assumption is based on the experimental data, which did not show the dependence on electrode thickness and is used for modeling simplification. The voltage of arbitrary profile is ap-

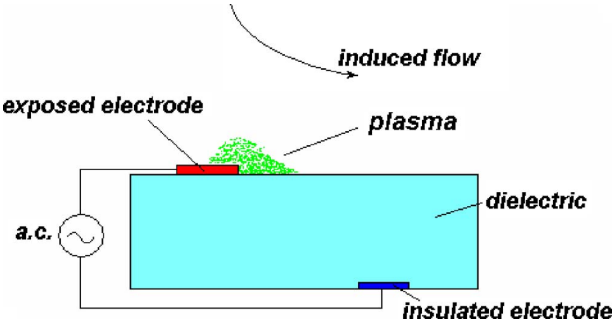

FIG. 1. (Color online) Asymmetric dielectric barrier discharge configuration.

plied to the upper electrode and the lower plate is considered grounded.

The modeled gas was air at room temperature (constant density) consisting of neutrals, electrons, positive, and negative ions. The air was considered as a mixture of oxygen and nitrogen. Air chemistry was not considered in detail. The voltage applied to the upper electrode resulted in weakly ionized plasma formation near the edge of electrode, which subsequently spread to above the dielectric. The formation of negative ions was due to attachment of electrons to oxygen (see Ref. 17). The plasma kinetics and interactions with neutral gas were modeled in a drift-diffusion approximation (see Ref. 11).

We denote number densities of electrons, positive and negative ions, and neutrals as n_e, n_+, n_-, and n, and fluxes of charged particles as Γ_e, Γ_+, and Γ_-. Rate coefficients of ionization, electron-ion recombination, ion-ion recombination, electron detachment from negative ions, and electron attachment to the neutrals will be denoted as α, β, β_{ii}, k_d, and ν_a. For simplicity, we assume that masses of both positive and negative ions are equal to the mass of a neutral molecule, and any of those greatly exceeds the electron mass m. D_e, D_i, μ_e, and μ_i are correspondingly the electron and ion diffusion coefficients and mobilities.

Equations of motion for a four-fluid mixture are then as follows: Continuity equation for electrons,

$$\frac{\partial n_e}{\partial t} + \nabla_j \Gamma_{ej} = \alpha|\Gamma_e| - \beta n_e n_+ + k_d n n_- - \nu_a n_e. \tag{1}$$

Continuity equation for positive ions,

$$\frac{\partial n_+}{\partial t} + \nabla_j \Gamma_{+j} = \alpha|\Gamma_e| - \beta n_e n_+ - \beta_{ii} n_+ n_-. \tag{2}$$

Continuity equation for negative ions,

$$\frac{\partial n_-}{\partial t} + \nabla_j \Gamma_{-j} = -\beta_{ii} n_+ n_- - k_d n n_- + \nu_a n_e. \tag{3}$$

Electron flux,

$$\Gamma_{ej} = -\mu_e E_j n_e - D_e \nabla_j n_e - D_e n_e \frac{\nabla_j T_e}{T_e}. \tag{4}$$

Positive ion flux,

$$\Gamma_{+j} = \mu_i E_j n_+ - D_i \nabla_j n_+. \tag{5}$$

Negative ion flux,

$$\Gamma_{-j} = -\mu_i E_j n_- - D_i \nabla_j n_-. \tag{6}$$

The electric potential and electric field distribution are calculated using the Poisson equation,

$$\nabla(\varepsilon \nabla \varphi) = e(n_e + n_- - n_+), \tag{7}$$

$$E_j = -\nabla_j \varphi, \tag{8}$$

where E is the electric field, e is the charge of the electron, ε is the dielectric permittivity, and φ is the electric potential. Ionization and recombination coefficients, as well as attachment, detachment rates, charged particles mobilities, and electron temperature, are considered as functions E/n, where E is local electric field. The numerical values for rate of ionization, electron-ion recombination, ion-ion recombination, ion mobilities, attachment, and detachment rates are standard and given in Ref. 17. Ion temperature is considered to be equal to gas temperature. Electron drift velocities V_{dr} and electron temperatures, as functions E/N, are given in Ref. 18. The electron mobilities are calculated using the following relation:

$$\mu_e = \frac{V_{\mathrm{dr}}}{E}. \tag{9}$$

The diffusion coefficients are calculated using the Einstein relation,

$$D_i = \mu_i T_i, \tag{10}$$

where i denotes the species (electrons, ions).

The boundary conditions at the electrode surface are

$$\Gamma_{en} = -\gamma_m \Gamma_{+n} \quad \text{if } E_n < 0, \tag{11}$$

$$\Gamma_{+n} = 0 \quad \text{if } E_n > 0, \tag{12}$$

and the boundary conditions at the dielectric surface are

$$\Gamma_{en} = -\gamma_d \Gamma_{+n} \quad \text{if } E_n < 0 \tag{13}$$

and

$$\Gamma_{+n} = 0 \quad \text{if } E_n > 0. \tag{14}$$

Here, γ_m and γ_d are the effective secondary emission coefficients from metal and dielectric, with numerical values 0.1 and 0.01 used in computations correspondingly; index n denotes the normal component of electric field and fluxes.

III. NUMERICAL METHODS

In our previous work (see Ref. 1), we used the second-order accurate MacCormack scheme (see Ref. 19) to model plasma kinetics. This model worked very well at low voltages and gave accurate results. Nevertheless, the transition to higher voltages could not be achieved because of the numerical instabilities that arose at sharp time gradients of the electric field. In order to overcome this problem, the flux corrected transport (FCT) (see Ref. 20) was added to the MacCormack scheme. The results, obtained using the FCT scheme, are smoother and more accurate. Figure 2 shows a

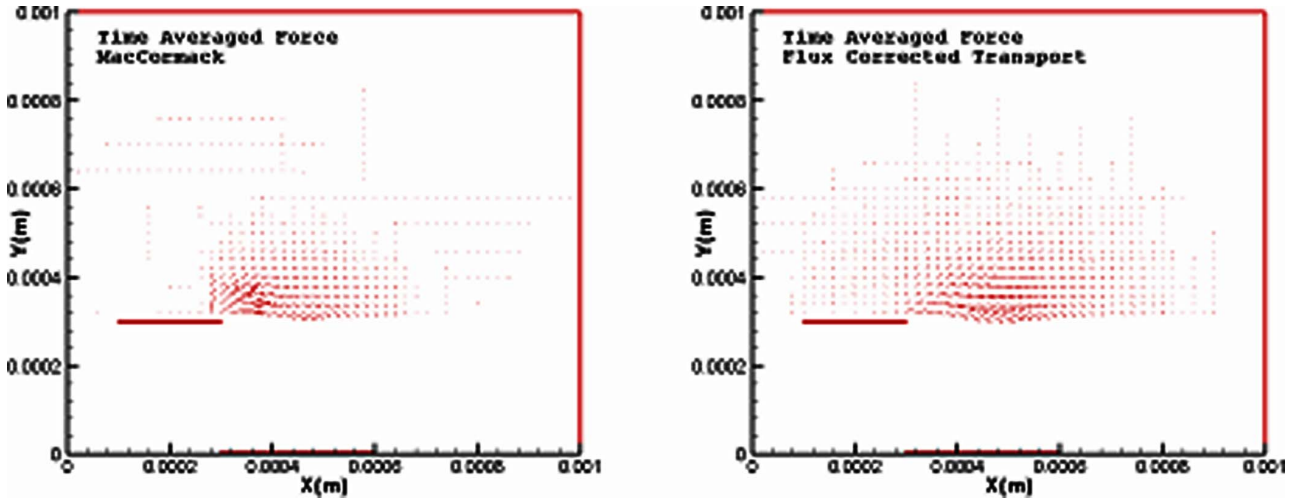

FIG. 2. (Color online) Time-averaged force on the neutral gas. The left plot corresponds to computations with the MacCormack method without FCT, and the right one to the FCT method. (Pulse voltage: 1.5 kV amplitude, 4 ns FWHM, 500 kHz repetition rate, and 500 V bias.)

comparison between time-averaged body forces on the neutral gas using these two methods after three pulses. The results obtained with and without FCT agree well: both produce similar downstream forces with only minor variations in the local force fields. A successive over-relaxation method was used to solve the Poisson equation (see Ref. 19).

Figure 3 shows the voltage-current characteristics during the breakdown for the two numerical schemes. After the pulse, the current is very small. These characteristics obtained with and without the FCT also agree well. A grid convergence study showed some dependence of the results on the grid size, however the qualitative results remained the same. Decreasing the mesh size results in plasma propagation somewhat farther downstream and thereby slightly increases the momentum transfer to the gas.

Using the second-order accurate MacCormack method, the low voltage cases (up to 2 kV) have been modeled (see Ref. 1). The results showed that at low voltages, the conventional sinusoidal voltage was not the optimal profile, and a new voltage profile was proposed: repetitive negative nanosecond pulses and positive bias. The addition of FCT now allows the calculation of DBD with applied low voltage repetitive positive nanosecond pulses with positive bias. Figure 4 shows the time-averaged force acting on the gas at positive pulse with amplitude 1.65 kV and positive bias of 500 V. It is worth mentioning that this is not the streamer case, because voltages are too low. It is a positive corona regime.

The question then arises as to whether the operation of the DBD will improve at higher voltages. What will happen if the amplitude of applied negative pulses increases? Or what is the effect of streamers on the gas in the case of high-voltage positive pulses? The second-order MacCormack scheme and FCT method could not give the answers to these questions due to numerical instabilities, which appear at high voltages. This difficulty has been overcome using the Scharfetter-Gummel method (see Refs. 21 and 22) for flux

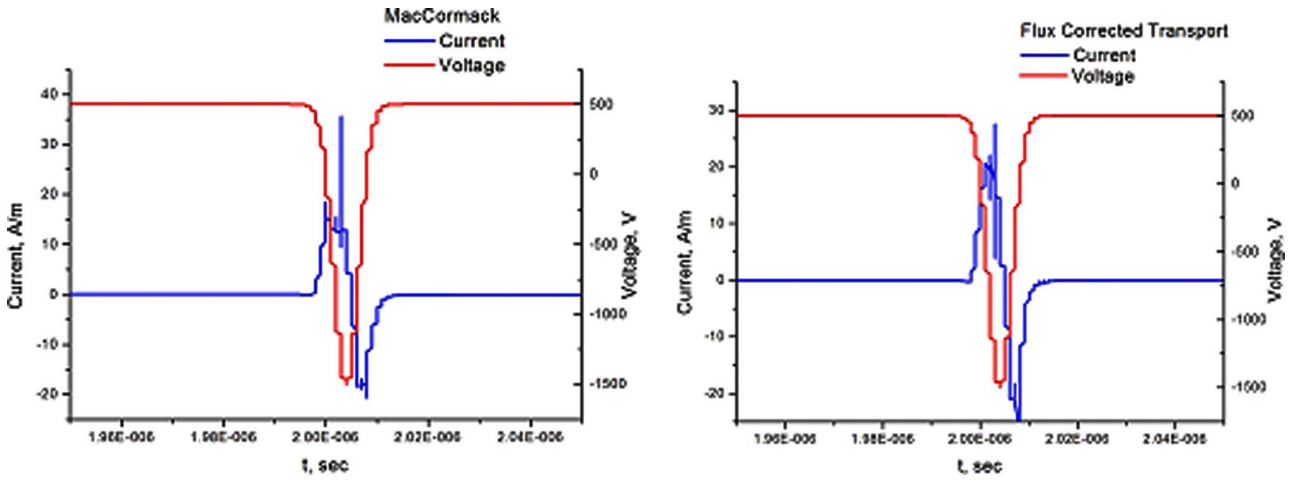

FIG. 3. (Color online) Current and voltage in a representative repetitive-pulse case in the quasi-steady-state regime. The red line shows the voltage, and the dashed line shows the current. The left plot corresponds to the MacCormack method without FCT, and the right one to the FCT method. (Pulse voltage: −1.5 kV amplitude, 4 ns FWHM, 500 kHz repetition rate, and 500 V bias.)

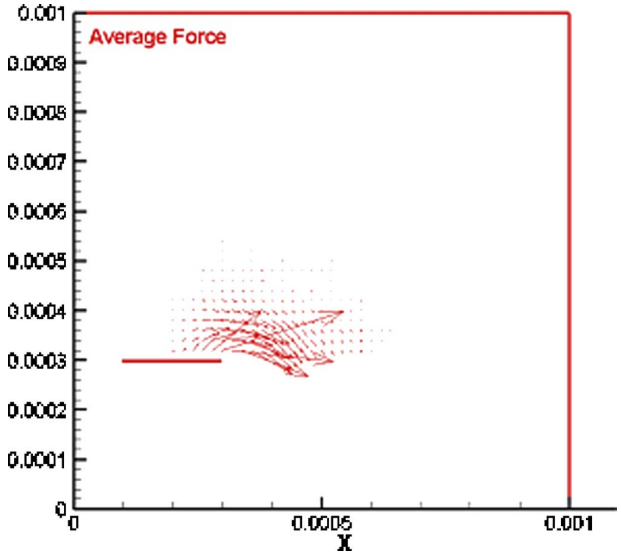

FIG. 4. (Color online) Average force acting on neutral gas during one cycle. (Pulse voltage: amplitude 1.65 kV, FWHM 4 ns, repetition rate 500 kHz, and bias 500 V.)

calculation and the Modified Euler method for solving continuity equations (see Ref. 23).

IV. HIGH-VOLTAGE RESULTS

A. Repetitive negative nanosecond pulses with positive dc bias

Based on the numerical calculations for low voltages, it was proposed to use negative nanosecond pulses and positive dc bias to increase the effect on gas pushing in the asymmetric DBD plasma actuator. The basic principle of this voltage performance was the creation of an ionization wave during the short pulse. When the pulse was applied, the electrons were created near the edge of an electrode due to the high electric field in this region, then they moved along the electric field lines, ionizing the gas, and finally they attached to the dielectric surface, creating a virtual cathode. Since a large number of electrons were attached to the dielectric surface and the pulse time was too short to make positive ions move, a positive ion cloud was formed above the dielectric surface. After the pulse, this positive cloud was pushed from the electrode toward the dielectric surface by an applied positive dc bias and by the attraction of the electrons on the dielectric.

The logical step to improve the performance of DBD plasma actuator with applied repetitive negative nanosecond pulses is to increase the peak voltage of the pulses. This voltage increase should lead to an increase of the positive ion number density in the air after the pulse, and therefore an increase in the force acting on the air in the downstream direction. In order to investigate this phenomenon, a numerical experiment has been carried out. The following geometry was chosen: lengths of upper and lower electrodes were 1.5 and 8 mms, the computational domain was 1×0.5 cm, and the grid size was 25×25 μm. The dielectric thickness was 100 μm and there were no gaps in the horizontal direction between electrodes. When the pulse is applied to the upper electrode, the breakdown occurs and the electrons move to the dielectric, producing weakly ionized plasma and leaving a positive ion cloud behind them. However, after the voltage reaches its peak, a reverse breakdown occurs. This reverse breakdown looks like a cathode-directed streamer (Figs. 5 and 6) and significantly decreases the performance of the DBD plasma actuator. Figure 7 shows the average force on the gas after the pulse. There is a component near the edge of the electrode, directed upstream, however the integral over the volume average force is still directed downstream and is greater than in the case of low voltages. The quantitative comparison of these results will be given later in the paper.

B. Repetitive positive nanosecond pulses with positive dc bias

Another possible way of pushing gas in a DBD plasma actuator is by applying high-voltage repetitive positive pulses plus a positive dc bias. The physics of the downstream force acting on the gas in this case is different from the case with negative pulses.

When a positive nanosecond pulse is applied to the upper electrode, at some voltage the electric field near the edge of the electrode will be sufficient for the initiation of cathode-directed streamer propagation. During the pulse, the streamer propagates along the dielectric until the electric field at the leading edge (head) of the streamer is not sufficient to produce further ionization in front of it. At that point the streamer stops. From the theory of streamers and from the calculations, it is well known that the body of the streamer is quasineutral, but the head of the streamer carries a positive charge in order to displace the electric potential and produce the ionization in front of it. Therefore, after the pulse there will be positive ion cloud in the front part of the decaying streamer. An applied dc bias after the pulse forces this cloud to move downstream and push the gas. Despite the body of the streamer being quasineutral plasma, its effect on the formation of force on the gas is negligible in comparison with the force from the positive ion cloud in front of the streamer. The reason is that the force is proportional to the difference between concentrations of positive and negative charge carriers. After the discharge, the electrons in the quasineutral streamer body are rapidly attached to the oxygen during the time scales of the order of 10 ns. Between the pulses, the drift of negative ions to the upper electrode is compensated by the drift of positive ions downstream.

C. The role of background electron density

In order to correctly model the streamer propagation, one has to solve the problem of radiation transfer and calculate the number density of photoelectrons ahead the streamer head. The number density of photoelectrons depends on the streamer and gas parameters. However, the problem of radiation transfer is quite complicated and solving this problem is time-consuming. The simplified model considers the background charge in the air as having been created in the photoprocesses (see Ref. 24). There are two important parameters we deal with: initial and background charge number

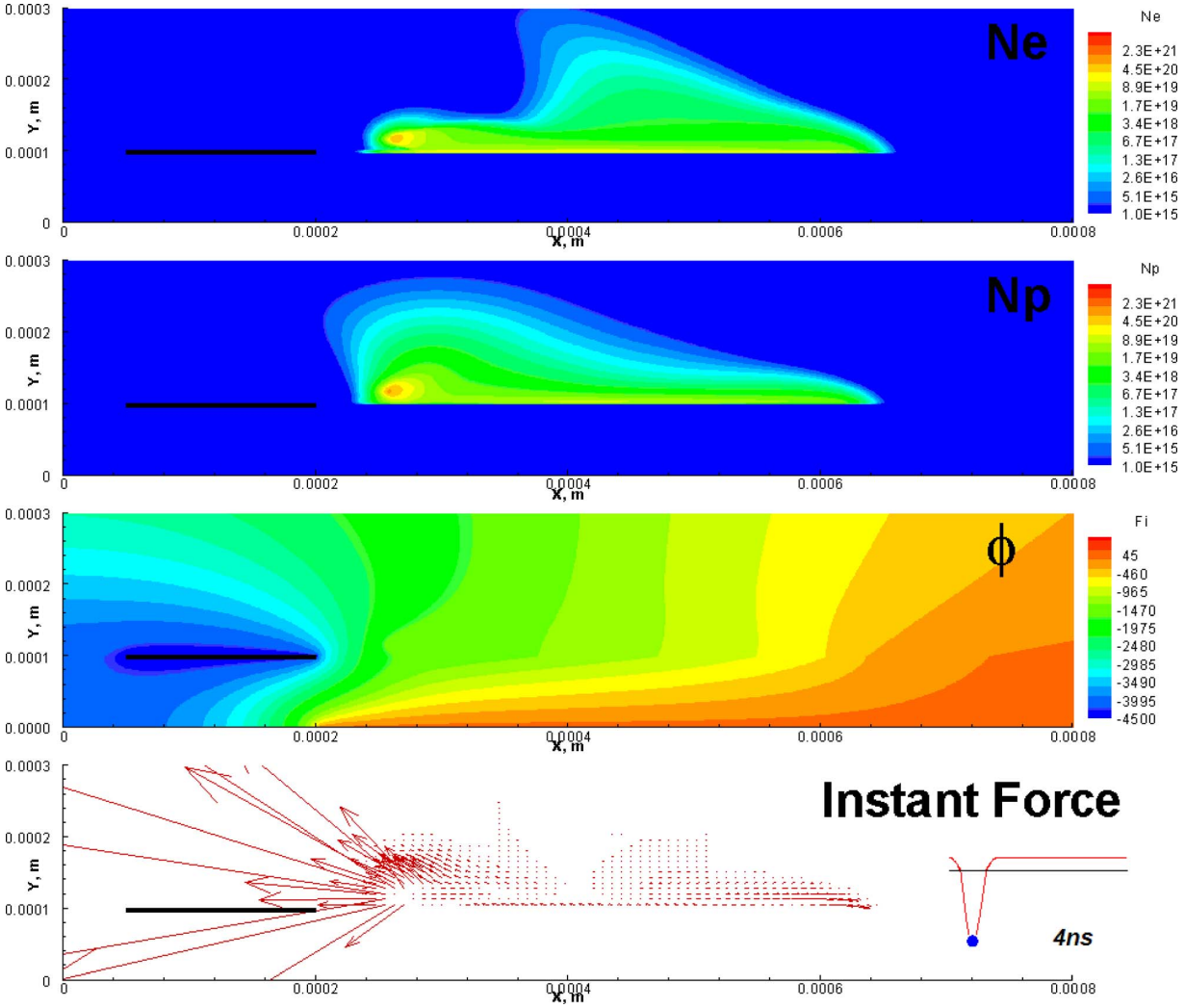

FIG. 5. (Color online) Reverse breakdown. Applied voltage: negative pulses with positive bias. Peak voltage is −4.5 kV, the bias is 0.5 kV, and the pulse FWHM is 4 ns. The figure shows the electron and positive ion number densities, electric potential, and the instantaneous force on the gas at the moment corresponding to the peak voltage.

density. The initial charge number density is the positive ion and electron number densities in the air at the beginning of calculations. Since plasma formation is an exponential process, without initial charges plasma cannot form. However, the initial number density has to be small to have no influence on plasma formation. This fact leads to the problem of streamer formation if the voltage of the upper electrode is positive. In this case, the electrons will be sucked to the electrode during hundreds of picoseconds and there will be no way for the streamer to propagate. In reality, photoelectrons, which are formed ahead of the streamer head, resolve this problem. In our model, we substitute them with background charge. It is the minimum charge number density in the computational domain. If charge number density is less than background in any computational point at some point of time, the charge number density becomes background. This addition of charge has a negligible influence on the precision of the model of plasma-gas interaction because the background charge number density is several orders of magnitude less than the plasma number density. The background charge number density should be chosen empirically to satisfy the experimental data on the streamer propagation speed and the propagation distance. The dependence of streamer propagation parameters on the background and the initial conditions has been investigated. For this, a geometry that is the same as for the negative pulses was chosen. Single positive Gaussian pulses with 4 ns FWHM and 3 kV amplitude have been applied to the upper electrode. Two parameters were changed—the initial charge density and the background charge density. If the initial and background charge density is of the order of $1-10\ 1/m^3$, the plasma cannot even appear. If the initial number density is very high (of the order of $10^{16}\ 1/m^3$) even without background charge, the plasma forms and a streamer propagates. The background does not play a role in this case, because the Debye length is less than the computational domain and electrons will always be able to come from the outside of the Debye sphere. When the initial number density drops to $10^{11}\ 1/m^3$, it plays a critical

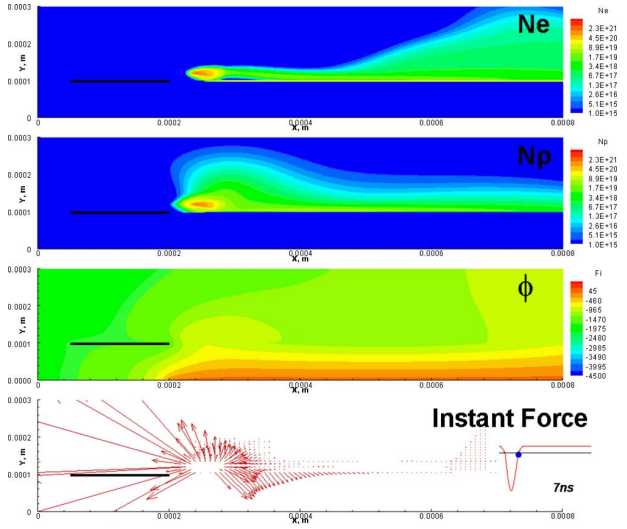

FIG. 6. (Color online) Reverse breakdown. Applied voltage is negative pulse with positive bias. Peak voltage is −4.5 kV, the bias is 0.5 kV, and the pulse FWHM is 4 ns. The figure shows the electron and positive ion number densities, electric potential, and the instantaneous force on the gas after the pulse.

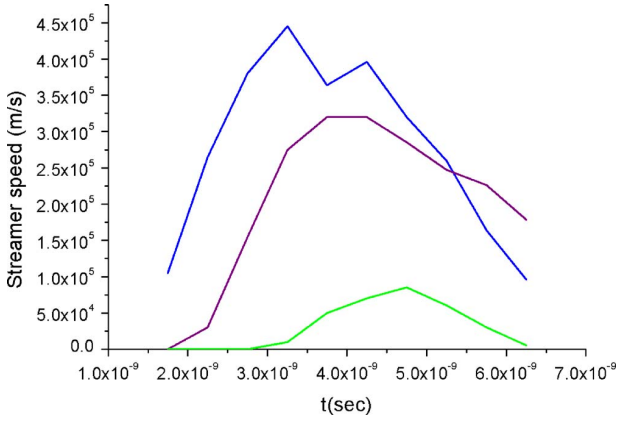

FIG. 8. (Color online) Streamer propagation speed in three different cases. The green line corresponds to the initial and background electron number density of 10^7 $1/m^3$; the purple line, to 10^{11} $1/m^3$; and the blue line, to the initial electron number density of 10^{16} $1/m^3$ and no background charge. Applied voltage waveform: positive pulses with positive bias. Peak voltage is 3 kV, the bias is 1 kV, and the pulse FWHM is 4 ns.

role in the streamer formation. Without it, all electrons will rapidly move to the electrode and there will be no "photo" electrons, and the streamer will not be able to propagate. The background charge supplies the electrons for the streamer. The streamer stops propagating when the electric field at its head is not enough for propagation. A similar situation happens when the background number densities drop to 10^7 $1/m^3$. Figure 8 shows a comparison of different initial and background charge number density. In our modeling, the background plasma was taken to be 10^7 $1/m^3$, corresponding to the values in the literature. Figure 9 shows the typical simulated streamer and Fig. 10 shows the time-average force on the gas distribution.

It is worth mentioning that the background charge is not essential for negative pulse modeling. In this case, the electrons appear on the electrode or dielectric due to secondary emission and then move along the electric field line, producing the plasma. The reverse breakdown is also easily resolved, despite its streamer-like appearance. After the electron avalanche, there is plasma with an ionization fraction much greater than 1 due to photoionization.

V. COMPARISON OF HIGH- AND LOW-VOLTAGE CALCULATIONS

As predicted before (see Ref. 1), higher voltages increase the DBD plasma actuator performance. Figure 11 shows a comparison of (i) low-voltage repetitive negative nanosecond pulses with positive bias, (ii) high-voltage negative pulses with positive dc bias, and (iii) repetitive positive nanosecond pulses with positive bias. The higher voltages transfer three times more momentum to the gas in contrast to the low ones. Note that positive pulses with amplitudes of 3 kV give the same effect as the negative pulses with amplitudes of 4.5 kV. Modeling high voltages also allows for the prediction of different ways of plasma formation in DBD and different momentum transfer. For example, at low voltages the streamer does not propagate in the case of positive pulses, but at high voltages it does. The obtained results also give an important conclusion about the scaling predictions in numerical modeling. DBD plasma actuators operate at different regimes not only at different voltage profiles, but at different voltage amplitudes. Further predictions of DBD performance at voltages of the order of 10–20 kV require more extensive computational capabilities and the application of parallel computing methods.

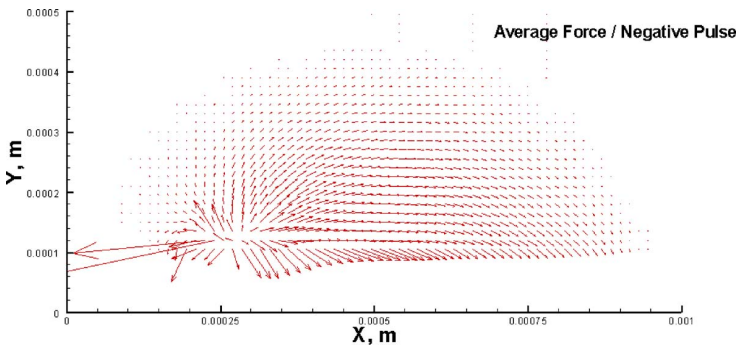

FIG. 7. (Color online) Average force acting on neutral gas during one cycle. (Pulse voltage: amplitude is −4.5 kV, FWHM is 4 ns, repetition rate is 500 kHz, and the bias is 0.5 kV.)

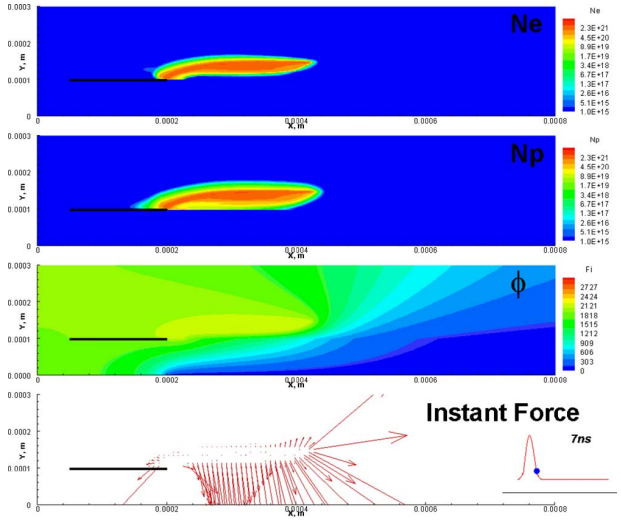

FIG. 9. (Color online) Streamer-like ionization wave. Applied voltage waveform: positive pulses with positive bias. Peak voltage is 3 kV, the bias is 1 kV, and the pulse FWHM is 4 ns. The figure shows the electron and positive ion number densities, electric potential, and the instantaneous force on the gas.

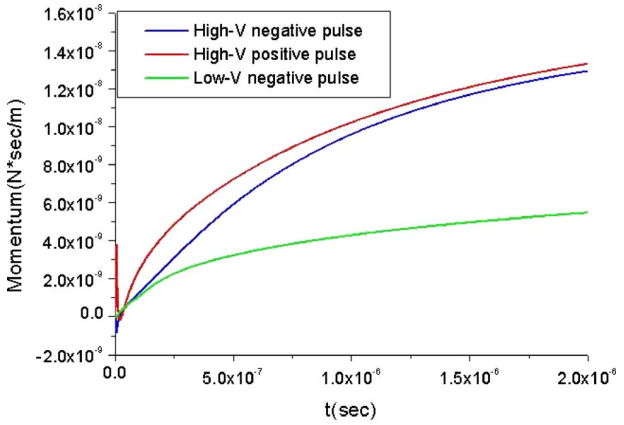

FIG. 11. (Color online) Momentum transferred to the gas. Blue and green lines correspond to the negative pulses with amplitudes −4.5 and −1.5 kV with positive bias of 0.5 kV, and the red line corresponds to the positive pulses with 3 kV amplitude and positive bias of 1 kV. FWHM for all pulses is 4 ns.

VI. CONCLUSIONS

The comprehensive physical and numerical model of DBD plasma actuators in air developed in this work allowed us to investigate the essential physics of DBD driven by repetitive short pulses with and without dc bias and to reveal the effects of varying the parameters of this type of voltage waveform. Modeling of high-voltage negative nanosecond pulses generally agrees with scaling predictions based on low-voltage cases, but a new effect, the reverse breakdown, takes place at the higher voltages. The physics of the reverse breakdown and its negative role in the DBD performance, consisting in upstream-directed force, has been shown. Nevertheless, at higher pulse voltages, stronger forces on the gas are produced and more momentum is transferred than at lower voltages.

A new voltage waveform—positive nanosecond pulses with positive dc bias—has been modeled. The results demonstrate that this waveform is promising for improvement of DBD plasma actuator performance. Although this voltage waveform is not very effective at low voltages, it becomes very effective at high voltages. With this waveform, a performance similar to that provided by the negative pulses with positive dc bias could be achieved with much lower voltage amplitudes.

Computations have demonstrated a crucial influence of background and initial electron densities on the DBD modeling of streamers in the anode stage. Although that background charge density can be several orders of magnitude

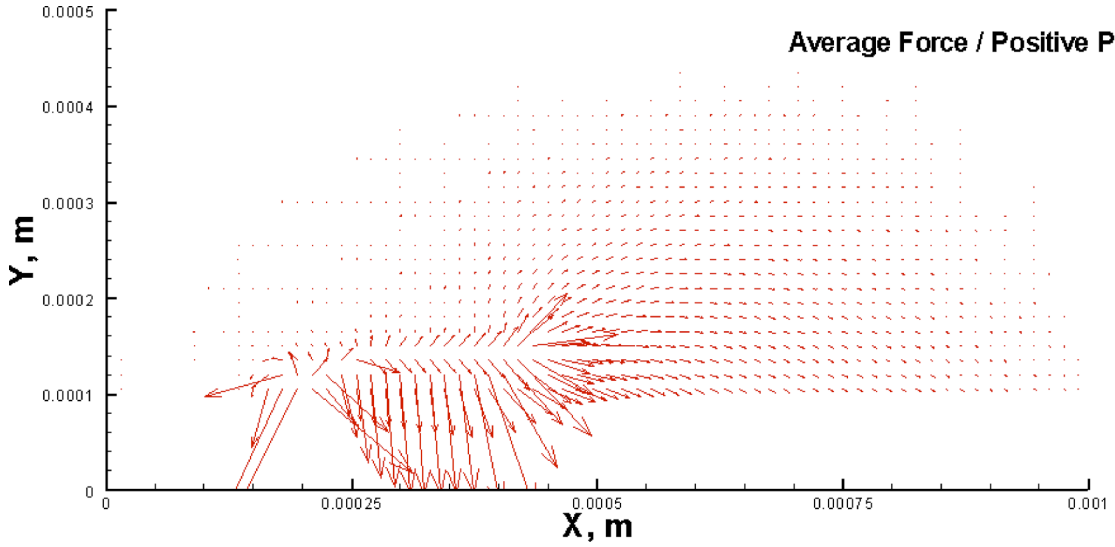

FIG. 10. (Color online) Average force acting on neutral gas during one cycle. (Pulse voltage: amplitude is 3 kV, FWHM is 4 ns, the repetition rate is 500 kHz, and the bias is 1 kV.)

lower than that in the fully developed plasma, streamer propagation characteristics are extremely sensitive to the background electron density.

A comparison of the results for low- and high-voltage amplitudes shows that, depending on the details of voltage waveform and on the voltage amplitude, different DBD regimes with different physics of plasma-air interaction can be realized. Therefore, one should be very cautious with scaling predictions, and such predictions must be based on full physical modeling and experiments.

ACKNOWLEDGMENTS

This work was supported in part by the Air Force Office of Scientific Research (Dr. John Schmisseur) and in part by Boeing, St. Louis. Fellowship support for one of the authors (A.V.L.) was provided by the Princeton Program in Plasma Science and Technology.

[1]A. V. Likhanskii, M. N. Shneider, S. O. Macheret, and R. B. Miles, *Proceedings of the 44th AIAA Aerospace Sciences Meeting and Exhibit, Reno, NV, 2006* (AIAA, Washington, D.C., 2006), Paper AIAA-2006–1204.
[2]C. L. Enloe, T. E. McLaughlin, R. D. VanDyken, K. D. Kachner, E. J. Jumper, and T. C. Corke, AIAA J. **42**, 89 (2004).
[3]C. L. Enloe, T. E. McLaughlin, R. D. VanDyken, K. D. Kachner, E. J. Jumper, T. C. Corke, M. Post, and O. Haddad, AIAA J. **42**, 595 (2004).
[4]M. Post and T. C. Corke, *Proceedings of the 35th AIAA Fluid Dynamics Conference and Exhibit, Toronto, Ontario, 2005* (AIAA, Washington, D.C., 2005), Paper AIAA-2005–4630.
[5]T. C. Corke, E. J. Jumper, M. L. Post, D. Orlov, and T. E. McLaughlin, *Proceedings of the 40th AIAA Aerospace Sciences Meeting & Exhibit, Reno, NV, 2002* (AIAA, Washington, D.C., 2005), Paper AIAA—2002–350.
[6]M. L. Post and T. C. Corke, AIAA J. **42**, 2177 (2004).
[7]D. F. Opaits, D. V. Roupassov, S. M. Starikovskaia, A. Yu. Starikovskii, I. N. Zavialov, and S. G. Saddoughi, *Proceedings of the 43rd AIAA Aerospace Sciences Meeting and Exhibit, Reno, NV, 2005* (AIAA, Washington, D.C., 2005), Paper AIAA-2005–1180.
[8]S. Roy and D. V. Gaitonde, *Proceedings of the 43rd AIAA Aerospace Sciences Meeting and Exhibit, Reno, NV, 2005* (AIAA, Washington, D.C., 2005), Paper AIAA 2005–160.
[9]S. Roy, Appl. Phys. Lett. **86**, 101502 (2005).
[10]K. P. Singh and S. Roy, J. Appl. Phys. **98**, 083303 (2005).
[11]J. P. Boeuf and L. C. Pitchford, J. Appl. Phys. **97**, 103307 (2005).
[12]D. M. Orlov and T. C. Corke, *Proceedings of the 43rd AIAA Aerospace Sciences Meeting and Exhibit, Reno, NV, 2005* (AIAA, Washington, D.C., 2005), Paper AIAA 2005–1083.
[13]J. R. Roth and X. Dai, *Proceedings of the 44th AIAA Aerospace Sciences Meeting and Exhibit, Reno, NV, 2006* (AIAA, Washington, D.C., 2006), Paper AIAA-2006–1203.
[14]D. V. Gaitonde, M. R. Visbal, and S. Roy, *Proceedings of the 44th AIAA Aerospace Sciences Meeting and Exhibit, Reno, NV, 2006* (AIAA, Washington, D.C., 2006), Paper AIAA-2006–1205.
[15]T. C. Corke, B. Mertz, and M. P. Patel, *Proceedings of the 44th AIAA Aerospace Sciences Meeting and Exhibit, Reno, NV, 2006* (AIAA, Washington, D.C., 2006), Paper AIAA-2006–1208.
[16]R. Anderson and S. Roy, *Proceedings of the 44th AIAA Aerospace Sciences Meeting and Exhibit, Reno, NV, 2006* (AIAA, Washington, D.C., 2006), Paper AIAA-2006–0369.
[17]S. O. Macheret, M. N. Shneider, and R. B. Miles, IEEE Trans. Plasma Sci. **30**, 1301 (2002).
[18]I. S. Grigoriev and E. Z. Meilikhov, *Handbook of Physical Quantities* (CRC, Boca Raton, FL, 1997), Chap. 20.
[19]D. A. Anderson, J. C. Tannehill, and R. H. Pletcher, *Computational Fluid Mechanics and Heat Transfer* (Hemisphere, New York, 1984).
[20]S. T. Zalezak, J. Comput. Phys. **31**, 335 (1979).
[21]H. K. Gummel, IEEE Trans. Electron Devices **11**, 455 (1964).
[22]D. L. Scharfetter and H. K. Gummel, IEEE Trans. Electron Devices **16**, 64 (1969).
[23]J. C. Butcher, *The Numerical Analysis of Ordinary Differential Equations: Runge-Kutta and General Linear Methods* (Wiley, New York, 1987).
[24]L. B. Loeb, Science **148**, 141 (1965).

JOURNAL OF APPLIED PHYSICS **104**, 043304 (2008)

Experimental investigation of dielectric barrier discharge plasma actuators driven by repetitive high-voltage nanosecond pulses with dc or low frequency sinusoidal bias

Dmitry F. Opaits,[1,a)] Alexandre V. Likhanskii,[1] Gabriele Neretti,[1] Sohail Zaidi,[1] Mikhail N. Shneider,[1] Richard B. Miles,[1] and Sergey O. Macheret[2]
[1]*Mechanical and Aerospace Engineering, Princeton University, Princeton, New Jersey 08544, USA*
[2]*Lockheed Martin Aeronautics Company, Palmdale, California 93599, USA*

(Received 14 August 2007; accepted 26 June 2008; published online 27 August 2008)

Experimental studies were conducted of a flow induced in an initially quiescent room air by a single asymmetric dielectric barrier discharge driven by voltage waveforms consisting of repetitive nanosecond high-voltage pulses superimposed on dc or alternating sinusoidal or square-wave bias voltage. To characterize the pulses and to optimize their matching to the plasma, a numerical code for short pulse calculations with an arbitrary impedance load was developed. A new approach for nonintrusive diagnostics of plasma actuator induced flows in quiescent gas was proposed, consisting of three elements coupled together: the schlieren technique, burst mode of plasma actuator operation, and two-dimensional numerical fluid modeling. The force and heating rate calculated by a plasma model was used as an input to two-dimensional viscous flow solver to predict the time-dependent dielectric barrier discharge induced flow field. This approach allowed us to restore the entire two-dimensional unsteady plasma induced flow pattern as well as characteristics of the plasma induced force. Both the experiments and computations showed the same vortex flow structures induced by the actuator. Parametric studies of the vortices at different bias voltages, pulse polarities, peak pulse voltages, and pulse repetition rates were conducted experimentally. The significance of charge buildup on the dielectric surface was demonstrated. The charge buildup decreases the effective electric field in the plasma and reduces the plasma actuator performance. The accumulated surface charge can be removed by switching the bias polarity, which leads to a newly proposed voltage waveform consisting of high-voltage nanosecond repetitive pulses superimposed on a high-voltage low frequency sinusoidal voltage. Advantages of the new voltage waveform were demonstrated experimentally. © *2008 American Institute of Physics*. [DOI: 10.1063/1.2968251]

I. INTRODUCTION

Electrohydrodynamic (EHD) and magnetohydrodynamic phenomena are being widely studied for aerodynamic applications. The major effects of these phenomena are heating of the gas, body force generation, and enthalpy addition or extraction.[1–35] In particular, asymmetric dielectric barrier discharge (DBD) plasma actuators are known to be effective EHD device in aerodynamic control.[30–35] A number of experiments have shown the potential of DBD for flow separation control at low-to-moderate flow velocities (1–100 m/s). There is an agreement that the DBD actuators generate near-surface synthetic jets. The induced near-surface flow velocities using sinusoidal or sawtooth voltage waveforms at frequencies of 1–100 kHz and amplitudes of 2–20 kV are of the order of 1–5 m/s. However, optimized voltage waveforms[36] allow the increase in the induced gas velocities in the vicinity of plasma-gas interaction region.

Recent numerical studies with a detailed model based on full plasma kinetics coupled with the dynamics of the electric field developed by Likhanskii *et al.*[37–40] provided consistent physical explanations for the observed phenomena and suggested ways for improvement of actuator performances. Specifically, it was shown that a voltage waveform consisting of high repetition rate short (nanosecond) pulses has the potential to produce a stronger effect on the flow than a conventional sinusoidal voltage. Additionally, it was predicted that adding a positive bias voltage to the pulses should increase the velocity of wall jet generated by the plasma actuator.

This paper presents results of experiments with a DBD asymmetric discharge driven by repetitive high-voltage nanosecond pulses. The purpose of the experiments was to provide a better understanding of the physical processes and to validate the numerical model. The experiments showed, as will be discussed below, that adding the bias voltage has a strong effect only for the first several hundred pulses. Then the surface charge builds up shielding the applied bias voltage and reducing performance. To remove the surface charge, we explored changing the bias voltage polarity periodically. Experiments reported in this paper have demonstrated that the new voltage profile which consists of nanosecond pulses superimposed on a high-voltage low frequency sinusoidal bias voltage does indeed lead to higher performance.

To conduct experiments with DBD actuators driven by repetitive voltage pulses, one needs to characterize and optimize the coupling of the pulses with the plasma and to develop reliable nonintrusive flow diagnostics. To address the

a)Electronic mail: dopaits@princeton.edu.

first problem, a numerical code for short pulse calculation with an arbitrary impedance load was developed. The code is based on Kirchhoff's laws and allowed minimization of pulse reflection from the actuator.

Regarding the second problem, flow diagnostics, difficulties of diagnostics of the actuator induced flow arise from its small (approximately centimeter) scale, low speed (~m/s), and closeness to the plasma and the dielectric surface. Most common techniques to diagnose the induced wall jet include particle image velocimetry, smoke visualization, Pitot probes, etc. Unfortunately, these methods are intrusive and must be used with great care. For example, in particle image velocimetry measurements the particles may get charged in the plasma and may not only depict the flow incorrectly but may also affect the plasma and the gas flow. The main disadvantage of Pitot-probe measurements is low sensitivity. The measurements have to be taken at some distance downstream from the actuator in order not to perturb the plasma. Pitot measurements are also local, and to obtain the entire flow pattern, a scan through the entire flow region should be performed. The task becomes much more complicated with nonstationary flows. Attempts to use nonintrusive optical methods were made in a number of works. A laser deflection technique was used to measure density by probing index of refraction gradients in the air.[41] Being nonintrusive, this approach, however, gives only local measurements and, like the Pitot-probe one, is hard to apply to nonstationary flows.

The use of the schlieren technique for DBD induced flow measurements was reported.[42,43] In the first paper[42] the authors used conventional schlieren technique for flow visualization. The technique is based on following thermal disturbances in the jet and extracting the flow speed from that. However, the authors[42] found this insufficient for quantitative speed measurements and used schlieren streak video instead. Another, similar, application of the schlieren technique to DBD plasma actuator was demonstrated in Ref. 43. Turbulent eddies were treated as tracers in the flow. A new, helium based technique of schlieren image processing was suggested to observe the flow field. In the region outside the turbulent flow a helium jet was injected in order to produce the necessary contrast. The helium jet, however, can disturb the plasma and the flow field. All of the above techniques are based on disturbances and/or turbulence in the induced flow. As noted in Ref. 43 the technique is not applicable for laminar flows.

In this paper, we used a new approach for the induced flow visualization and velocity measurements. Since the discharge slightly heats the air, it is possible to visualize the induced wall jet. The principal feature of our schlieren technique, distinguishing it from other studies, is the modulation of the voltage waveform applied to the discharge so that the plasma actuator is operated in pulse-burst mode. In the burst mode, separate pulse jets are created by each burst. The advantage of the proposed technique is the ability to visualize two-dimensional (2D), laminar, low speed, small, nonstationary plasma induced jets. An advantage of studies with quiescent air is that it is possible to notice some features of the induced flow which otherwise would be washed out by an external flow. A numerical model based on 2D Navier–Stokes equations predicts similar structures and allows us to extrapolate the entire flow pattern by matching the schlieren images of a single vortex. The numerical modeling also allows us to infer the magnitude of the body forces exerted by the DBD actuator on the gas.

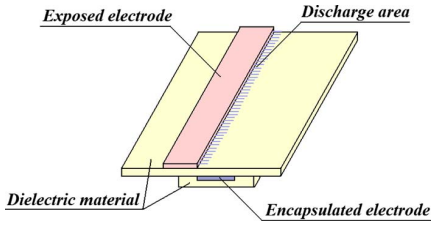

FIG. 1. (Color online) Asymmetric DBD plasma actuator.

As will be discussed in the paper, the schlieren imaging in the pulse-burst mode demonstrated that the DBD actuator produces vortices. Note that similar structures were observed in DBD experiments using smoke visualization[44] and schlieren technique,[45] in DBD induced flow numerical simulations,[46,47] and also in plane wall jet experiments and numerical simulations.[48–50] However, in this work, we demonstrate that the strength of the vortices and frequency of their generation can be controlled by the voltage waveform, which has practical implications.

II. EXPERIMENTAL SETUP

The plasma actuator consisted of two electrodes placed asymmetrically on either side of the dielectric, with one electrode encapsulated, and the other exposed to the atmospheric air, as shown at Fig. 1.[51] The electrodes were made of copper foil. The width of the electrodes was equal to 25 mm and their spanwise dimension was 50 mm. A 100 μm thick kapton tape was used as the dielectric. The discharge was ignited by applying high voltage to one of the electrodes. The other electrode was grounded. The actuator was placed inside a sealed cylindrical aluminum chamber (45 cm high and 40 cm in diameter) to eliminate the interaction between the plasma induced flow (~1 m/s) and air in the room and to enable experiments at different pressures and with different gases.

For the plasma actuator induced flow visualization we used a conventional schlieren system (Fig. 2)[52] which consisted of a mercury lamp, a 50 μm pinhole, and two lenses

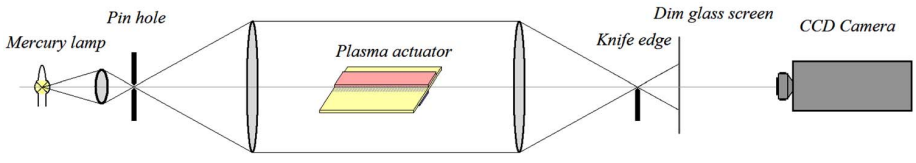

FIG. 2. (Color online) Schlieren system.

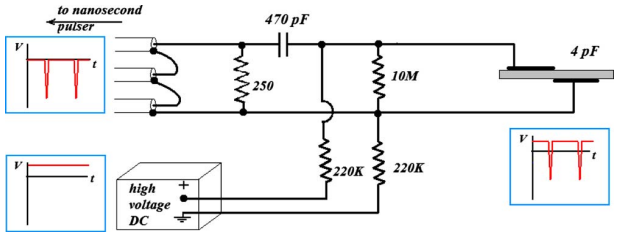

FIG. 3. (Color online) Electric circuit. The circuit is designed so as to combine short pulses with a low frequency bias voltage without interference between the pulser and the low frequency power supply. In experiments with sinusoidal bias, the dc power supply was replaced by a high-voltage transformer.

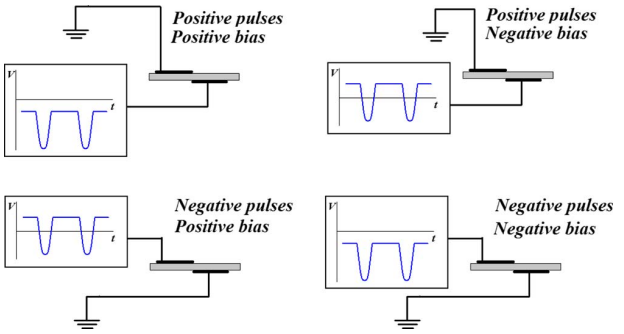

FIG. 4. (Color online) Terminology used in the paper for the pulse and bias voltage polarities. The encapsulated electrode is always considered to be at zero potential. The sign of potential of the exposed electrode relative to the encapsulated one determines the pulse and bias polarity.

(FL=25 cm, D=6 cm). A vertical knife edge was put into the focus of the second lens. The image was projected on a ground glass screen and then captured by a Princeton Scientific Instruments 4-D charge coupled device camera. The camera took 28 consecutive images with 1 ms exposure time and no significant delay between the images.

In the experiments, we used a voltage waveform consisting of repetitive nanosecond pulses in burst mode superimposed on a bias voltage. Although during the experiments the bias voltage waveform evolved from constant to sinusoidal, the same electric circuit, shown in Fig. 3, was used. The circuit is designed so as to superimpose short pulses on a low frequency bias voltage without interference between the pulser and the low frequency power supply. Adding a 470 pF capacitor in series with the actuator shielded the pulser from the bias voltage. Since the capacitance of the actuator was only 4 pF, the main voltage drop occurred just at the plasma actuator. The 220 kΩ resistors did not let the pulse go to the power supply. The charging time for the capacitor through the corresponding resistors was $\tau=RC=220$ kΩ 470 pF ≈ 100 μs, which corresponds to 10 kHz$\gg$60 Hz. The 10 MΩ resistor was put in parallel with the actuator for safety reasons. It discharged the high-voltage electrode after experiments. Its high impedance did not influence the circuit in any way. Also, a noninductive 250 Ω resistor was added in parallel with the actuator to minimize the pulse reflection.

The pulser used in the experiments was a FID Technology 4 ns full width at half maximum (FWHM) pulser capable of running with pulse repetition rate (PRR) of up to 100 KHz and triggered by a ~10 V pulse from a Stanford Box. The peak output voltage of the pulser was up to 10 kV which was fed to three separate 3 m long 75 Ω coaxial lines. The three copropagating pulses were converted into a single pulse by taking advantage of the short physical "length" of the pulses (less than 1 m). By connecting the center conductor of the first coaxial line to the outer conductor of the second and the center conductor of the second to the outer conductor of the third, an amplified pulse is produced between the center conductor of the third line and the outer conductor of the first. This essentially is a transformer made of sections of transmission lines, and it is well described in the literature.[53]

A source of constant bias voltage used in the experiments was High Voltage DC Supply model 412 by John Fluke MFG Co, Inc., capable of producing output voltages up to 2 kV both polarities. Ozone generator transformer by Plasma Technics, Inc., was used for producing sinusoidal bias voltage.

The pulser was able to produce pulses of negative polarity only. The bias voltage could be of any polarity but could be added to the pulsed electrode only due to the circuit properties. The terminology used in this paper came from the numerical simulations, where the encapsulated electrode was supposed grounded, and the voltage waveform was applied to the exposed electrode. Following the same terminology, we consider the encapsulated electrode to be at zero potential. That means that the term "positive" refers to a case when the electric field is directed from the exposed electrode to the encapsulated one, i.e., parallel to the induced jet, and negative when in the opposite direction. Thus, applying negative pulses to the lower (encapsulated) electrode will henceforth be referred to as positive pulses. Further, applying negative bias voltage to the top (exposed) electrode will be called a negative bias, whereas applying negative bias voltage to the lower (encapsulated) electrode will be referred to as positive bias. See Fig. 4 for further examples.

III. NANOSECOND PULSE PROFILE

Special attention was paid to the electric pulse waveform. It was measured by a LeCroy high-voltage probe PPE6 kV (400 MHz bandwidth, 50 MΩ input resistance, <6 pF input capacitance) connected to a Tektronix digital oscilloscope TDS 380 (400 MHz bandwidth). Since the pulses were only several nanoseconds long, they were reflected back from the plasma actuator and then reflected again by the pulser toward the actuator. Therefore, each pulse actually looked like a series of damped pulses. To reduce this ringing, a computer code incorporating the actuator's and the probe's capacitances was developed. The code calculated the reflection of a pulse from a *RLC* load. The code was based on Kirchhoff's laws written for an *LRC* load connected to a 3 ×75 Ω=225 Ω cable. A schematic of the transformer made of sections of transmission lines connected to a *RLC* load is shown in Fig. 5(a). In the figure, Z is the cable impedance, Z_0 is defined by parasitic impedances and/or impedance of cable connecting wires, C is the capacitance of the actuator and the voltage probe, R is resistance of a noninductive matching

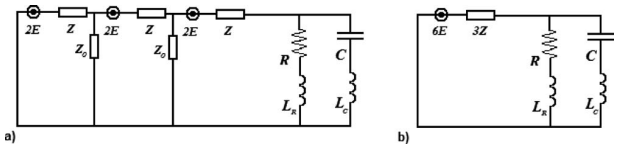

FIG. 5. An equivalent scheme of the transformer made of sections of transmission lines connected to the *RLC* load. (a) Full circuit; (b) reduced circuit.

resistor, and *LR* and *LC* are inductances of the connecting wires. Note that usually $Z_0 \gg nZ$, where n is the number of the cables. This simplifies the circuit to the one shown in Fig. 5(b). Kirchhoff's laws for this circuit can be written as

$$6E = 3Z_0(I_{RL} + I_{LC}) + I_{RL}R + L_R\frac{dI_{RL}}{dt}, \tag{1}$$

$$6E = 3Z_0(I_{RL} + I_{LC}) + V + L_C\frac{dI_{LC}}{dt}, \tag{2}$$

$$V = \frac{1}{C}\int_o^t I_{LC}d\tau. \tag{3}$$

From these, we get the following set of two integrodifferential equations for the currents:

$$\frac{dI_{RL}}{dt} = \frac{1}{L_R}(6E - 3Z_0(I_{RL} + I_{LC}) - I_{RL}R), \tag{4}$$

$$\frac{dI_{LC}}{dt} = \frac{1}{L_C}\left(6E - 3Z_0(I_{RL} + I_{LC}) - \frac{1}{C}\int_o^t I_{LC}d\tau\right). \tag{5}$$

Solving the set of equations using first order explicit Euler's method, we obtain the dependence of the currents on time. From that, the time-dependent voltage on the plasma actuator and of the reflected pulse is calculated as

$$V_{\text{reflected}} = 3Z_0(I_{RL} + I_{LC}) - 3E. \tag{6}$$

In the absence of a reactive load, this gives a well-known result—the ringing can be eliminated by a matching load. In our case, it was 225 Ω. In the experiments, the connecting wires had finite dimensions, i.e., inductances. To evaluate the inductances, we used an approximate expression for circular loop inductance,

$$L_{\text{circle}} \approx R\mu_0\left[\ln\left(\frac{8R}{a}\right) - 2\right], \tag{7}$$

where R is the radius of the loop, a is the radius of the wire, and μ_0 is the permeability of free space. In the experiments, the wires connecting the resistance formed a loop with ~1 cm radius, while the wires connecting the actuator were longer and the corresponding radius was ~5 cm. This corresponds to inductances of $L_R = 0.038$ μH and $L_R = 0.294$ μH. Substituting these numbers into the numerical code, the pulse reflection can be calculated. Calculations showed that at these values of inductances, there is almost no difference if a 250 Ω resistor is used as the matching impedance instead of the 225 Ω one. Therefore, in the experiments, 250 Ω resistor was used due to its availability in the laboratory. Unfortunately, the reflection of the pulse from the pulser back to the actuator could not be calculated because of the complex structure of the pulser. Therefore, the numerical results are for single reflection only, whereas the experimental ones show all the ringing which takes place between the actuator and the pulser. Note that increasing the actuator's capacitance leads to a lower peak voltage and to increased pulse duration. The voltage over the actuator and the reflected pulse is shown in Fig. 6. By choosing the right resistance, we were able to reduce the ratio of the reflected pulse to the voltage over the actuator from 60% to 40%. The main reason for the 40% reflection is the inductance of the connecting wires. The numerical model also predicted the pulse duration increase from 4 to ~5.5 ns. This result agrees well

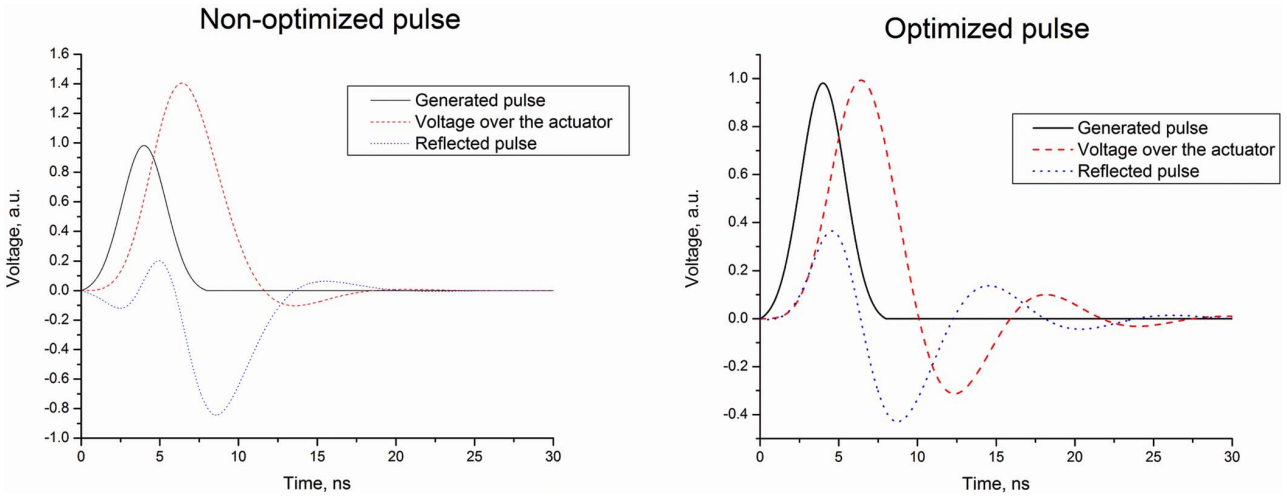

FIG. 6. (Color online) Numerical calculation of the nanosecond pulses. The plots show profiles of the pulse originally generated by the pulser, the voltage profile over the actuator, and the pulse reflected back into the cables. Left plot is for nonoptimized load. Right plot is for optimized load with 250 Ω noninductive resistor. Adding the resistor decreases the ratio of the reflected pulse to the voltage on the actuator from 60% to 40%. These 40% are due to inductances of the connecting wires.

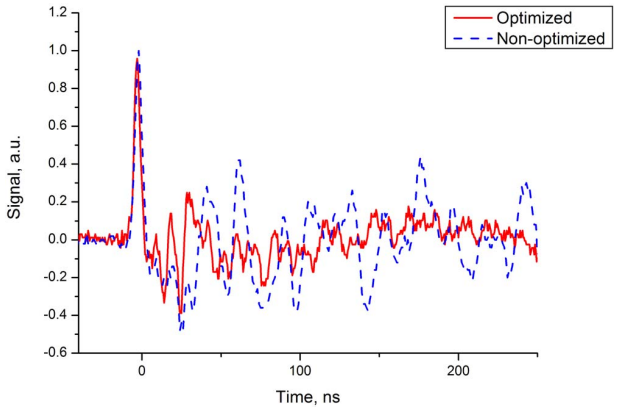

FIG. 7. (Color online) The measured pulse profile before and after optimization.

with the experiment. The measured pulse profiles before and after optimization are shown in Fig. 7.

Experiments showed that covering the exposed electrode by a kapton tape, thus preventing the discharge ignition, changed the amplitude of reflected pulse by only a few percent. Thus it was concluded that the plasma impedance plays an insignificant role in the impedance matching problem.

IV. RESULTS

The schlieren technique provides the coupling between the theoretical investigation of the plasma-gas interaction and the experiment. The plasma model predicts the heating rate and the force exerted on the gas. The output parameters from the plasma calculations can be then used as an input for the time-accurate numerical computational fluid dynamics (CFD) model based on 2D Navier–Stokes equations. The experiments showed that the DBD actuator run in pulse-burst mode generates periodic wall jets which evolve into vortical structures. The numerical model predicts similar vertical structures and allows us to restore the entire flow pattern by matching the schlieren images of a single vortex.

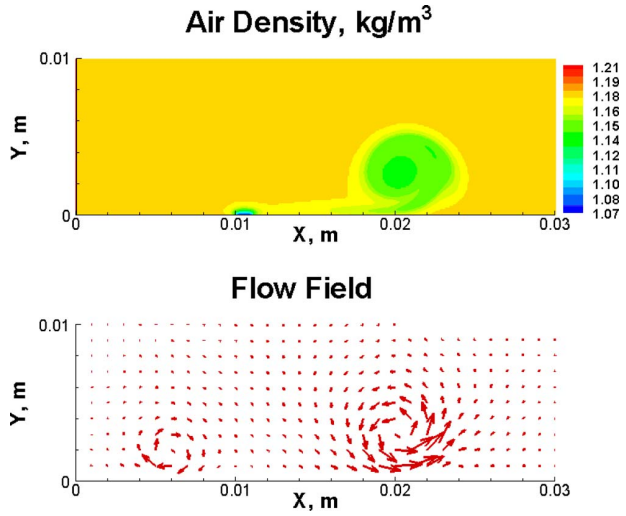

FIG. 8. (Color online) Air density and velocity distribution 14 ms after the burst.

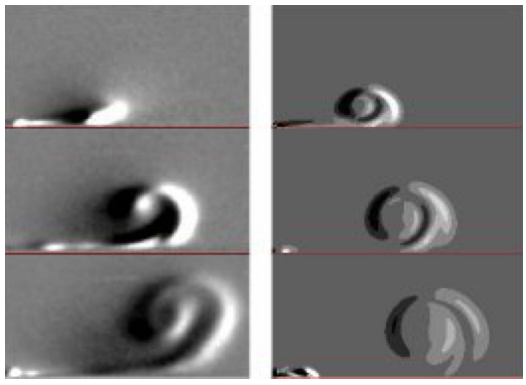

FIG. 9. (Color online) An example of experimental (left) and simulated (right) schlieren images of the DBD plasma jets. The images are 20 $\times$ 10 mm^2 each and correspond to 7, 14, and 21 ms after the burst start.

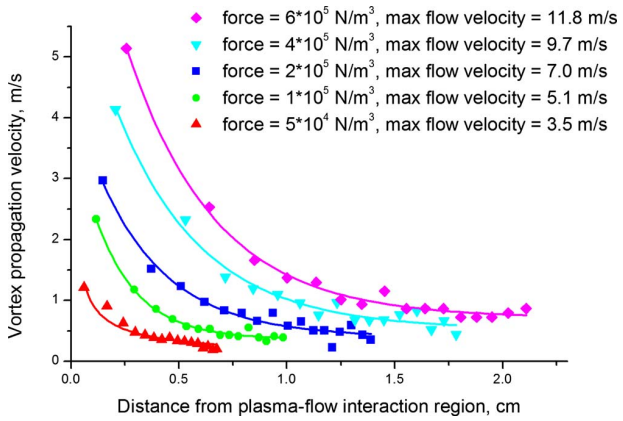

FIG. 10. (Color online) Vortex propagation velocity as a function of the distance from DBD at different forces in the interaction region. The maximum velocities of the induced flow at the vicinity of interaction region are designated as "max flow velocities."

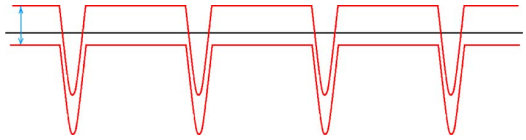

FIG. 11. (Color online) Varying the bias voltage in constant bias experiments. The pulse voltage is unchanged, thus change in bias voltage leads to the same change in the peak voltage.

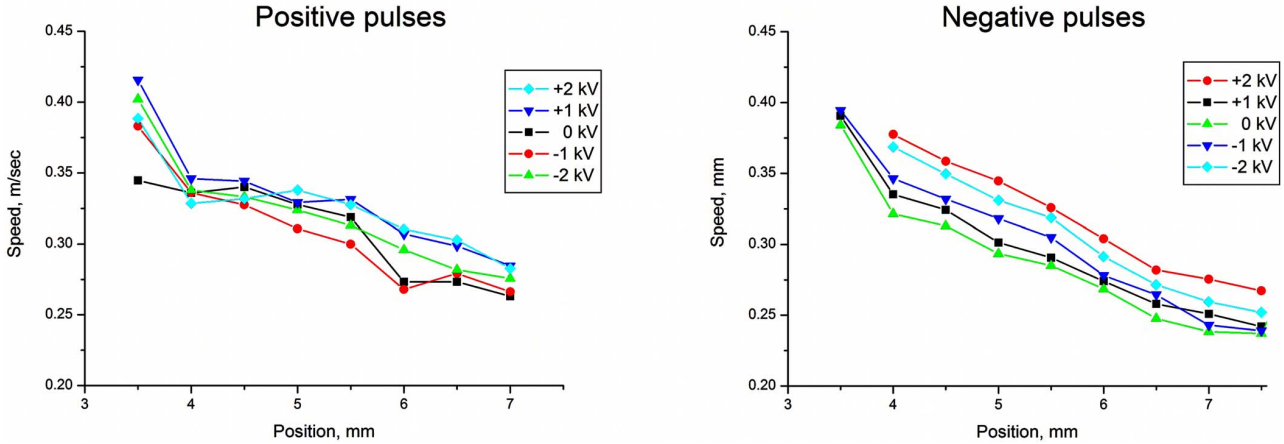

FIG. 12. (Color online) The induced flow speed vs distance at different constant bias voltages. The error bar is ~0.04 m/s.

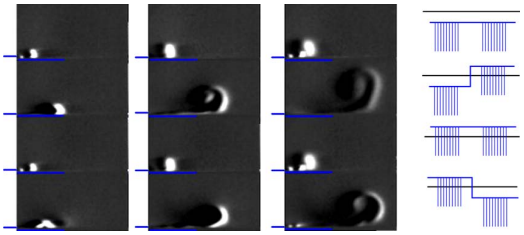

FIG. 13. (Color online) Bias voltage switch experiments. The columns represent images taken 7, 14, and 21 ms after the burst started. Different rows represent different bias profiles. The electrode arrangement is indicated. The results are presented for 5 kV negative pulses, 50 kHz, 50% duty cycle. The bias voltage was +/−2 kV. The view field is 20×10 mm^2.

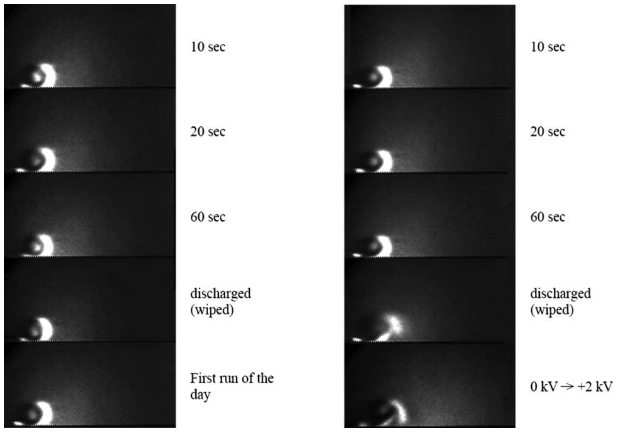

FIG. 14. Surface wipe experiments. The experiments were done for 0 kV (left column) and +2 kV (right column) bias voltages with 5 kV, 50 kHz, 50% duty cycle positive pulses and time delays of 10, 20, and 60 s. Wiped runs were done with 10 s time delay during which the charge was removed from the surface by a grounded wet cloth. The last picture in the left column shows the very first run of the day, when the surface was still charge-free. The last picture in the right column shows a bias switch experiment in which the bias voltage was changed from 0 to +2 kV. The images were taken 12 ms after the burst start. The field of view of each image is 20×10 mm^2.

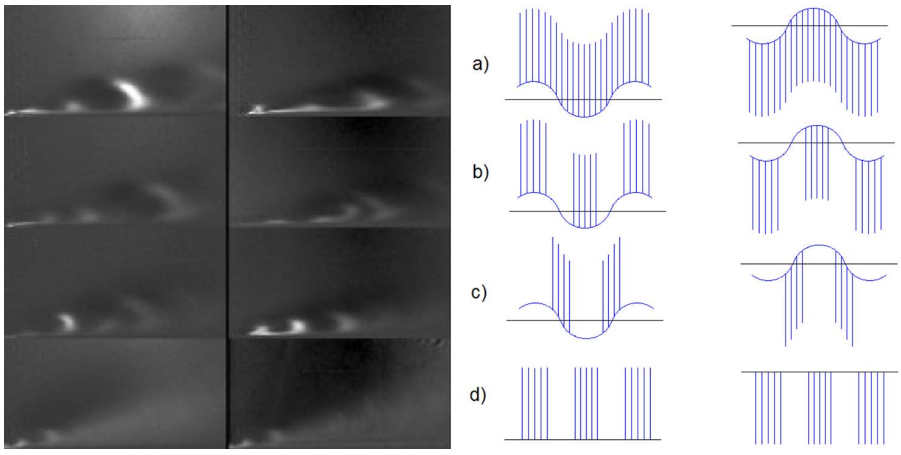

FIG. 15. (Color online) Nanosecond pulses combined with sinusoidal bias voltage. 5 kV, 50 kHz positive (left column) and negative (right column) pulses combined with 2.6 kV peak-to-peak 60 Hz sinusoidal bias voltage. The field of view of each image is 20×10 mm^2.

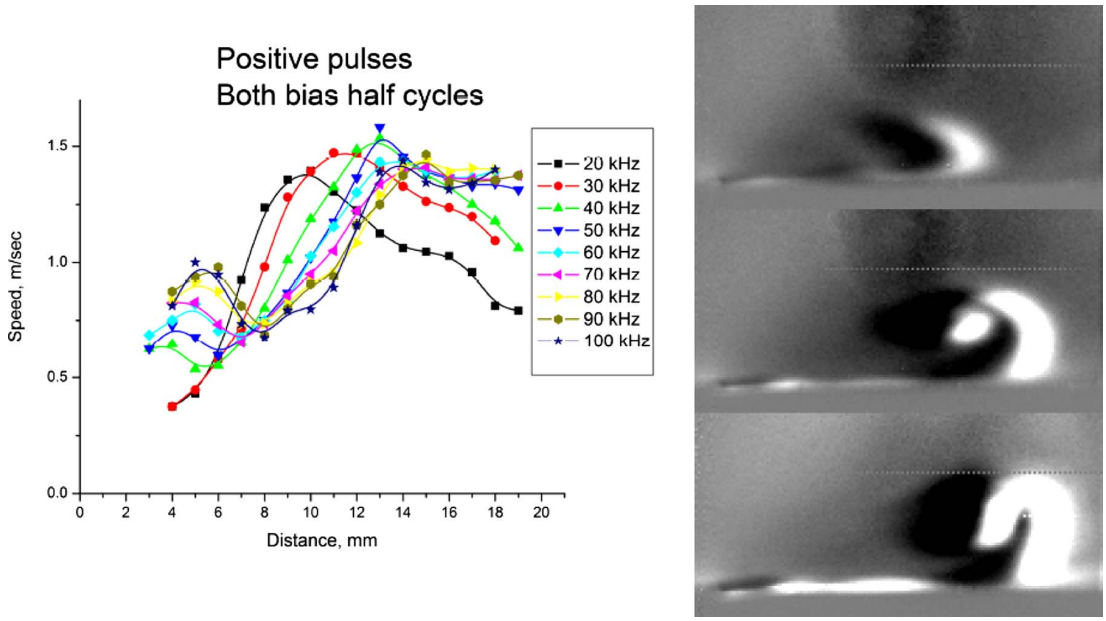

FIG. 16. (Color online) Vortex speed vs distance for different PRRs with positive polarity of the pulses. The schlieren images were taken at the same moment of time for 20, 50, and 100 kHz. A slow vortex is created by a jet from positive bias half-cycle, then from ~5–7 mm it is accelerated by a jet from the negative bias half-cycle burst. The field of view of each schlieren image is 20×10 mm^2.

The 2D Navier–Stokes equations were solved using second order accurate MacCormack scheme.[54] The computational domain was 5×2 cm^2. The time step was determined by the Courant-Friedrichs-Lewy (CFL) condition. The modeling has been performed for quiescent air at initial temperature of 300 K. The gas constants have been taken from Ref. 54. The dielectric surface temperature 1 mm downstream from the exposed electrode was considered to be 350 K. Several cases have been studied. We considered the plasma region to be 100×500 μm. The force on the gas was considered to act only in horizontal direction downstream and to be uniformly distributed in the interaction region. In the simulations, the force magnitude and heating in the interaction region were varied.

In the experiment the pulser was run in burst mode at 50 kHz PRR and 50% duty cycle, giving 10 ms bursts with 500 pulses in each burst every 20 ms. The pulse voltage was 5 kV. In addition 2 kV bias voltage was applied to the electrodes.

Consider the flow induced by the DBD plasma actuator in pulse-burst mode. When the DBD is on, the gas in the interaction region is being heated and receives momentum in the downstream direction (from left to right). The motion of the gas generates pressure gradient in the vicinity of interaction region. The gas is being sucked in that region from the left and from above, creating an upstream vorticity. At the same time another vortex is generated by the induced gas jet (Fig. 8). There are important differences between the two vortices. One of them is the sign of vorticity. The vorticities of upstream and downstream vortices are negative and positive, respectively. Another principal difference is the gas density in these vortices. The upstream vortex involves motion of the quiescent air at room temperature, thus its temperature is constant. In contrast, the downstream vortex is generated due to the motion of heated gas jet. Thus, it is characterized by well-defined temperature and density profiles. In the schlieren experiments on DBD induced flow, only density gradients can be visualized, i.e., the downstream vortex is observed and the upstream one is not detected. These results can be important in theoretical investigations of the flow separation control using DBD: the gas flow will interact not only with the observed downstream vortex but also with the "hidden" upstream one. Representative examples of such vortical structures, both experimental and reproduced in the numerical modeling, are shown in Fig. 9. By comparing the experimental and computational results, it was thus possible to reconstruct the entire evolving flow pattern and to infer both induced velocity field and the magnitude of plasma induced body force. For this example the motion of the vortex was around 0.5 m/s 17 mm downstream and that was driven by a surface jet with a velocity of 7 m/s in the plasma vicinity.

In our previous work[37–40] we calculated the integral momentum transferred to the gas by means of positive and negative nanosecond pulses with dc bias, as well as the heating rate in the interaction region. We have now extracted that data and used it as an input to the Navier–Stokes solver. An important assumption in the modeling was that there are no saturation effects due to surface charging. The pulser was considered to operate at 500 kHz repetition rate. The computed vortex propagation velocity as a function of distance from the exposed electrode is shown in Fig. 10. Taking the results for momentum transfer from Refs. 38 and 39 for positive 3 kV pulses (4 ns FWHM) with 1 kV dc bias and distributing it equally in the interaction region, we get the force in that region, 1.4×10^5 N/m^3. The numerical results for this calculation are between the green (round) and blue (square) data points in Fig. 10. The other curves correspond

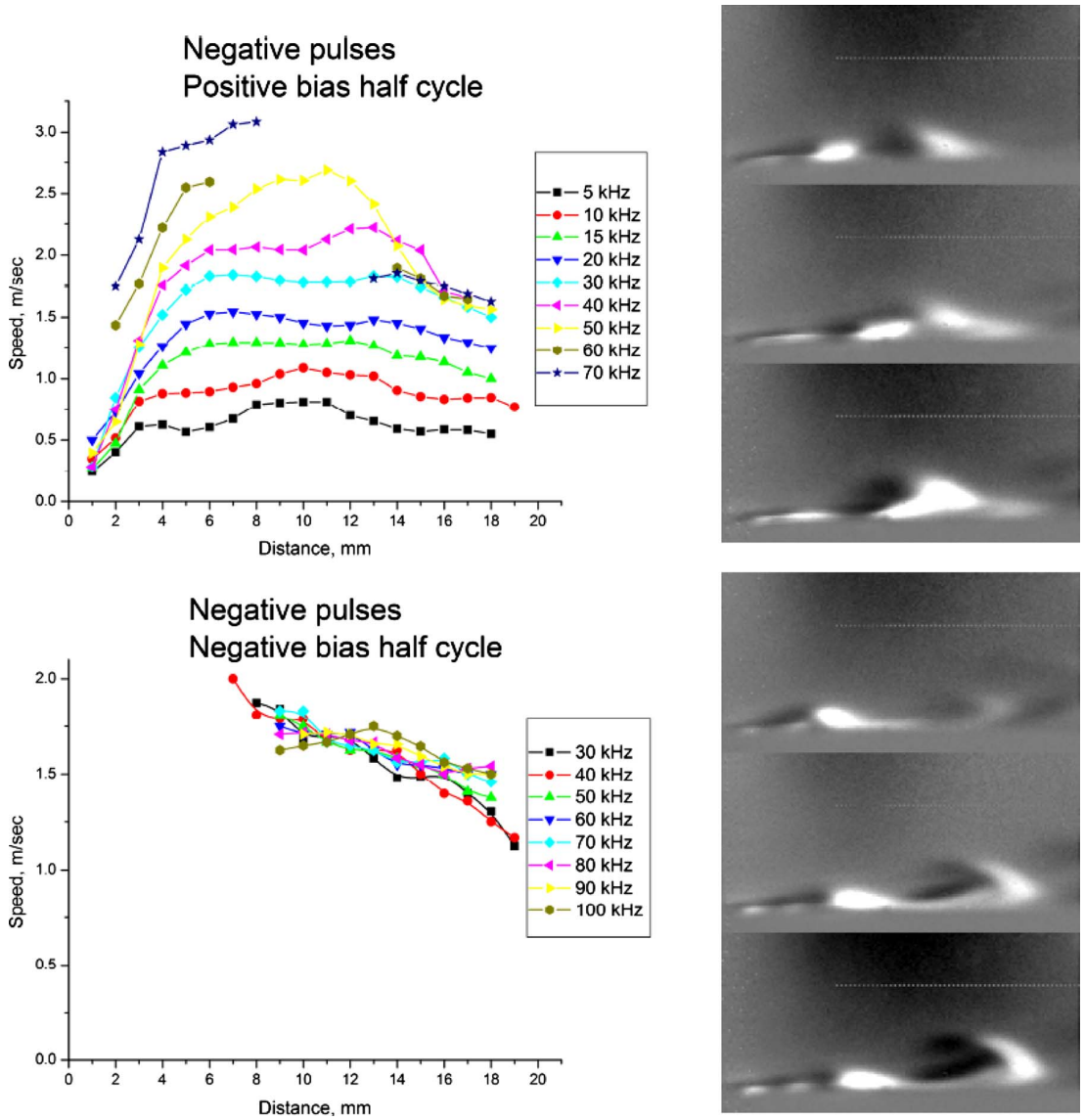

FIG. 17. (Color online) Vortex speed vs distance for different PRRs with negative polarity of the pulses. The schlieren images were taken at the same moment of time for 30, 50, and 70 kHz. In the bottom images, a vortex from the negative bias half-cycle is shown. The vortex consists of two parts: head vortex and tail vortex. In the top image, jet from positive bias half-cycle hitting the tail part of the negative vortex is shown. The speed of the positive vortex greatly depends on the PRR, while the speed of the negative one does not. The field of view of each schlieren image is 20×10 mm^2.

to the different force magnitudes in the interaction region at constant heating rate. It can be clearly seen that the translational vortex velocity significantly drops with the propagation along the surface. This fact is very important, since using the schlieren technique in the experiments we can extract the density gradients at several temporal points and thus determine the vortex propagation speed. The developed model thus allows inferring the induced flow velocity right at the edge of the plasma and the force magnitude in the interaction region by matching the experimental pictures with numerically obtained ones. The effect of heating was also investigated; however, the results showed that the vortex size has almost no dependence on the heating in the interaction region. Only the temperature of the gas within the vortex varies. Note that the gas temperature cannot be measured by the schlieren technique, and additional measurements with other techniques should be used to provide an additional insight into the plasma-flow interaction.

To examine experimentally how the actuator induced flow speed depends on the constant bias voltage, we ran experiments with fixed pulse voltage and different bias voltages, as shown in Fig. 11. The vortex translational speed versus coordinate at different bias voltages is shown in Fig. 12 for both polarities of the pulses. The experiments showed that in the case of negative pulses there is only a weak, within the error bars, dependence of the induced flow velocity on the bias voltage. Bias voltage of either polarity increased the induced jet speed only slightly. For the positive pulses, there was no clear dependence on the bias voltage. These results did not agree with the expectations based on

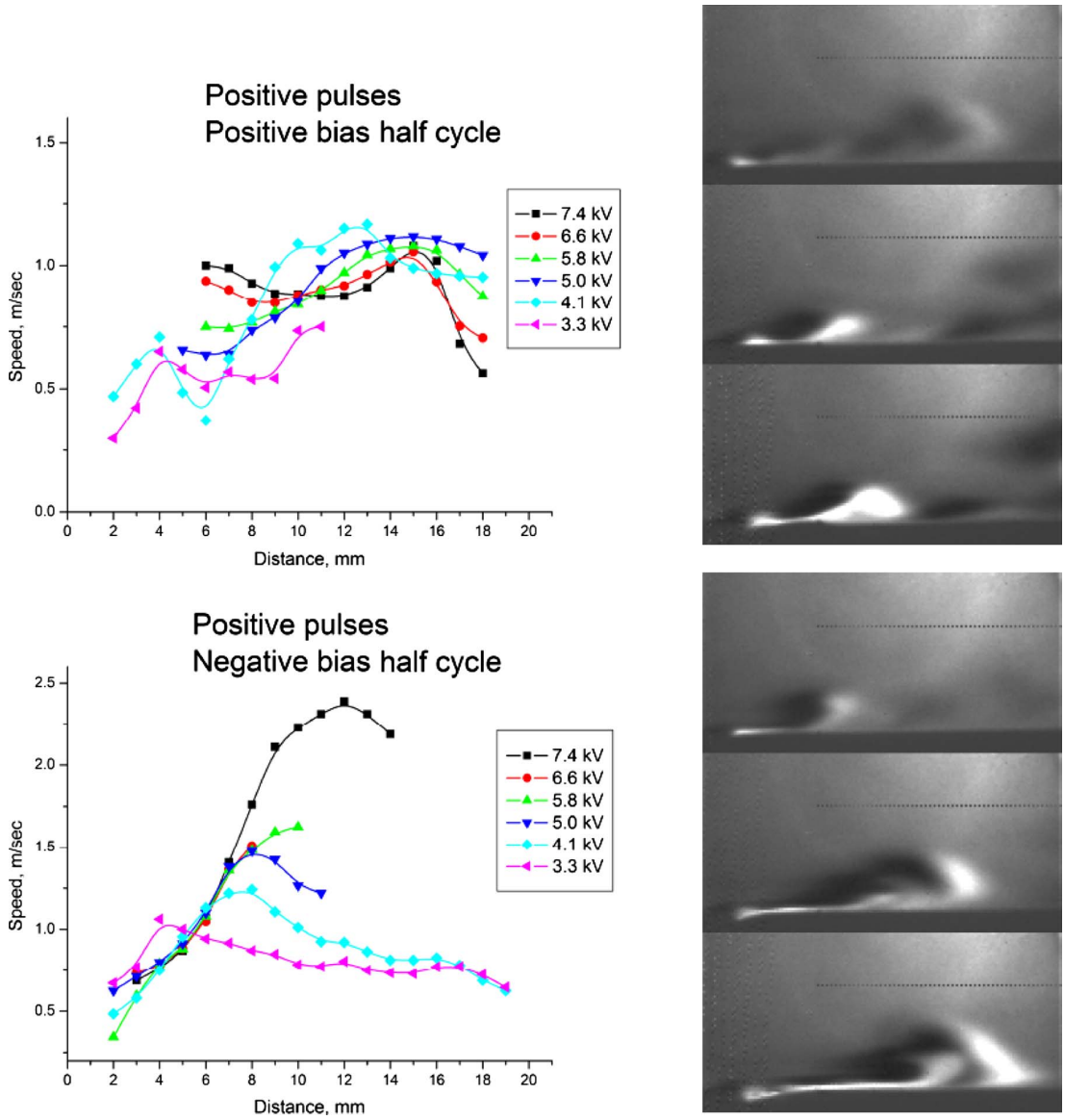

FIG. 18. (Color online) Vortex speed vs distance for different pulse voltages with positive polarity of the pulses. The schlieren images were taken at the same moment of time for 3.3, 5.0, and 7.4 kV. In the top images, slow jet from positive bias half-cycle is shown. In the bottom images, a vortex from the negative bias half-cycle is shown. The speed of this vortex is high and depends strongly on the pulse voltage. In the pictures for 5.0 and 7.4 kV, this vortex is colliding with the positive one. The field of view of each schlieren image is 20×10 mm^2.

the numerical plasma model that predicted significant increase in the induced flow velocity with the bias voltage.

However, during the experiment, an interesting phenomenon was noticed: a rapid switch of the bias polarity increased the jet velocity for the first several pulse bursts. To observe the details of the first vortices after the bias switch, the camera was triggered at the very beginning of every run so that it captured the first bursts. The actuator was thus run at some value of the bias voltage for 5 s, and then the pulses were turned off. After 10 s off, the pulses were turned on again, and the first burst of this second run was captured. This second run was done at either the same or a different value of the bias voltage compared to the first run. As in the previous experiments, the pulser was run in burst mode at 50 kHz PRR and 50% duty cycle, giving 10 ms bursts with 500 pulses in each burst every 20 ms. The pulse voltage was 5 kV, and the bias voltage was changed from −2 to +2 kV. The results are presented in Fig. 13. Columns represent images taken 7, 14, and 21 ms after the burst started. Different rows represent different biases. The electrode arrangement is indicated. The results show that switching the polarity of the bias voltage has a dramatic effect on the DBD operation: much faster jets and vortices are generated compared to the constant bias cases. An interesting feature can also be seen when switching from positive to negative bias. The induced wall jet from the first burst makes what looks like a jump. The jet created by the second burst, however, does not "jump" anymore. The location of the jump is around the region where the plasma ends. In the case of positive pulses, a similar jump can be observed when switching from nega-

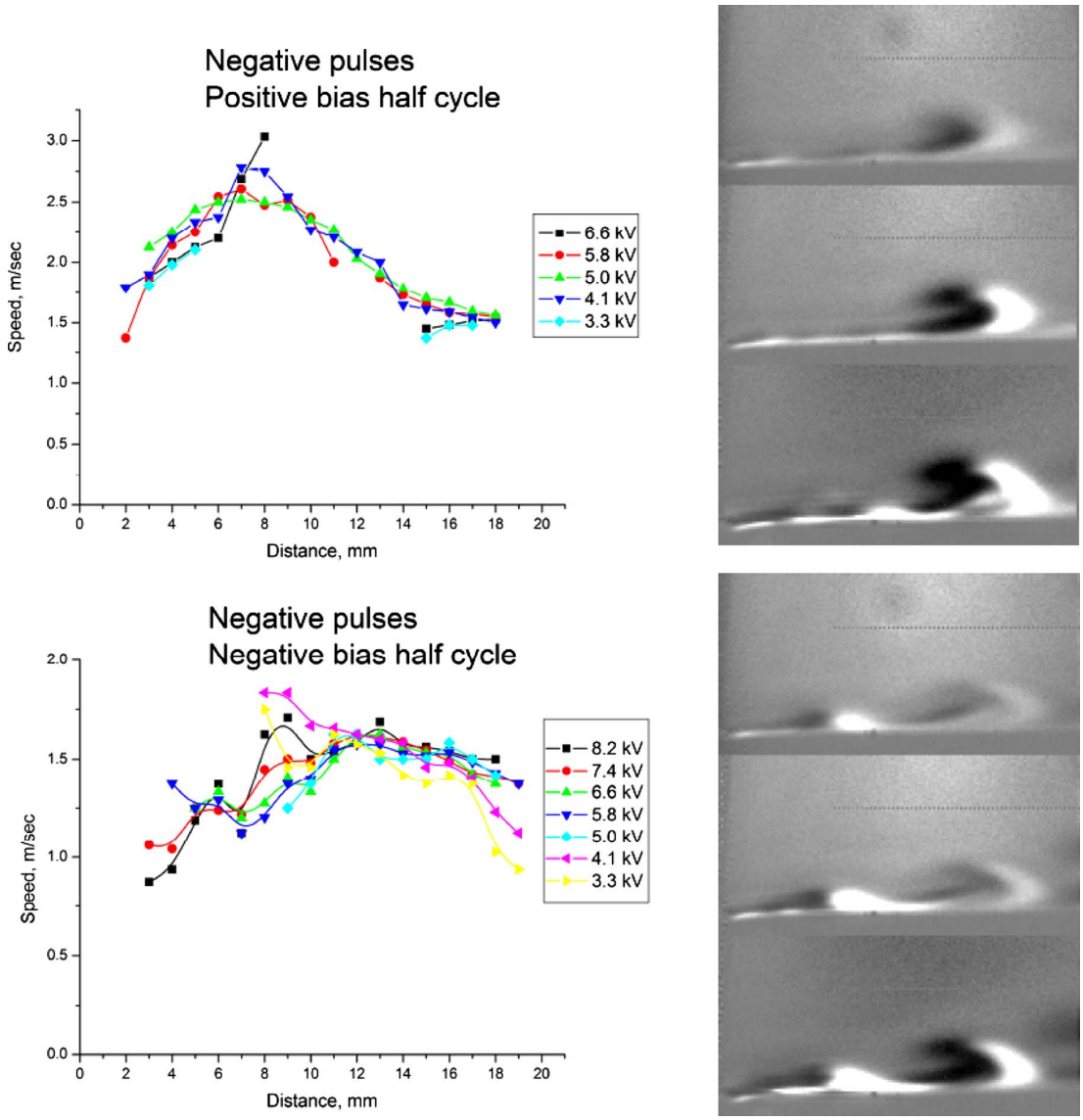

FIG. 19. (Color online) Vortex speed vs distance for different pulse voltages with negative polarity of the pulses. The schlieren images were taken at the same moment of time for 3.3, 5.0, and 7.4 kV. In the top images, jet from positive bias half-cycle is shown. In the bottom images, a jet from the negative bias half-cycle is shown, consisting of two parts: head vortex and tail vortex. There is no dependence of the speed of the vortices on the pulse voltage. The field of view of each schlieren image is 20×10 mm^2.

tive to positive bias voltage. In addition, in that case the second vortex also "jumps." The same behavior was observed during switches from −2 to 0, 0 to −2, 0 to +2, and +2 to 0 kV for both polarities of the pulses. However, the jet velocity increase and the jump were not as strong as in the cases of switching between negative and positive polarities of the bias voltage.

Likely explanation for the observed behavior is accumulation of surface charge on the dielectric. During the run, the dielectric surface is charged, and shielding of the applied bias electric field occurs, reducing the force on the gas and the jet velocity. This explains why in the first series of experiments the effect was determined by the difference between the peak voltage and the bias voltage and not so much by the peak voltage or the bias voltage separately. Switching the polarity of the bias removes the surface charge and enhances the actuator performance for a short time, until the surface charge builds up again. One reason for the jump behavior could be an interaction of residual space charge with the surface charge. More studies are needed to better understand these phenomena.

To check if there really is a surface charge accumulated on the dielectric, the next set of experiments was conducted. The conditions were similar to the previous experiments. First the actuator was run for 5 s. Then after some time being off it was run again *without* switching the bias voltage. The first burst of the second run was captured. The aim was to see how the generated vortex depends on the time delay between the runs. The experiments were done for −2, 0, and +2 kV bias voltages with 5 kV, 50 kHz, 50% duty cycle positive pulses and time delays of 10, 20, and 60 s. Another run was done with 10 s time delay during which the charge

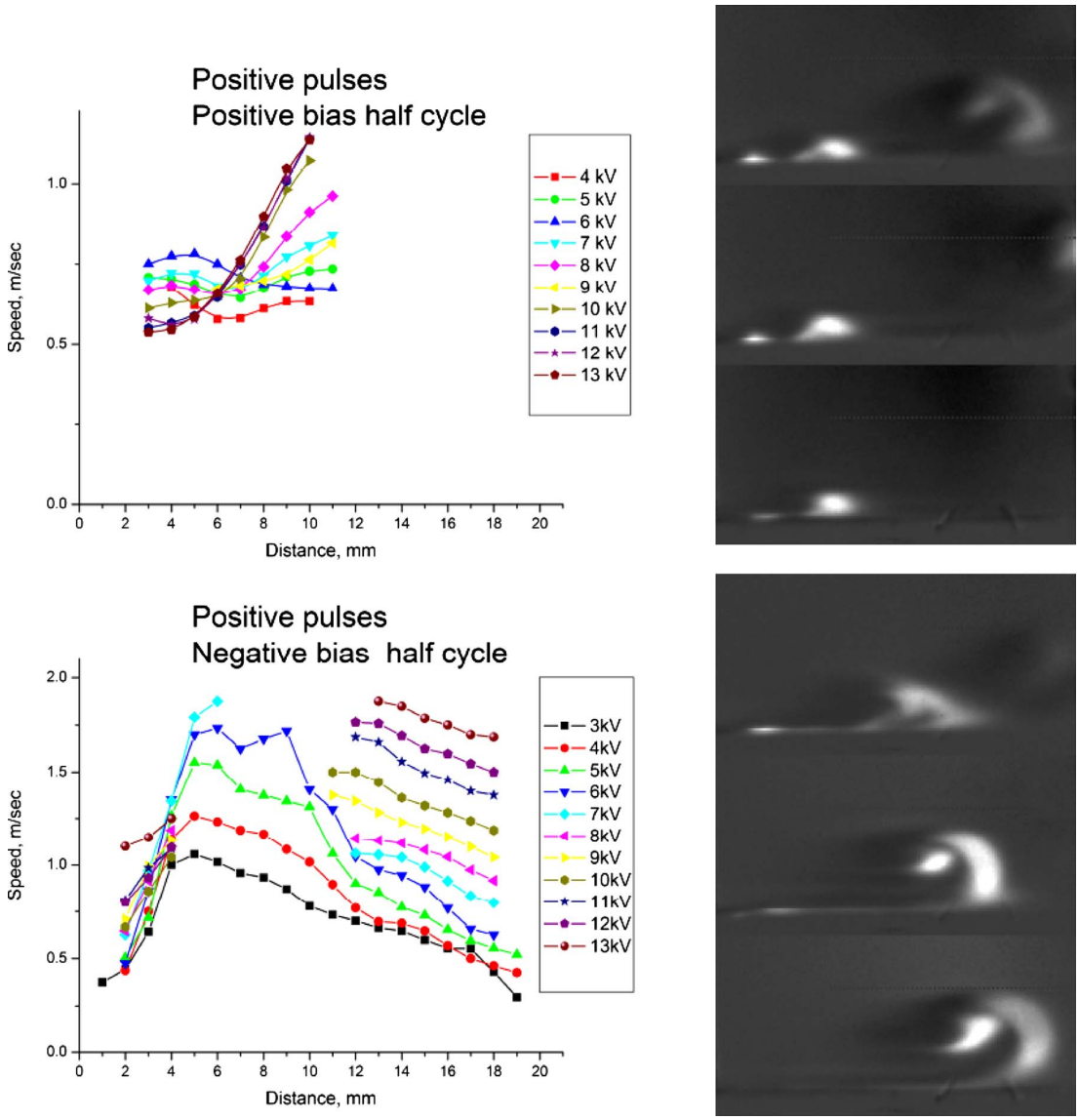

FIG. 20. (Color online) Vortex speed vs distance for different peak-to-peak sinusoidal bias voltages with positive polarity of the pulses. The schlieren images were taken at the same moment of time for 5, 10, and 13 kV. In the top images, a slow jet from positive bias half-cycle is shown; when a strong jet from the negative half-cycle arrives, it pushes the positive jet forward, which explains the acceleration in 6–11 mm range. In the bottom images, a vortex from the negative bias half-cycle is shown. Its speed is high and strongly depends on the pulse voltage. In the pictures for 5.0 kV, the collision is still in progress, which explains the complex shape of the vortex. The field of view of each schlieren image is 20×10 mm^2.

was removed from the surface. The surface charge removal was done with a wet grounded cloth. The water provided a good contact with the entire surface, and after a wipe the surface was slightly wet and quickly dried out by itself. The whole procedure took less then 10 s at the end of which the surface was dry and discharged. (Wiping the surface with a dry cloth to remove the water might lead to charging through friction). The results are presented in Fig. 14. It is seen that the vortex-generating performance persists for the times up to 1 min. If the observed behavior was due to some heating effects, there would not have been such a long hysteresis as 1 min. This provides evidence in favor of the surface charge. Also the wiped-surface runs with bias look like a switch from zero bias voltage. This shows that the effect does occur due to the surface charge which depends on the bias voltage. It can be seen that the vortex is very similar to the one from the wiped-surface run, which means that both the wipe and the run at 0 kV bias voltage discharge the surface. Again it can be seen that the surface charge shields the applied bias voltage. However, if the surface charge is removed, the plasma feels the bias voltage, but only until new charge builds up on the dielectric surface.

It was not possible to conduct similar experiments with the negative pulses. As mentioned above, the bias voltage was applied to the same electrode as the pulses, i.e., for the negative pulses that would be the exposed electrode. Manually wiping the surface to remove the charge in the close vicinity of the electrode at a few kilovolts potential would be unsafe.

Since the jet-enhancement effect disappears as soon as

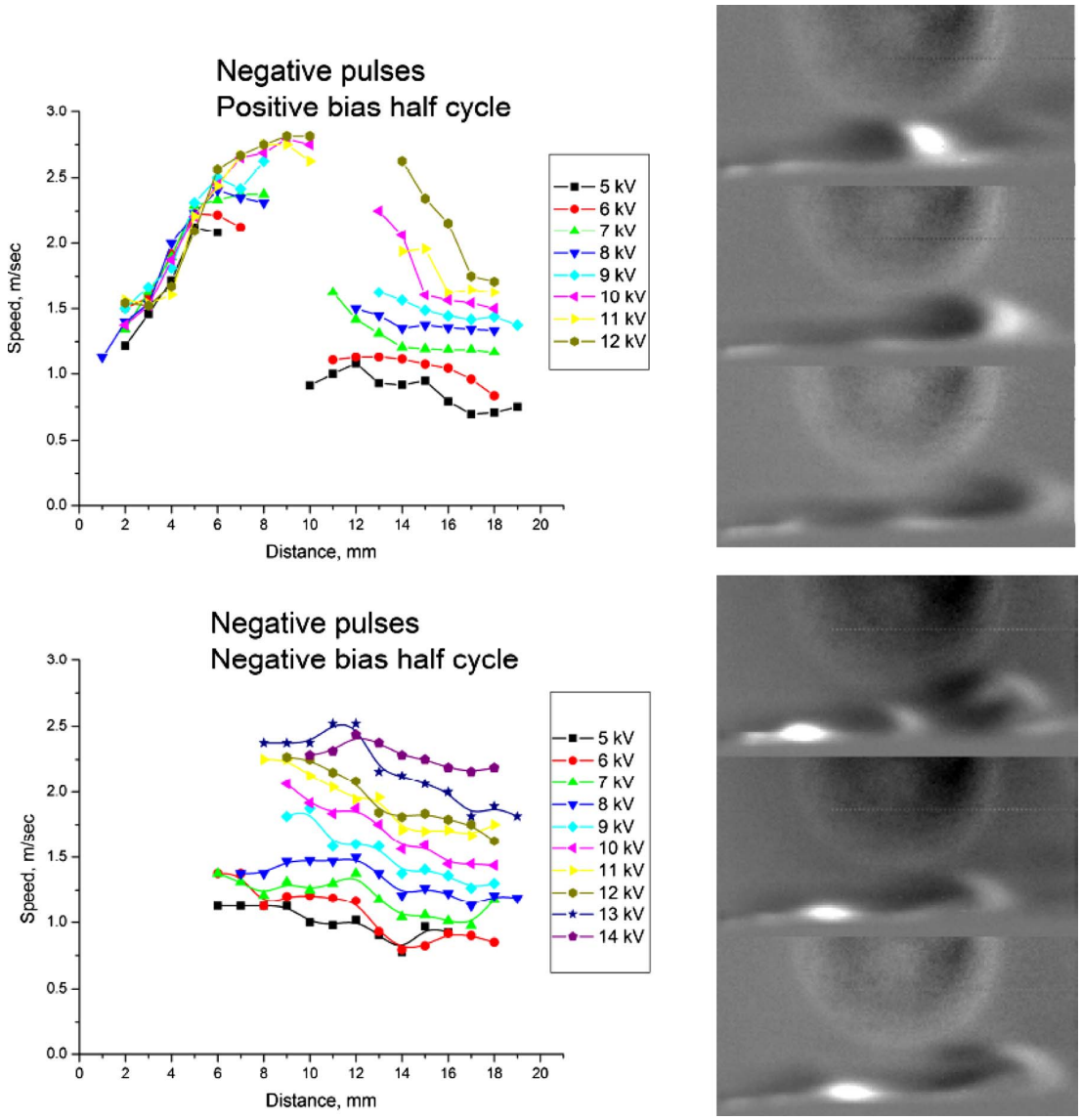

FIG. 21. (Color online) Vortex speed vs distance for different peak-to-peak sinusoidal bias voltages with negative polarity of the pulses. The schlieren images were taken at the same moment of time for 5, 10, and 13 kV. In the top images, jet from positive bias half-cycle is shown. The vortex speed strongly depends on the negative pulse voltage. The field of view of each schlieren image is 20×10 mm^2. The circle in the images is due to water condensation in the camera.

the charge builds up on the dielectric and shields the bias field, to let the effect go on continuously, one needs to keep switching the bias. Thus, a new voltage waveform was used in the subsequent experiments: high-voltage sinusoidal signal (2.6 kV peak to peak, 60 Hz) plus nanosecond pulses (50 kHz, 5 kV, positive or negative). Three versions of the voltage waveform were examined: (a) 100% duty cycle pulses +sinusoidal bias voltage, (b) 50% duty cycle pulses, bursts near the peak of the sinusoidal voltage+sinusoidal bias voltage, and (c) 50% duty cycle pulses, bursts at the slopes of the sinusoidal voltage+sinusoidal bias voltage, and were compared with the pulses without any bias voltage: (d) 50% duty cycle pulses with no bias.

Since this set of experiments involved 60 Hz sinusoidal signal, a new modulation of the pulses had to be used. The pulses were generated in bursts with 208 pulses per burst and 120 bursts per second. The results are presented in Fig. 15.

From the experimental results we can see that the sinusoidal bias significantly improves the actuator performance. The jet speed increases from ~30 cm/s near the discharge in case (d) to ~80 cm/s at 10 mm downstream in case (a). Thus, even a relatively low bias voltage (1.3 kV amplitude comparing to 5 kV of the pulses) has a great effect on the DBD actuator operation. Note that the bias voltage itself could not ignite the plasma in the absence of the pulses. Also, vortices are still observed in case (a) despite the fact that the pulses are on all the time. This means that the in-

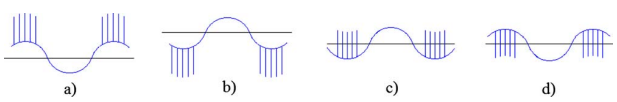

FIG. 22. (Color online) Voltage profiles with pulses near the bias voltage peaks of one polarity only.

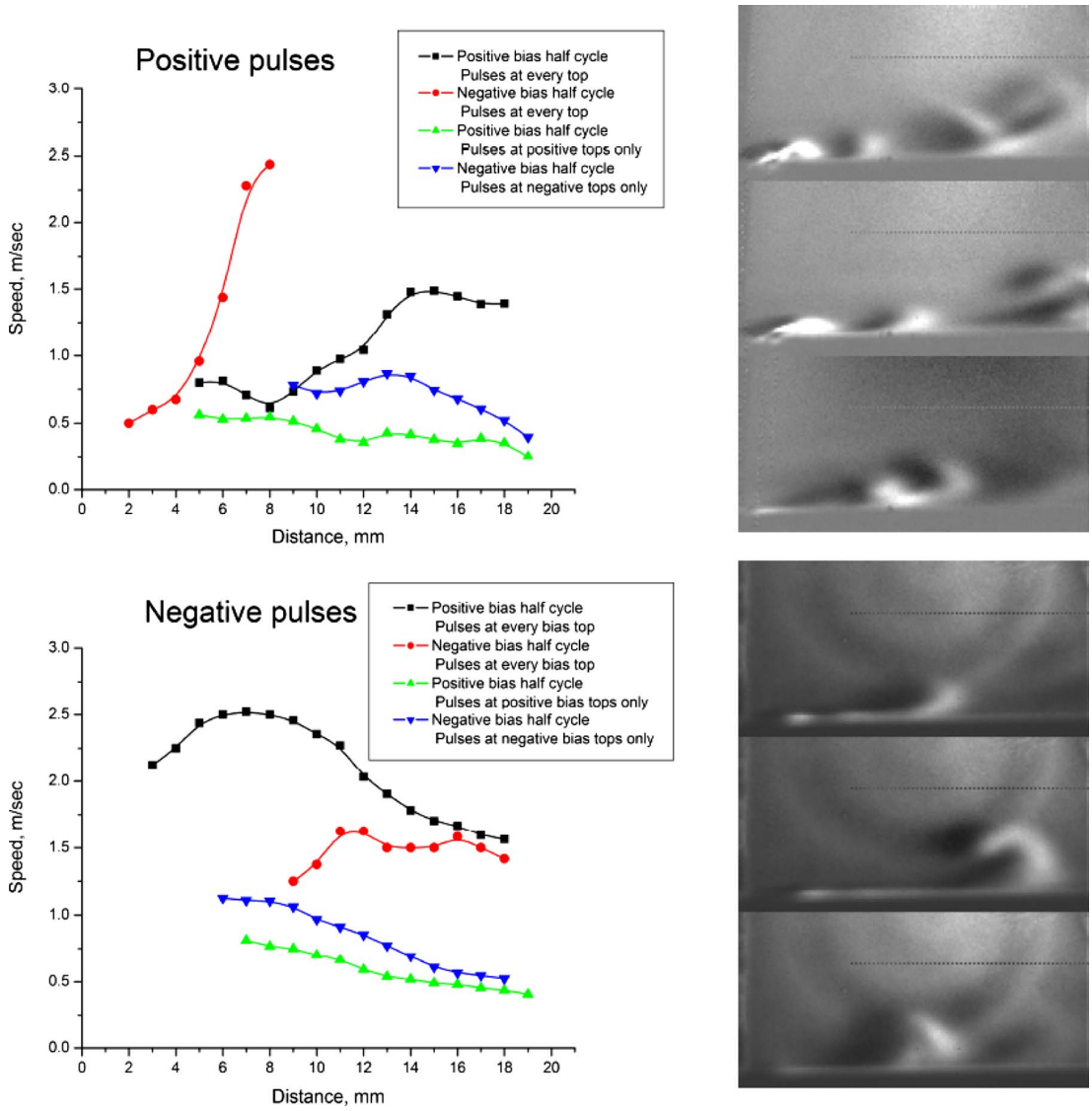

FIG. 23. (Color online) Vortex speed vs distance for different voltage waveforms, see Fig. 20. The schlieren images were taken at the same moment of time for pulses during negative half-cycle only, both half-cycles, and positive half-cycle only. The field of view of each schlieren image is 20×10 mm^2.

duced wall jet speed strongly depends on instantaneous bias voltage as well as on the surface charge on the dielectric. In addition, vortices coming out of different bursts, i.e., of bursts at different bias voltages, are different. The vortex speed and size depend on whether it was generated during positive/negative bias/slope of the bias voltage.

For further investigation we selected voltage waveform with pulses near the peaks of the bias voltage, since this waveform was more effective than the one with the pulse bursts at the bias voltage slopes. Additionally, with this waveform, it can be determined unambiguously which burst the vortex came from, which makes the data easier for interpretation.

DBD actuator operation dependence on the new voltage waveform parameters was investigated. As a baseline voltage waveform, we chose 5 kV pulses at 50 kHz and 50% duty cycle near the peaks of 10 kV peak-to-peak 60 Hz sinusoidal bias voltage. Then varying one of the parameters at a time (the bias voltage, pulse voltage, and repetition rate) we observed the vortices for each polarity of the pulses. As mentioned above, the vortices coming out of different bias half-cycles differ in speed and size. Thus plots for both kinds of vortices are presented in the figures when possible.

Consider first the actuator performance dependence on PRR for positive pulses (Fig. 16). The vortex coming out of the positive bias half-cycle is slow. It does not move far away from the plasma region by the time the next vortex appears. The next vortex, which comes out of the negative bias have-cycle, is very fast. It actually does not evolve into a vortex immediately; it is still in its jet phase and thus is hard to notice. Then, upon collision with the earlier generated slow vortex, it also becomes a vortex. Thus, actually there is only one vortex in the schlieren image at a time. As seen in Fig. 16, there is some weak dependence on the PRR.

The dependence of vortex parameters on PRR for negative pulses (Fig. 17) is different. The vortices created during

the negative bias half-cycles consist of two parts. The head part is not observed for pulses repetition rate lower than 30 kHz. Its speed is relatively high and does not depend on the PRR. The tail part is brighter and much slower. The vortex created during positive bias half-cycle is faster. Its speed strongly depends on the PRR, as seen in Fig. 17.

The next parameter varied in the experiments was the pulse voltage. The results for the positive pulses are presented in Fig. 18. The speed of positive (i.e., generated during the positive half-cycle of the bias voltage) vortices weakly depends on the pulse voltage. However, their brightness (temperature) strongly depends on the pulse voltage. The pulse voltage has a dramatic effect on the speed of negative (i.e., generated during the negative half-cycle of the bias voltage) vortices. For the negative polarity of the pulses, the vortex speed is quite high, and the only effect of the higher pulse voltage is stronger heating. The details are shown in Fig. 19.

Among all the parameters, the sinusoidal bias voltage has perhaps the strongest influence on the DBD plasma actuator operation. The results for the positive pulses are presented in Fig. 20. Again, positive vortices are rather slow, and it is unclear if changing the bias voltage has any effect on them because they propagate only several millimeters before the vortices from the negative bias half-cycles hit them from behind. The speed of vortices from the negative half-cycles depends strongly on the bias voltage. For negative pulses, the increase in bias voltage leads to a significant increase in effect in both half-cycles of the bias voltage. The results are presented in Fig. 21.

Starting from 5 kV peak-to-peak bias voltage, self-sustained discharge was ignited in the absence of the high-voltage pulses. This discharge could remove the surface charge by itself. Since positive pulses create a strong force on the gas only during the negative bias half-cycle, it was interesting to check if it is still important to have pulse bursts during the positive half-cycle of the bias. Thus experiments were run with the pulses during half-cycles of one polarity only. The voltage waveforms are shown in Fig. 22. The results of the experiments are shown in Fig. 23. It can be seen that in the absence of the pulse burst during the other half-cycle, the induced wall jet speed becomes two to three times lower in all cases. This means that although some of the pulse bursts do not create a strong wall jet, they still play an important role in the DBD operation. Their task is to discharge/recharge the dielectric surface and thus to increase the efficiency of the other bursts. The experiments also clearly show that the wall jets induced by negative pulses evolve into two-vortex formations, whereas the ones from the positive pulses do not. The mechanism of this behavior should be investigated in future studies.

V. CONCLUSIONS

We have used a burst mode of plasma actuator operation in conjunction with nonintrusive schlieren diagnostic of the actuator induced flows in quiescent gas. With this technique, the DBD actuator was observed to generate periodic pulsed wall jets that evolve into vortices, and parametric studies of the vortex speed and size versus parameters of the waveform (pulses in repetitive-burst mode plus dc or ac bias voltage) were performed. Matching 2D numerical fluid modeling to the experimental results allowed us to infer the magnitude of plasma-generated body force exerted on the gas. The knowledge of the body force magnitude can then be used to compute the entire flow field in both burst and continuous modes of plasma actuator operation.

The experiments showed that although repetitive short pulses do efficiently generate the plasma, a dc bias voltage cannot push the gas efficiently because the charge buildup on the dielectric surface shields the applied dc electric field.

To remove the surface charge, periodic switching of the bias voltage polarity is required. Thus, we proposed a new voltage waveform, consisting of high-voltage nanosecond repetitive pulses superimposed on a high-voltage low frequency sinusoidal or square-wave bias voltage.

The advantages of the new voltage waveform in significantly enhancing the wall jets and the vortices have been demonstrated experimentally.

Note that in conventional DBD actuators driven by sinusoidal voltages, ionizing pulses (streamer breakdowns) also occur, but the magnitude and frequency of those ionizing pulses depend entirely on the parameters of the sinusoidal driving voltage. In contrast, we proposed and used what is essentially non-self-sustained discharge: the plasma is generated by repetitive short pulses, and the pushing of the gas occurs primarily due to the low frequency (bias) voltage. The advantage of this non-self-sustained discharge is that the parameters of ionizing pulses and the driving bias voltage can be varied independently, which adds flexibility to control and optimization of the actuator performance.

Future work should involve investigation of different dielectric surfaces (due to the importance of surface charge buildup) and parametric studies of the induced flow velocity versus frequency of the sinusoidal bias voltage. Nonsinusoidal bias voltage waveforms should also be investigated.

ACKNOWLEDGMENTS

This work was supported in part by NASA Glenn Research Center (Dr. David Ashpis), in part by the Air Force Office of Scientific Research (Dr. John Schmisseur). Fellowship support for one of the authors (A.V.L.) was provided by Princeton Program in Plasma Science and Technology.

[1] S. O. Macheret, M. N. Shneider, and R. B. Miles, AIAA J. **42**, 1378 (2004).
[2] S. O. Macheret, M. N. Shneider, R. B. Miles, and R. J. Lipinski, AIAA J. **39**, 1127 (2001).
[3] S. O. Macheret, M. N. Shneider, and R. B. Miles, AIAA J. **40**, 74 (2002).
[4] S. O. Macheret, M. N. Shneider, and R. B. Miles, J. Propul. Power **18**, 424 (2002).
[5] M. N. Shneider, S. O. Macheret, and R. B. Miles, AIAA J. **42**, 2303 (2004).
[6] S. O. Macheret, M. N. Shneider, and R. B. Miles, 34th AIAA Plasmadynamics and Lasers Conference, Orlando, FL, 23–26 June 2003, (unpublished), Paper No. AIAA-2003-3763.
[7] R. C. Murray, L. Vasilyak, M. R. Carraro, S. H. Zaidi, S. O. Macheret, M. N. Shneider, and R. B. Miles, 42nd Aerospace Sciences Meeting and Exhibit, Reno, NV, 5–8 January 2004 (unpublished), Paper No. AIAA-2004-1025.
[8] S. O. Macheret, M. N. Shneider, and G. V. Candler, 42nd Aerospace

Sciences Meeting and Exhibit, Reno, NV, 2004 (unpublished), Paper No. AIAA 2004-1024.
[9]M. N. Shneider and S. O. Macheret, 35th AIAA Plasmadynamics and Lasers Conference, Portland, OR, 2004 (unpublished), Paper No. AIAA-2004-2662.
[10]M. N. Shneider and S. O. Macheret, 43rd AIAA Aerospace Sciences Meeting and Exhibit, Reno, NV, 10–13 January 2005 (unpublished), Paper No. AIAA-2005-0979.
[11]R. B. Miles, S. O. Macheret, M. N. Shneider, C. Steeves, R. C. Murray, T. Smith, and S. H. Zaidi, 43rd AIAA Aerospace Sciences Meeting and Exhibit, Reno, NV, 10–13 January 2005 (unpublished), Paper No. AIAA-2005-0561.
[12]A. L. Kuranov and E. G. Sheikin, 40th AIAA Aerospace Sciences Meeting and Exhibit, Reno, NV, 14–17 January 2002 (unpublished), Paper No. AIAA-2002-0490.
[13]A. Vatazhin, V. Kopchenov, and O. Gouskov, Third AIAA Weakly Ionized Gases Workshop, Norfolk, VA, 1–5 November 1999, Paper No. AIAA-1999-4972.
[14]V. A. Bityurin, A. I. Klimov, S. B. Leonov, A. N. Bocharov, and J. T. Lineberry, Third AIAA Weakly Ionized Gases Workshop, Norfolk, VA, 1–5 November 1999 (unpublished), Paper No. AIAA-1999-4820.
[15]M. Nishihara, N. Jiang, J. W. Rich, W. R. Lempert, I. V. Adamovich, and S. Gogineni, Phys. Fluids **17**, 106102 (2005).
[16]M. Nishihara, J. W. Rich, W. R. Lempert, I. V. Adamovich, and S. Gogineni, Phys. Fluids **18**, 086101 (2006).
[17]D. Gaitonde, 43rd AIAA Aerospace Sciences Meeting and Exhibit, Reno, NV, 10–13 January 2005 (unpublished), Paper No. AIAA-2005-560.
[18]S. T. Surzhikov and J. S. Shang, 43rd AIAA Aerospace Sciences Meeting and Exhibit, Reno, NV, 10–13 January 2005 (unpublished), Paper No. AIAA-2005-0406.
[19]S. T. Surzhikov and J. S. Shang, J. Comput. Phys. **199**, 437 (2004).
[20]S. T. Surzhikov and J. S. Shang, 42nd Aerospace Sciences Meeting and Exhibit, Reno, NV, 5–8 January 2004 (unpublished), Paper No. AIAA-2004-0508.
[21]S. T. Surzhikov and J. S. Shang, High Temp. **43**, 19 (2005).
[22]R. Kimmel, J. Hayes, J. Menart, and J. S. Shang, 42nd Aerospace Sciences Meeting and Exhibit, Reno, NV, 5–8 January 2004 (unpublished), Paper No. AIAA-2004-0509.
[23]J. Poggie, 35th AIAA Plasmadynamics and Lasers Conference, Portland, OR, 28 June–1 July 2004 (unpublished), Paper No. AIAA-2004-2858.
[24]J. S. Shang, R. Kimmel, J. Hayes, C. Tyler, and J. Menart, J. Spacecr. Rockets **42**, 780 (2005).
[25]J. S. Shang and S. T. Surzhikov, AIAA J. **43**, 1633 (2005).
[26]J. Menart, J. Shang, C. Atzbach, S. Magoteaux, M. Slagel, and B. Bilheimer, 43rd AIAA Aerospace Sciences Meeting and Exhibit, Reno, NV, 10–13 January 2005 (unpublished), Paper No. AIAA-2005-947.
[27]S. B. Leonov, D. A. Yarantsev, V. G. Gromov, and A. P. Kuriachy, 43rd AIAA Aerospace Sciences Meeting and Exhibit, Reno, NV, 10–13 January 2005 (unpublished), Paper No. AIAA-2005-0780.
[28]S. O. Macheret, 44th AIAA Aerospace Sciences Meeting and Exhibit, Reno, NV, 9–12 January 2006 (unpublished), Paper No. AIAA-2006-1005.
[29]S. H. Zaidi, T. Smith, S. O. Macheret, and R. B. Miles, 44th AIAA Aerospace Sciences Meeting and Exhibit, Reno, NV, 9–12 January 2006 (unpublished), Paper No. AIAA-2006-1006.
[30]C. L. Enloe, T. E. McLaughlin, R. D. VanDyken, K. D. Kachner, E. J. Jumper, and T. C. Corke, AIAA J. **42**, 589 (2004).
[31]C. L. Enloe, T. E. McLaughlin, R. D. VanDyken, K. D. Kachner, E. J. Jumper, T. C. Corke, M. Post, and O. Haddad, AIAA J. **42**, 595 (2004).
[32]M. Post and T. C. Corke, 35th AIAA Fluid Dynamics Conference and Exhibit, Toronto, Ontario, 6–9 June 2005 (unpublished), Paper No. AIAA-2005-4630.
[33]T. C. Corke, E. J. Jumper, M. L. Post, D. Orlov, and T. E. McLaughlin, 40th AIAA Aerospace Sciences Meeting and Exhibit, Reno, NV, 14–17 January 2002 (unpublished), Paper No. AIAA-2002-350.
[34]M. L. Post and T. C. Corke, AIAA J. **42**, 2177 (2004).
[35]D. F. Opaits, D. V. Roupassov, S. M. Starikovskaia, A. Yu. Starikovskii, I. N. Zavialov, and S. G. Saddoughi, 43rd AIAA Aerospace Sciences Meeting and Exhibit, Reno, NV, 10–13 January 2005 (unpublished), Paper No. AIAA-2005-1180.
[36]D. Opaits, A. Likhanskii, M. Shneider, G. Neretti, S. Zaidi, S. Macheret, and R. Miles, 38th AIAA Plasmadynamics and Lasers Conference, Miami, Florida, 25–28 June 2007 (unpublished), Paper No. AIAA-2007-4532.
[37]A. Likhanskii, M. Shneider, S. Macheret, and R. Miles, 44th AIAA Aerospace Sciences Meeting and Exhibit, Reno, Nevada, 9–12 January 2006 (unpublished), Paper No. AIAA-2006-1204.
[38]A. Likhanskii, M. Shneider, S. Macheret, and R. Miles, 45th AIAA Aerospace Sciences Meeting and Exhibit, Reno, NV, 10–13 January 2007 (unpublished), Paper No. AIAA-2007-633.
[39]A. Likhanskii, M. Shneider, S. Macheret, and R. Miles, Phys. Plasmas **14**, 073501 (2007)
[40]A. Likhanskii, M. Shneider, D. Opaits, S. Macheret, and R. Miles, 38th AIAA Plasmadynamics and Lasers Conference, Miami, Florida, 2007 (unpublished), Paper No. AIAA-2007-4533.
[41]C. Enloe, T. McLaughlin, G. Font, and J. Baughn, 44th AIAA Aerospace Sciences Meeting and Exhibit, Reno, NV, 2006 (unpublished), Paper No. AIAA-2006-166.
[42]S. Leonov, D. Yarantsev, and A. Kuriachy, 43rd AIAA Aerospace Sciences Meeting and Exhibit, Reno, NV, 2005 (unpublished).
[43]R. Sosa, E. Arnaud, and G. Artana, International Simposium on Electrohydrodonamics (ISEHD), Buenos Aires, Argentina, 2006 (unpublished).
[44]T. Jukes, K. Choi, G. Johnson, and S. Scott, Third AIAA Flow Control Conference, San Francisco, CA, 2006 (unpublished), Paper No. AIAA-2006-3693.
[45]A. M. Konchakov, V. M. Krivtsov, S. B. Leonov, V. R. Soloviev, and D. A. Yarantsev, preprint of Institute of High Temperature RAS 2-491, 2006 (unpublished).
[46]G. I. Font, S. Jung, C. L. Enloe, T. E. McLaughlin, W. L. Morgan, and J. W. Baughn, 44th AIAA Aerospace Sciences Meeting and Exhibit, Reno, NV, 2006 (unpublished), Paper No. AIAA-2006-167.
[47]M. R. Visbal and D. V. Gaitonde, 44th AIAA Aerospace Sciences Meeting and Exhibit, Reno, NV, 2006 (unpublished), Paper No. AIAA-2006-505.
[48]M. R. Visbal, D. V. Gaitonde, and S. P. Gogineni, 29th Fluid Dynamics Conference, Albuquerque, NM, 1998 (unpublished), Paper No. AIAA-1998-2643.
[49]S. Gogineni, M. Visbal, and C. Shih, Exp. Fluids **27**, 126 (1999).
[50]S. Gogineni, M. Visbal, and C. Shih, 35th AIAA Aerospace Sciences Meeting and Exhibit, Reno, NV, 1998 (unpublished), Paper No. AIAA-1997-0071.
[51]J. R. Roth, D. M. Sherman, and S. P. Wilkinson, 36th AIAA Aerospace Sciences Meeting and Exhibit, Reno, NV, 1998 (unpublished), Paper No. AIAA-1998-0328.
[52]G. S. Settles, *Schlieren and Shadowgraph Techniques* (Springer, NY, 2001).
[53]G. A. Mesiats, S. A. Nasibov, and V. V. Kremnev, *Formirovanie Nanosecundnih Impulsov Visokogo Napriazhenia* (Energia, Moscow, 1970) (in Russian).
[54]D. A. Anderson, J. C. Tannehill, and R. H. Pletcher, *Computational Fluid Mechanics and Heat Transfer* (Hemisphere, New York, 1984).

JOURNAL OF APPLIED PHYSICS **103**, 053305 (2008)

Modeling of dielectric barrier discharge plasma actuator in air

Alexandre V. Likhanskii,[1,a)] Mikhail N. Shneider,[2] Sergey O. Macheret,[3] and Richard B. Miles[2]
[1]*Department of Engineering Science and Mechanics, The Pennsylvania State University, University Park, Pennsylvania 16802, USA*
[2]*Department of Mechanical and Aerospace Engineering, Princeton University, Princeton, New Jersey 08544, USA*
[3]*Lockheed Martin Aeronautics Company, Palmdale, California 93599, USA*

(Received 24 January 2007; accepted 29 November 2007; published online 11 March 2008)

A detailed physical model for asymmetric dielectric barrier discharge (DBD) in air at low voltages (1.5–2 kV) is developed. Modeling of DBD with an applied sinusoidal voltage is carried out in two dimensions. The leading role of charging the dielectric surface by electrons in the cathode phase is shown to be critical, acting as a harpoon that pulls positive ions forward and accelerates the gas in the anode phase. The positive ion motion back toward the exposed electrode is shown to be a major source of inefficiency in the sinusoidal or near-sinusoidal voltage cases. Based on understanding of the DBD physics, an optimal voltage waveform is proposed, consisting of high repetition rate, short (a few nanoseconds in duration), negative pulses combined with a positive dc bias applied to the exposed electrode. © *2008 American Institute of Physics*. [DOI: 10.1063/1.2837890]

I. INTRODUCTION

Plasma and magnetohydrodynamic (MHD) devices can potentially be used for internal and external flow control and power extraction (Refs. 1–37, and references therein). Body forces can be exerted by electric and magnetic fields on charged species (electrons and ions) and coupled to the bulk gas by collisions. These forces can then be used to extract power or to control the flow. Plasma-induced gas heating can also modify the flow (Refs. 1–26, and references therein). Both body forces and heating can be used as virtual shapes for flow control in the absence of moving parts (Refs. 1–27, and references therein). There is also an increasing interest in near-surface plasmas with and without magnetic field to control both laminar and turbulent boundary layers, shock-boundary layer interactions, and particularly flow separation. Air Force Research Laboratory researchers (Kimmel, Shang *et al.*) studied dc surface plasmas in a Mach 5 tunnel.[16–26] Leonov *et al.* at the Institute of High Temperatures (Moscow, Russia) investigated flow control with high-current quasi-equilibrium surface arcs.[27] Adamovich *et al.* at the Ohio State University has demonstrated MHD effects on the supersonic turbulent boundary layer[15] and flow deceleration by Lorentz force.[16] Recently, the Princeton University group has proposed and demonstrated cold (nonequilibrium) constricted surface discharges ("snowplow arcs") that are magnetically driven downstream or upstream at high velocity and impart momentum to the boundary layer.[11,28,29] All those studies were devoted to high-speed, supersonic, or hypersonic flow control.

Significant and impressive experimental results have been obtained by Corke and colleagues at Notre Dame University and the U.S. Air Force Academy,[30–34] and by Starikovskii *et al.*[35] in Russia on the use of asymmetric dielectric barrier discharges (DBD) for low-speed separation control. Despite the successful demonstration of DBD plasma actuators for flow control and the seeming simplicity of DBD devices, the fundamental understanding of the underlying physics of their operation is still incomplete. It is accepted that the experimentally observed near-surface gas acceleration to several meters per second is due to the transfer of momentum from ions which are accelerated by the electric field to the bulk gas molecules.

Challenges in modeling and understanding DBD plasma actuators stem from the physics of the problem. Generation, decay, drift, and diffusion of electrons and both positive and negative ions must be correctly described by the model and resolved by the numerical scheme. Since it is the electric space charge that is responsible for the net force acting on the gas, the Poisson equation for the electric potential must be fully coupled with the other equations. The processes on both dielectric and metallic surfaces, such as attachment of electrons to the dielectric surface and the secondary electron emission from both metallic and dielectric surfaces, must be included. Additional complexity is due to the high gas density (about 1 sea-level atmospheric density) at which DBD actuators operate. This high density reduces both time and length scales relevant to the problem. For example, avalanche ionization and sheath formation occur on a subnanosecond time scale, and sharp gradients of the electric field and net charge density occur on a micron length scale. At the same time, the model should also be able to compute the plasma dynamics and kinetics on macroscopic time (milliseconds) and length (millimeters or centimeters) scales.

Because of this complexity, several recent modeling efforts[38–42] did not capture some essential features of kinetics and dynamics of asymmetric DBD plasmas. The first attempts at DBD modeling were performed in Refs. 38–42. However, the modeled regimes did not explain the observed experimental results. Reference 41 shows the relevant plasma kinetics and discharge development, but lacks the

a)Electronic mail: alikhans@princeton.edu.

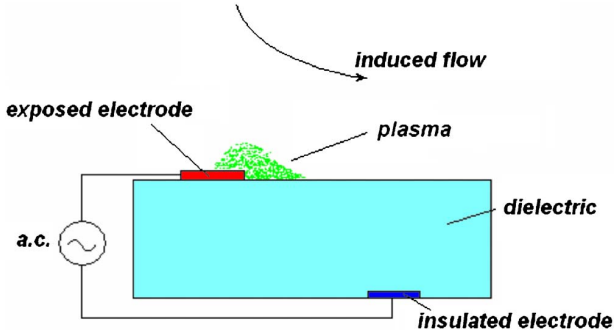

FIG. 1. (Color online) Asymmetric dielectric barrier discharge configuration.

modeling of voltages used in DBD operation. The empirical results, based on the DBD experiments, are shown in Ref. 42. But, this model has not resolved the processes in plasma. All previous plasma modeling has been done in inert gases, which did not allow an explanation of the features of DBD operation, experimentally observed in air. For example, the fact of DBD operation in "push-push" mode in a negative half-cycle for sinusoidal voltages can be explained only by the presence of negative ions, which are not present in inert gases plasmas.

Therefore, it is necessary to develop a consistent, comprehensive, and physically based model that would qualitatively and quantitatively explain the operation of dielectric barrier plasma actuators. This paper describes the successful development of such a model. The ultimate goal of the model development is to find a way of improving the DBD actuator performance.

II. THE MODEL

The asymmetric DBD plasma actuator[30–34] consists of two electrodes separated by a dielectric layer (Fig. 1). The lower electrode is covered by the dielectric and is grounded, and the voltage is applied to the upper (exposed) electrode. The electrodes are shifted with respect to each other (thus, the term "asymmetric"). Near the right edge of the upper electrode the plasma is created, and according to the experimental data[30–34] the gas is pushed from left to right.

The modeling was performed for air. The weakly ionized air plasma was modeled as a four-fluid mixture: neutral molecules, electrons, and positive and negative ions. Note that the presence of negative ions in air (unlike the models for inert gases or pure nitrogen) is quite important for understanding of DBD physics, as will be shown later in this paper. The motion of the charged particles was considered in the drift-diffusion approximation. We denote the number densities of electrons, positive and negative ions, and neutrals as n_e, n_+, n_-, and n fluxes as $\Gamma_e, \Gamma_+, \Gamma_-$. The rate of ionization is α, rates of electron-ion and ion-ion recombination are β and β_{ii}, the rate of electron detachment from negative ions is k_d, the rate of electron attachment to the neutrals is υ_a, electron and ion diffusion coefficients and mobilities are D_e, D_i and μ_e, μ_i, correspondingly; the thermodiffusion relation is k_t.

The continuity equations for electrons, positive and negative ions are then

$$\frac{\partial n_e}{\partial t} + \nabla_j \Gamma_{ej} = \alpha|\Gamma_e| - \beta n_e n_+ + k_d n n_- - \nu_a n_e, \tag{1}$$

$$\frac{\partial n_+}{\partial t} + \nabla_j \Gamma_{+j} = \alpha|\Gamma_e| - \beta n_e n_+ - \beta_{ii} n_+ n_-, \tag{2}$$

$$\frac{\partial n_-}{\partial t} + \nabla_j \Gamma_{-j} = -\beta_{ii} n_+ n_- - k_d n n_- + \nu_a n_e, \tag{3}$$

where

$$\Gamma_{ej} = -\mu_e E_j n_e - D_e \nabla_j n_e - k_t D_e n_e \frac{\nabla_j T_e}{T_e}, \tag{4}$$

$$\Gamma_{+j} = \mu_i E_j n_+ - D_i \nabla_j n_+, \tag{5}$$

$$\Gamma_{-j} = -\mu_i E_j n_- - D_i \nabla_j n_-. \tag{6}$$

Since the gas velocity is low in comparison with the drift velocities of charged particles, for plasma behavior calculations the gas was considered stationary. Ionization and recombination coefficients, as well as attachment, detachment rates, charged particles mobilities, and electron temperature are considered as functions E/n, where E is the local electric field .The numerical values for the rate of ionization, electron-ion recombination, ion-ion recombination, ion mobilities, attachment and detachment rates are standard and given in Refs. 43–45. The ion temperature is considered to be equal to the gas temperature. Electron drift velocities V_{dr} and electron temperatures, as functions E/N, are given in Ref. 46. The electron mobilities are calculated using the following relation:

$$\mu_e = \frac{V_{\mathrm{dr}}}{E}. \tag{7}$$

The diffusion coefficients are calculated using the Einstein relation,

$$D_i = \mu_i T_i, \tag{8}$$

where i denotes the species (electrons, ions).

The boundary conditions at the electrode surface are, for the cathode,

$$\Gamma_{en} = -\gamma_m \Gamma_{+n}, \tag{9}$$

and, at the anode,

$$\Gamma_{+n} = 0. \tag{10}$$

And, the boundary conditions at the dielectric surface are

$$\Gamma_{en} = -\gamma_d \Gamma_{+n}, \quad \text{if } E_n < 0, \tag{11}$$

and

$$\Gamma_{+n} = 0, \quad \text{if } E_n > 0. \tag{12}$$

Here, γ_m and γ_d are the effective secondary emission coefficients from metal and dielectric.

The electric field and potential are related to the density of charged species according to the Poisson equation,

$$\nabla(\varepsilon \nabla \varphi) = e(n_e + n_- - n_+), \tag{13}$$

$$E_j = -\nabla_j \varphi. \tag{14}$$

The volumetric force on neutral gas can be generally expressed the following way:[41]

$$F = e(n_+ - n_- - n_e)E + \left(m_e\mu_e\frac{dn_e}{dt} - m_+\mu_+\frac{dn_+}{dt} + m_-\mu_-\frac{dn_-}{dt}\right)E - \nabla(n_e kT_e + n_+ kT_+ + n_- kT_-). \tag{15}$$

For the simulations, the following geometry was chosen. The problem is considered two-dimensional, corresponding to the plane of Fig. 1. The electrodes are considered infinitely thin. This is justified, since a number of experiments performed with both slightly protruding and buried electrodes showed no considerable difference in DBD actuator performance.[30–34] The sizes of the electrode was from 0.1 to 1.5 mm, depending on the plasma length at different voltage profiles. The cell size for the rectangular grid was chosen according to the characteristic plasma and voltage scales and geometrical sizes. Since the maximum charge density in the DBD plasma was found to be on the order of 10^{21} – 10^{22} m^{-3}, and the applied voltage is on the order of kilovolts, the voltage drop on the order of several volts (much less than the applied voltage) corresponds to the cell size on the order of 1–10 microns. It also explains the computational difficulties of DBD numerical simulation in large scales. Note that the maximum cell size should be the same even as the size of DBD plasma is increased, in order to resolve the relevant plasma dynamics, and increasing the geometrical size would increase the number of computational points.

Two different numerical schemes were used in DBD plasma kinetics modeling. For low voltages, a second-order explicit McCormack scheme[47] was able to resolve all physical processes. Using this scheme the low-voltage sinusoidal case and low-voltage repetitive negative nanosecond pulses were calculated. Some "wrinkles" on the presented figures are due to dispersion of this numerical scheme. However, for higher voltages this scheme could not resolve some plasma phenomena, such as streamer propagation and back breakdown, due to the scheme dispersion. The Scharfetter-Gummel[48,49] method resolved these problems and the high-voltage case was modeled using this scheme.

The successive over-relaxation method[47] was used to solve the Poisson equation. One of the difficulties in kinetic simulations is the choice of time step. In the plasma modeling in this work, two parameters determine it. First, the time step should allow the resolution of plasma formation and sheath dynamics time (which is of the order of nanoseconds), and second, the time step should satisfy the CFL (Courant-Friedrichs-Lewy) condition. The combination of these two requirements leads to the time step of the order of picoseconds. In the modeling, the time step was recalculated on each step according to the CFL condition and was from 1 to 10 picoseconds.

The complexity of the stated problem, such as resolution of micron geometrical scales, picosecond time scale for the nonlinear problem with particle generation, and the necessity to compute the micro- to milliseconds time intervals and the geometrical scales of the order of millimeters, sets some limitations on the model for single-processor calculations. First of all the model is two-dimensional. This fact does not allow resolution of the 3D filament structures, experimentally observed in DBD investigations. However, due to overlapping of the streamers, the plasma becomes of diffusion form, making the 2D assumption work quite well. Another issue is that the 2D modeling qualitatively explains many DBD features, but it would be better to compare the 2D calculations with 3D ones, done on a multiprocessor cluster, in order to verify the code. The second limitation is the geometrical and the time domain of the problem. Usually in the modeling the size of the domain was 1 by 1 mm and the computational time was several microseconds. The payoff for increasing either the geometrical or time domain to experimental sizes was the decrease in the remaining domain. Another issue is the range of applied voltages. The higher the voltages applied, the smaller the grid should be. The decrease of the grid size twice leads to the 8-times increase of the computational times. The model allowed calculations for the peak voltages up to 3–4 kV. The above listed issues can be possibly resolved using parallel computations, on which our group is currently working.

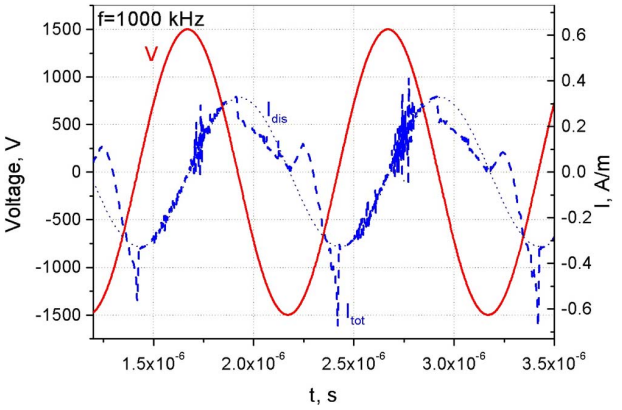

FIG. 2. (Color online) Applied voltage and calculated current for 1.5 kV, 1000 kHz sinusoidal voltage. Red line shows the voltage shape, dashed blue line the calculated total current, and dotted line the displacement current.

III. LOW-VOLTAGE SINUSOIDAL SIGNAL

In a number of experiments,[27,30–34] the sinusoidal shape of the applied voltage on the exposed electrode was used as a baseline. In order to understand the physics of DBD plasmas and the nature of the force exerted on the gas in those experiments, a series of computations with small-scale geometry (several hundred microns, see Sec. II) and high ac frequency (1000 kHz) was performed. The small scales allow DBD simulations to be performed in a reasonable time while showing the essential physics. However, it is very important to compare the results with those obtained with larger plasma sizes in order to understand the scaling issues.

Figure 2 shows the applied voltage and calculated total and displacement currents in a representative case with small plasma size and sinusoidal voltage. During the negative half-

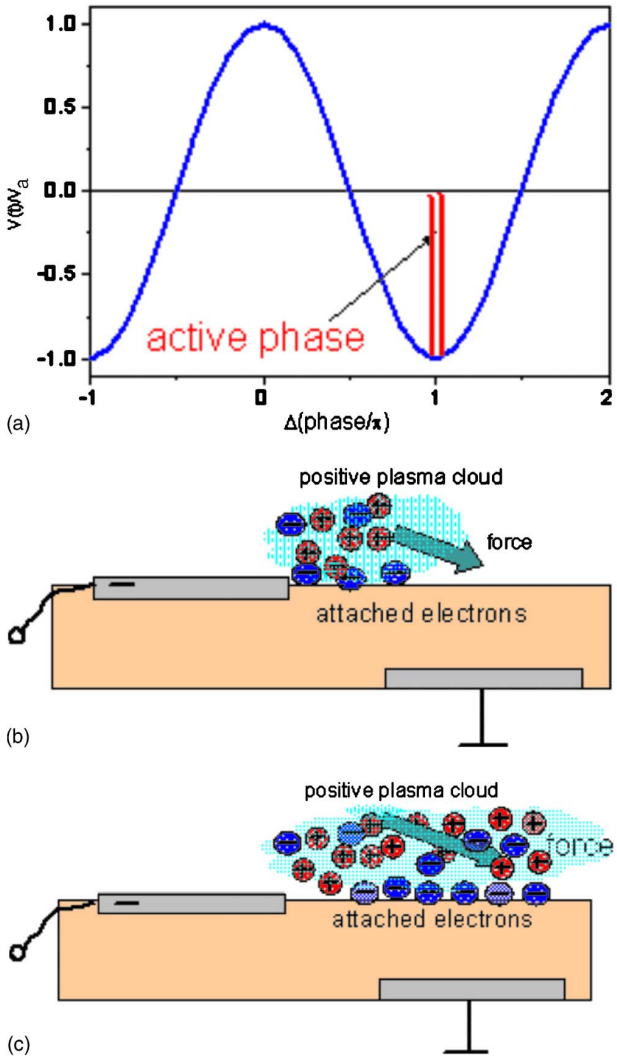

FIG. 3. (Color online) Negative half-period: (a) sine voltage waveform with short active phase; (b) illustration of processes during the active phase (avalanche breakdown of the gas, charging of the dielectric surface, and propagation of the plasma); (c) illustration of processes during the decaying phase (positive space charge, ions drift toward the surface and away from the exposed electrode, imparting momentum to the gas and recombining with electrons deposited on the dielectric surface).

cycle, the difference between the total and displacement currents is due to the breakdown. In the positive half-cycle the difference can be explained by the motion of both negative ions and the secondary electrons (emitted from the dielectric surface) to the exposed anode.

Consider separately two half-cycles of sinusoidal-voltage DBD operation.

A. Negative half-cycle

During the first half of the negative half-cycle (the exposed electrode is negative, its potential is decreasing, and the covered electrode is grounded), the breakdown starts when the instantaneous voltage reaches its critical value. If the amplitude of the applied voltage is not very high, the plasma development starts near the voltage peak, as shown in Figs. 3(a) and 3(b). Electrons are generated at the cathode surface due to the secondary emission, and avalanche ionization then occurs in the strong electric field. Being light and fast, electrons separate from positive ions and attach to the dielectric surface, leaving behind a cloud of positive ions. Some electrons, i.e., those at the front and upper edges of the plasma, attach to oxygen and form negative ions [Fig. 3(b)]. The plasma thus propagates along the surface and negatively charges the surface during the propagation (Fig. 4). The propagation stops and the current is cut off when the negative potential on the dielectric surface becomes sufficiently high, so that the difference in potential of the exposed electrode and the dielectric falls below the critical breakdown value.

Increasing the applied voltage amplitude increases the duration of this active phase, and also allows the plasma to propagate farther along the surface. Under typical conditions, the active (avalanche) phase duration is on the order of 100 ns (for small-scale actuator) to about 1 microsecond (for a large-scale device), much shorter than the half-cycle of the applied voltage. Therefore, during most of the negative half-period, no avalanche ionization occurs, and the plasma is decaying. During this part of the cycle the negative ions push the gas to the right (downstream), while the cloud of positive ions is attracted to the exposed electrode and pushes the gas upstream and down, toward the surface (Fig. 5).

Since the magnitude of the negative potential on the dielectric surface is always somewhat lower than the peak negative potential on the exposed electrode-cathode, the positive ion cloud always moves toward the cathode, creating the backward-directed force on the gas and reducing the efficiency of generation of downstream-directed gas jet. Moreover, in the computations for small-scale DBD actuator, this backward motion of ions was found to be strong enough to cause the overall negative (backward-directed) force during the cathode half-period.

However, when the length scale of the plasma was increased (the streamwise length of the electrode was increase by a factor of 7, to several millimeters), the voltage amplitude increased to 3.5 kV, and the ac frequency decreased by a factor of 10, then the reversal of the integrated force in the cathode phase was reached. This is due to the fact that the backward-directed force caused by the positive ions moving to the cathode was found to vary only slightly with the scaling, while the downstream-directed force caused by the negative ions increases with the increase in plasma size and voltage amplitude. Consequently, the integrated force is now directed downstream (Fig. 6), as observed in the experiments.[26,29–33]

Therefore, three factors are especially important in understanding why the force on the gas is directed downstream even if the exposed electrode is at a negative potential: (i) the charging of dielectric surface by the attached electrons; (ii) the formation of negative ions and their motion; and (iii) the relatively large scale of DBD actuators. It is also important to note that the attraction of positive ions to the exposed electrode in the cathode phase significantly reduces (if not reverses) the overall average force that pushes the gas. This is a major source of inefficiency of plasma actuators.

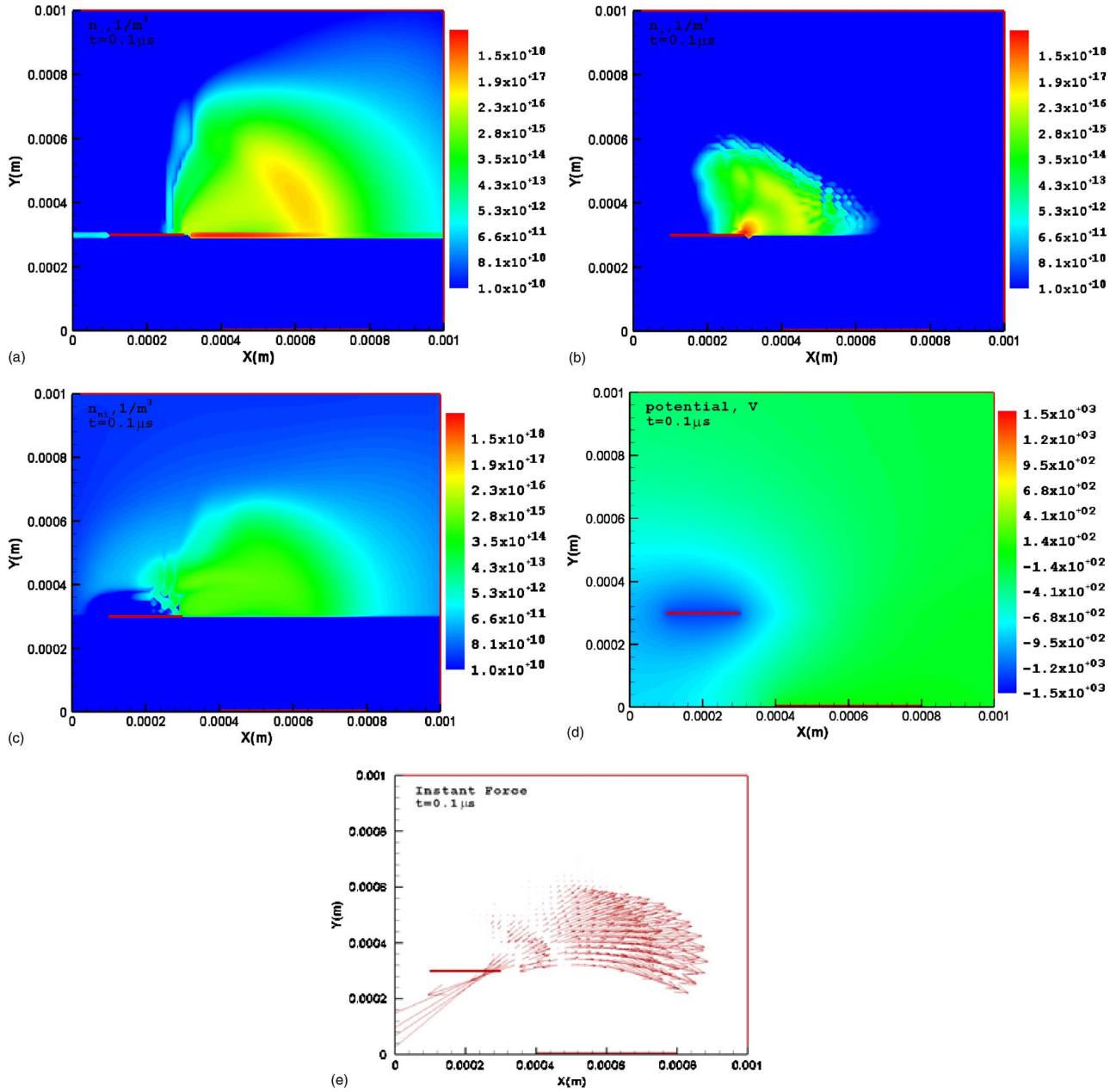

FIG. 4. (Color online) (a) Instantaneous electron density distribution during the ionization avalanche (sinusoidal voltage, amplitude 1.5 kV, frequency 1000 kHz). (b) Instantaneous positive ion density distribution during the ionization avalanche (sinusoidal voltage, amplitude 1.5 kV, frequency 1000 kHz). (c) Instantaneous negative ion density distribution during the ionization avalanche (sinusoidal voltage, amplitude 1.5 kV, frequency 1000 kHz). (d) Instantaneous electric potential distribution during the ionization avalanche (sinusoidal voltage, amplitude 1.5 kV, frequency 1000 kHz). (e) Instantaneous force on neutral gas during the ionization avalanche. The force always pushes the gas to the surface. The electrons push the gas downstream, and the positive ion cloud pushes the gas upstream (sinusoidal voltage, amplitude 1.5 kV, frequency 1000 kHz).

B. Positive half-cycle

Two distinctly different regimes are possible in the positive half-cycle (Fig. 7). If the applied voltage frequency is low (lower than about 2–3 kHz in millimeter or centimeter-scale plasmas), then by the end of the negative half-period almost all the electrons at the dielectric surface have been destroyed in recombination with ions. Therefore, the plasma around the positive exposed electrode can only exist as a positive corona, as shown in Fig. 7(b). Electrons generated in the strong field when the electrode potential is near its peak drift toward the exposed positive electrode (anode), leaving behind positive ions. The positive ions move in the opposite direction, i.e., upwards (away from the surface) and along the dielectric surface, imparting momentum to the gas. Thus, the momentum imparted to the gas is in the same direction (away from the exposed electrode) as in the negative half-period. However, in this corona regime, the gas also can receive some momentum directed from the surface.

Note that in this low-frequency corona regime the cloud of positive ions near the tip of exposed electrode partially

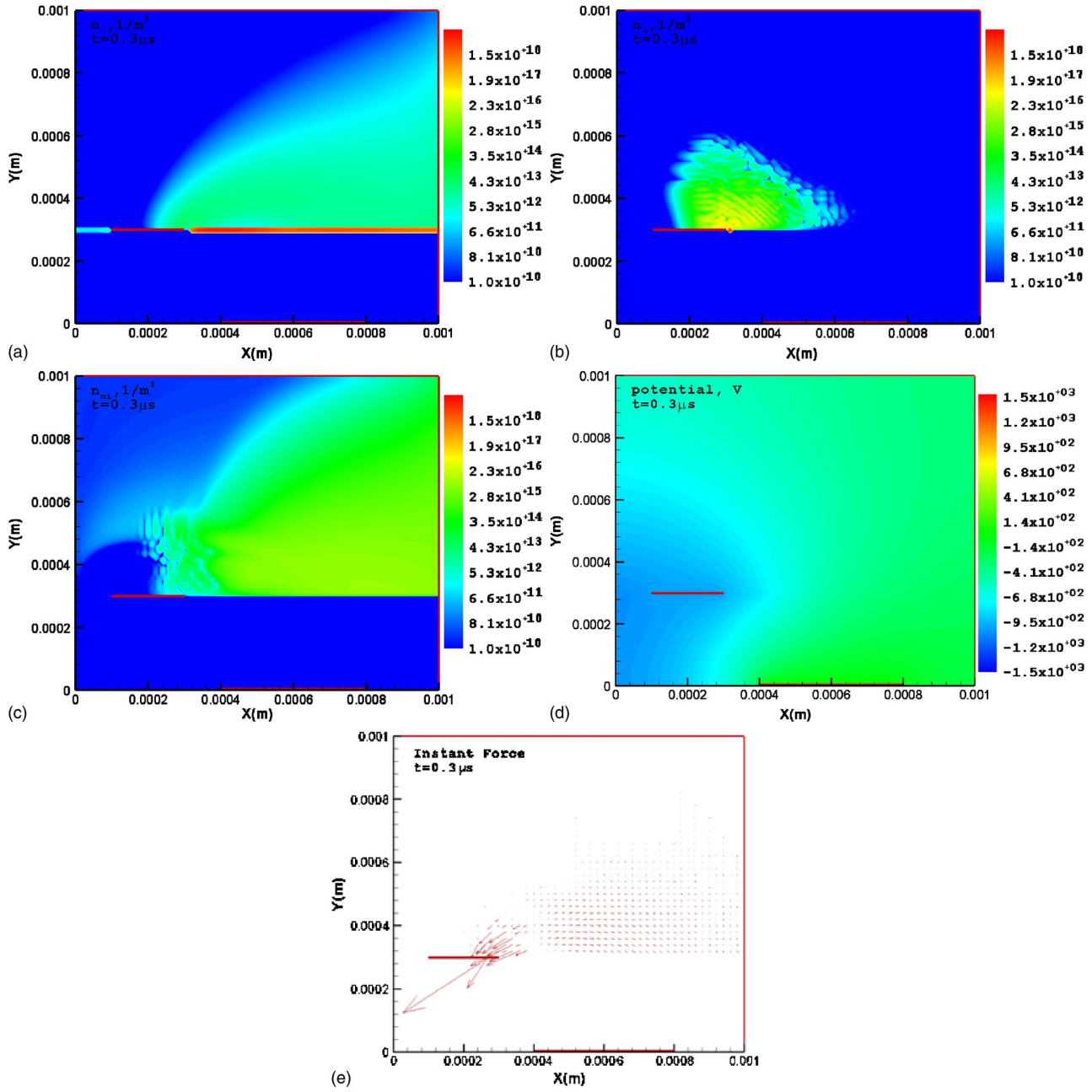

FIG. 5. (Color online) (a) Instantaneous electron density distribution during the negative half-cycle after the ionization avalanche. The electrons are attached to the dielectric surface (sinusoidal voltage, amplitude 1.5 kV, frequency 1000 kHz). (b) Instantaneous positive ion density distribution during the negative half-cycle after the ionization avalanche. The positive cloud is attracted to the cathode (sinusoidal voltage, amplitude 1.5 kV, frequency 1000 kHz). (c) Instantaneous negative ion density distribution during the negative half-cycle after the ionization avalanche. Negative ions drifts downstream (sinusoidal voltage, amplitude 1.5 kV, frequency 1000 kHz). (d) Instantaneous electric potential distribution during the negative half-cycle after the ionization avalanche (sinusoidal voltage, amplitude 1.5 kV, frequency 1000 kHz). (e) Instantaneous force on neutral gas during the negative half-cycle after the ionization avalanche. Positive ion cloud is attracted to the exposed electrode and pushes gas upstream (sinusoidal voltage, amplitude 1.5 kV, frequency 1000 kHz).

shields the field and limits the current, stopping the avalanches. When the ions drift away, the shielding is removed, and the breakdown can start again. This indicates the possibility of high-frequency oscillations superimposed on the low-frequency discharge operation.

If the applied voltage frequency is high enough (according to the calculations, at least 5–10 kHz, which agrees well with experimental observations) so that the electrons attached to the dielectric surface are not significantly destroyed

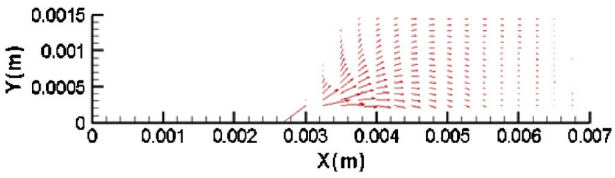

FIG. 6. (Color online) Average force during the negative half-cycle for sinusoidal applied voltage (amplitude 3.5 kV, frequency 100 kHz).

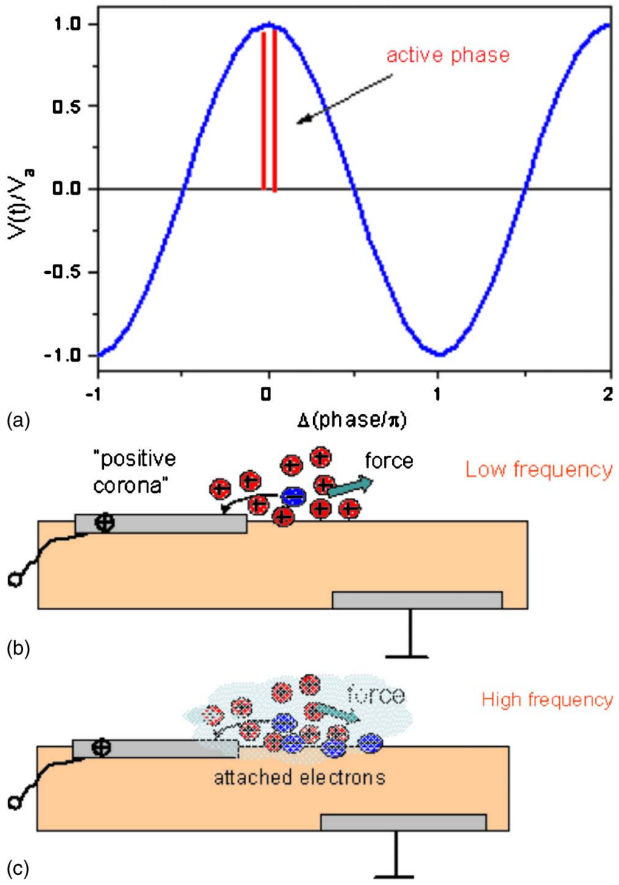

FIG. 7. (Color online) Positive half-period: (a) sine voltage waveform with short active phase; (b) illustration of "positive corona" regime at low frequency (no charge on dielectric surface, electrons are drawn to the exposed electrodes, ion clouds expand upward and away from the exposed electrode, imparting momentum to the gas); (c) illustration of processes at high frequency (negative charge remaining on dielectric surface from the negative half-period, ions drift toward the surface and away from the exposed electrode, imparting momentum to the gas and recombining with electrons deposited on the dielectric surface).

by the end of the negative half-period, then the electrons can be pulled from the surface in the positive half-period by secondary emission (impacts of high-energy ions and UV photons on the surface). These electrons can then generate avalanche ionization. The dielectric then plays the role of a cathode in this half-period, as illustrated in Fig. 7(c). The motion of positive ions that imparts momentum to the gas is toward the surface and along it (Fig. 8). Note that in the positive half-cycle, the negative ions move upstream, toward the exposed electrode, and impart an upstream-directed momentum to the gas, thus reducing the overall downstream-directed gas velocity.

C. Summary of the force exerted on the gas in sinusoidal applied voltage cases

The average force acting on the gas for the small-scale case is shown in Fig. 9. The first observation is that the gas experiences a strong force normal to the surface and toward it. This normal suction force, noted in Refs. 29–33, is due primarily to the motion of positively charged ion cloud to the exposed cathode in the negative half-cycle. In fact, this suction force turns out to be stronger than the average tangential force. However, the same positive ion motion to the cathode also creates a strong upstream-directed force. This upstream force is even greater than the downstream-directed force created by the negative ions in the negative half-cycle, if the device scale is small (less than 1 mm). In a large-scale (at least several millimeters) device, computations showed that the negative ion generated downstream force becomes stronger than the upstream force due to positive ions, so that the overall force is directed downstream even in the negative half-cycle and the total force over the cycle is also in the downstream direction (see Fig. 6). However, the motion of positive ions to the negatively biased exposed electrode remains a major source of inefficiency in generating tangential velocity of the gas. Note also that negative ions play diametrically opposing roles in the negative and positive half-cycles. In the negative half-cycle, the negative ions are primarily responsible for the downstream force, while in the positive half-cycle the negative ions move upstream and impede the downstream gas motion. The obtained results provide the first qualitative explanation of the DBD operation in atmospheric air with applied sine voltage. The previous DBD models[38–42] had several weaknesses, which reflected the provided results. For example, all plasma modeling has been done in inert gases. Thus, the formation of negative ions, which explains the downstream-directed force in the cathode cycle, was absent. Models[38–40] used unreasonably large time steps, which did not correctly resolve the ionization processes. Boeuf *et al.* developed a comprehensive model for DBD simulations in nitrogen,[41] but the real experimental cases, such as applied sine voltage in air, were not considered.

Overall, despite the dominant downstream directionality of the force, it is clear that a sinusoidal or near-sinusoidal voltage signal is an inefficient way of generation of a downstream-directed gas jet. In order to maximize the tangential force and the gas jet velocity, the inefficiencies discussed above should be eliminated or at least minimized.

IV. OPTIMAL WAVE FORM FOR LOW VOLTAGES: REPETITIVE SHORT PULSES WITH DC BIAS

A. The physical principles

As shown in the discussion of the DBD actuator operation with a sine voltage signal, the gas is pushed downstream due to the attraction of positive ions to the negatively charged dielectric surface in the positive half-period and due to negative ions in the negative half-period.

The charging of the dielectric plays the key role in understanding and optimizing the process. In the computed DBD examples, this has been accomplished by the removal of electrons from the plasma ionization wave onto the surface. However, in principle, other methods of charging the dielectric surface can be used. A newly proposed principle puts dielectric charging at the center.

Indeed, to push the gas along the surface in the direction away from the exposed electrode, the motion of positive ions should be predominantly in that direction. For that, the ex-

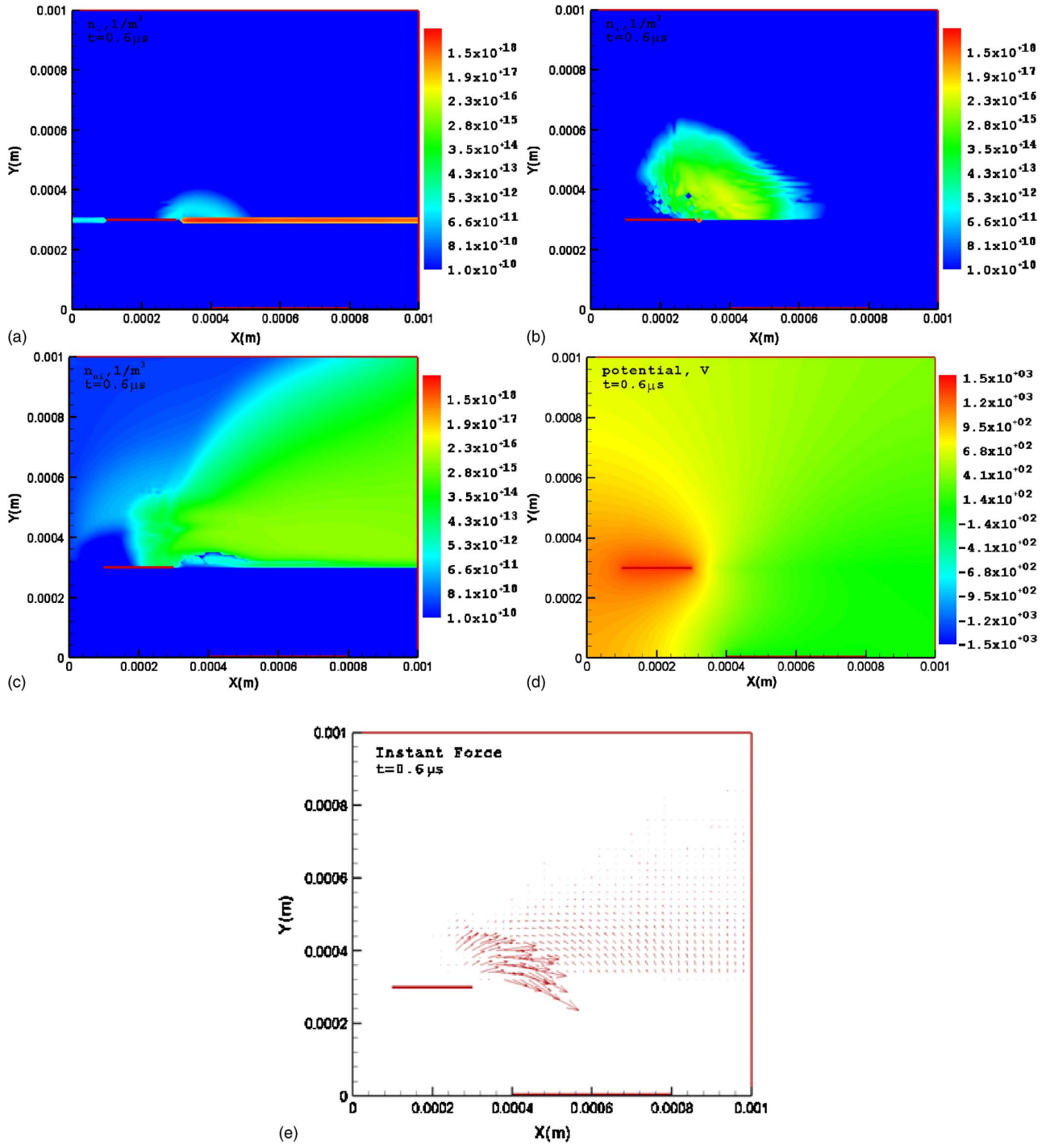

FIG. 8. (Color online) (a) Instantaneous electron density distribution during the positive half-cycle (sinusoidal voltage, amplitude 1.5 kV, frequency 1000 kHz). (b) Instantaneous positive ion density distribution during the positive half-cycle. The positive cloud pushes the gas downstream (sinusoidal voltage, amplitude 1.5 kV, frequency 1000 kHz). (c) Instantaneous negative ion density distribution during the positive half-cycle. The negative low density ion cloud pushes the gas upstream (sinusoidal voltage, amplitude 1.5 kV, frequency 1000 kHz). (d) Instantaneous electric potential distribution during the positive half-cycle (sinusoidal voltage, amplitude 1.5 kV, frequency 1000 kHz). (e) Instantaneous force on neutral gas during positive half-cycle. The unbalanced positive ions drift from the anode to the dielectric surface (sinusoidal voltage, amplitude 1.5 kV, frequency 1000 kHz).

posed electrode should be positively biased. However, dc current cannot just flow between neutral dielectric and the positive exposed electrode. (The dielectric itself is needed in order to limit the current and thus to prevent transformation of the plasma into hot, constricted, unstable arc). To make the current flow possible in the regime when the exposed electrode is positive, electrons should be deposited onto the dielectric surface. That way, the electrons would be "lifted" from the surface by recombination with ions that drift and arrive at the surface and by secondary emission (due to impact of energetic positive ions), and the operation would be similar to the cathode in glow discharge.

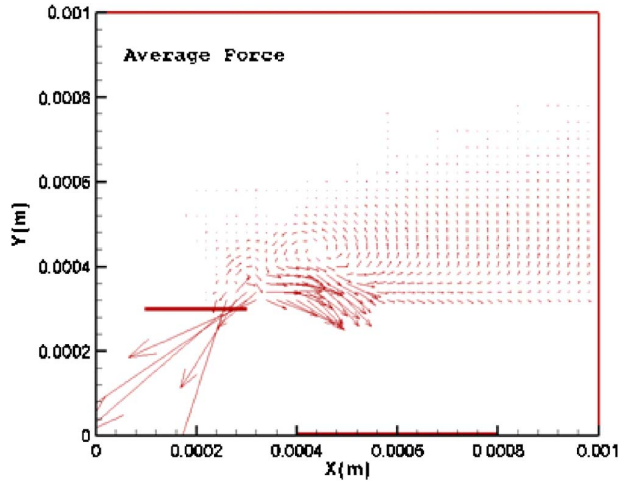

FIG. 9. (Color online) Average force acting on neutral gas during the cycle (sinusoidal voltage, amplitude 1.5 kV, frequency 1000 kHz).

Since the actuator operation will entail the removal of electrons from the surface, these surface-deposited electrons should be periodically replenished.

The periodic replenishment of negative charge on the dielectric should be done very rapidly to minimize the time period of backward-directed positive ion motion. This can indeed be accomplished by periodic application (with repetition rate from tens to hundreds of kHz) of very short (2–5 ns), strong, negative voltage pulses. In these short pulses, the ionization avalanche developing from the exposed electrode would quickly reach the dielectric surface and would deposit electrons onto it, leaving behind the positive ions, so that the main plasma actuator operation could resume.

B. Numerical results

The applied voltage and the corresponding calculated current in the circuit in the representative repetitive-pulse case is presented in Fig. 10. The breakdown occurs during the pulse and the peak in the current curve corresponds to it.

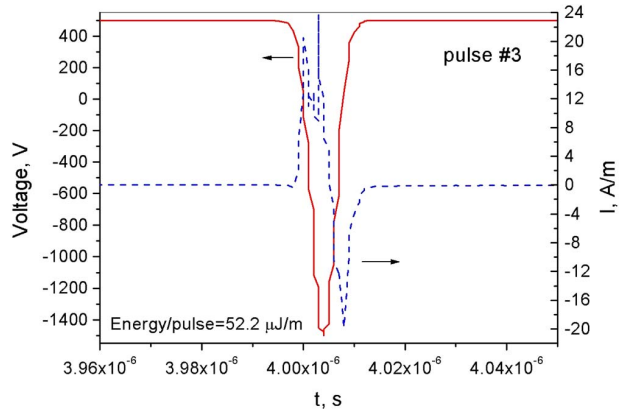

FIG. 10. (Color online) Current and voltage in a representative repetitive-pulse case in quasi-steady-state regime. The solid line shows the voltage and the dashed line shows the current. (Pulse voltage: amplitude −1.5 kV, FWHM is 4 ns, repetition rate is 500 kHz, and the bias is 500 V.)

In the representative case the following parameters were chosen: the Gaussian pulse width was 4 ns, the pulse amplitude was −1.5 kV, the dc bias was 0.5 kV, and the repetition rate was 500 kHz (so that the interval between the pulses was 2 μs). The small-scale geometry was the same as in the sine-voltage cases. Figure 11 shows that after the pulse there is a very high concentration of positive ions near the exposed electrode. The electrons are attached to the dielectric surface, creating an effective "cathode" which attracts the positive cloud. Figures 11–13 show the evolution of the positive cloud from the anode to the dielectric and the corresponding instantaneous potential distributions. The cloud moves to the right, neutralizing the surface charge and gradually dispersing. Figure 14 shows the average force acting on the gas between two pulses. Comparison of Figs. 14 and 9 clearly shows that the waveform with short repetitive pulses eliminates the upstream-directed force that was the principal inefficiency source in the sine-voltage cases.

A simple physical model can describe the pushing action of plasma on the gas. Consider the gas in a region of length L (Fig. 15). A positive ion cloud with average ion number density n_+ and the width S is created near the exposed electrode.

The moving ion cloud acts as a porous piston: it moves faster than the gas and accelerates the gas molecules that experience collisions with ions. Since at thermal energies the ion-molecule collision cross section is approximately $\sigma_{in} \approx 1.5 \times 10^{-14}$ cm^2,[50] and the ion number density is typically $n_+ \approx 10^{11} - 10^{12}$ cm^{-3}, the mean-free path of the molecule with respect to collisions with ions is on the order of 1–10 m—much longer than the 0.3–3 mm width of the ion cloud. Therefore, only a small fraction of molecules experiences collisions with ions during the single sweep of the ion cloud, which justifies the porous piston analogy.

The force on a molecule inside the plasma column is

$$f = k_{in} n_+ M (u_+ - u), \tag{16}$$

where $k_{in} \approx 1.1 \times 10^{-9}$ cm^3/s is the ion-molecule momentum-transfer rate constant,[51] M is the ion mass (assumed equal to the molecule's mass), u_+ is the ion cloud (drift) velocity, and u is the gas velocity. Since the residence time of a molecule inside the ion cloud is approximately $t \approx S/(u_+ - u)$, the gas velocity increment in a single sweep of the ion cloud is

$$\Delta V_1 = k_{in} n_+ S. \tag{17}$$

As the gas element in the boundary layer slowly moves along the wall, it experiences many "hits" by the consecutive rapidly moving ion clouds. The number of these hits is approximately equal to $L/(\tilde{u}\Delta t)$, where $\tilde{u}$ is the average gas velocity, and Δt is the smaller of the interval between the pulses and the time of ion drift over the distance L. Denoting the initial gas velocity (i.e., the velocity at the entrance to the interaction region) as V_0 and the final (i.e., exit) gas velocity as V, we obtain

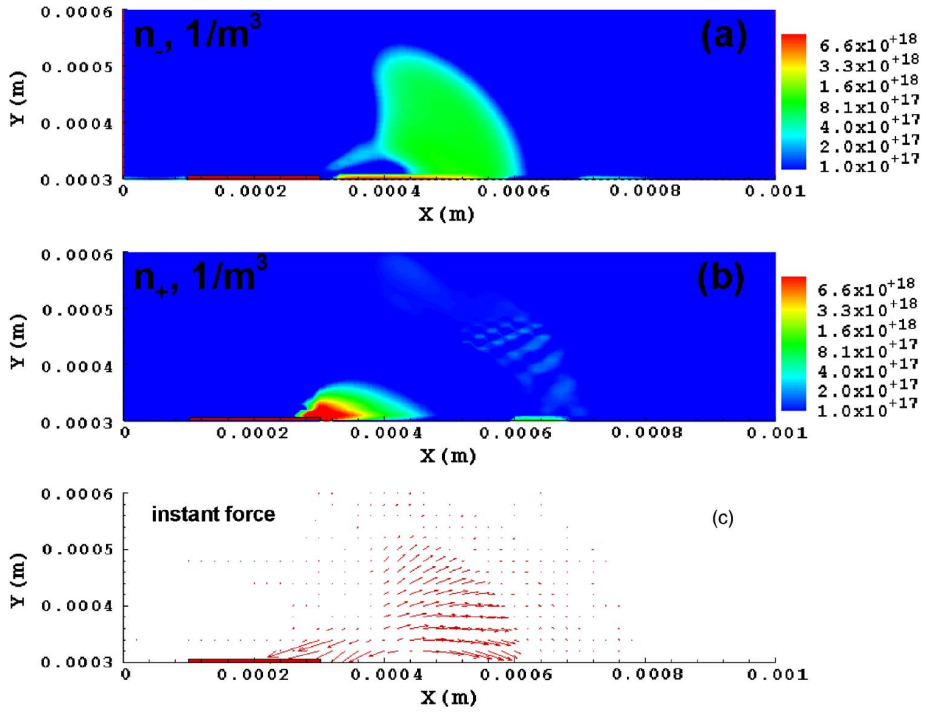

FIG. 11. (Color online) (a) Electron density distribution at the peak pulse voltage. The electron avalanche charges the dielectric surface during the pulse. (Pulse voltage: amplitude −1.5 kV, FWHM is 4 ns, repetition rate is 500 kHz, and the bias is 500 V.) (b) Positive ion density distribution at the peak pulse voltage. The positive ion cloud is formed near the exposed electrode during the pulse. (Pulse voltage: amplitude −1.5 kV, FWHM is 4 ns, repetition rate is 500 kHz, and the bias is 500 V.) (c) Instantaneous force on neutral gas at the peak pulse voltage. The gas is pushed by electrons downstream and by ions upstream, but during a very short time. (Pulse voltage: amplitude −1.5 kV, FWHM is 4 ns, repetition rate is 500 kHz, and the bias is 500 V.)

$$V - V_0 = \frac{L}{\frac{1}{2}(V + V_0)\Delta t}\Delta V_1. \tag{18}$$

From Eqs. (17) and (18), we obtain

$$V^2 - V_0^2 = \frac{2Lk_{\text{in}}n_+S}{\Delta t}, \tag{19}$$

and assuming that initially the gas is at rest,

$$V = \sqrt{\frac{2Lk_{\text{in}}n_+S}{\Delta t}}. \tag{20}$$

In the computed small-scale case with repetitive (500 kHz), short (4 ns FWHM) 2 kV pulses and 500 V dc bias, the approximate values of the parameters in Eq. (20) are $L=0.3$ mm, $S=0.1$ mm, $\Delta t=2\times10^{-6}$ s, and $n_+=5\times10^{11}$ cm^{-3}. Equation (20) then gives the induced gas velocity of $V=4$ m/s. It is important to recognize that this

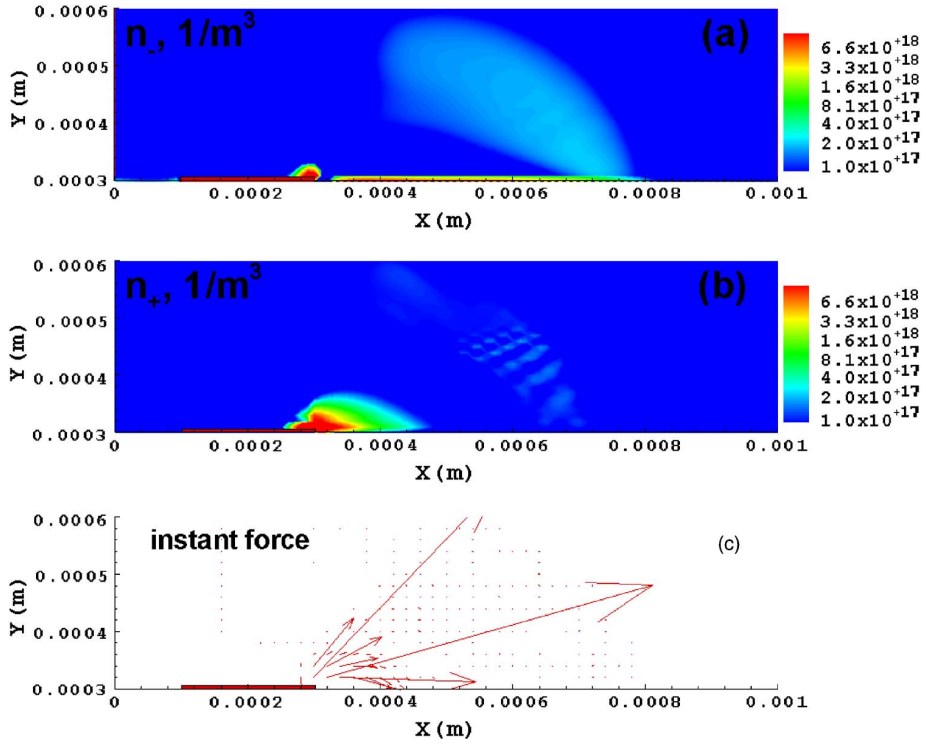

FIG. 12. (Color online) (a) Electron density distribution immediately after the pulse. The electron avalanche has charged the dielectric by the end of the pulse. (Pulse voltage: amplitude −1.5 kV, FWHM is 4 ns, repetition rate is 500 kHz, and the bias is 500 V.) (b) Positive ion density distribution immediately after the pulse. Positive ions start to move to the dielectric surface. (Pulse voltage: amplitude −1.5 kV, FWHM is 4 ns, repetition rate is 500 kHz, and the bias is 500 V.) (c) Instantaneous force on neutral gas immediately after the pulse. Positive ions start to push the gas downstream. (Pulse voltage: amplitude −1.5 kV, FWHM is 4 ns, repetition rate is 500 kHz, and the bias is 500 V.)

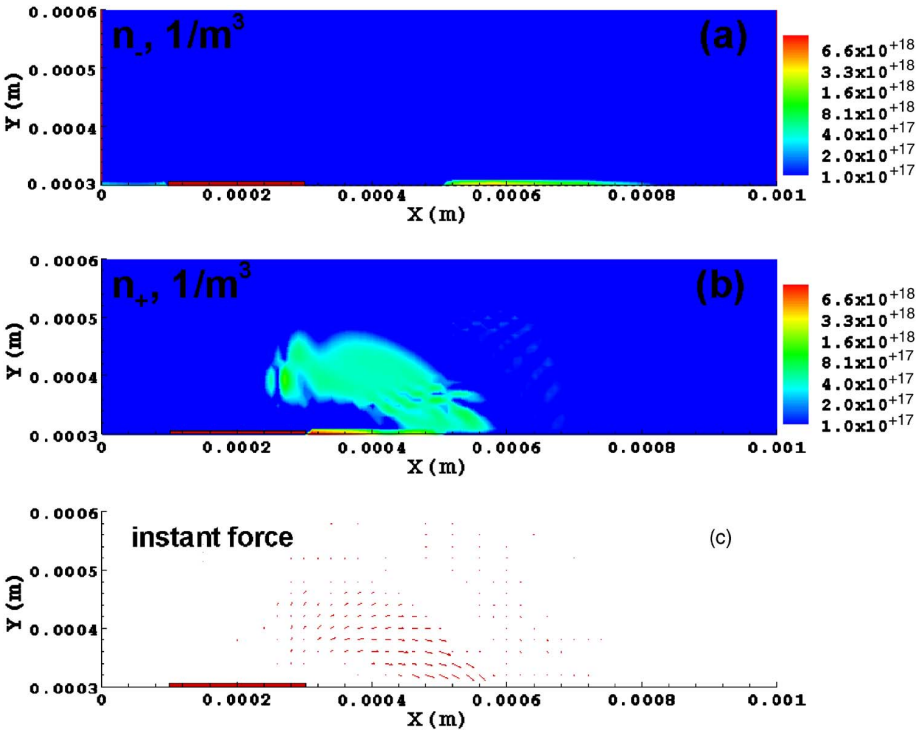

FIG. 13. (Color online) (a) Electron density distribution 0.5 μs after the pulse. The electrons are neutralized on the surface by positive ions. (Pulse voltage: amplitude −1.5 kV, FWHM is 4 ns, repetition rate is 500 kHz, and the bias is 500 V.) (b) Positive ion density distribution 0.5 μs after the pulse. The ions drift to the negatively charged dielectric surface. (Pulse voltage: amplitude −1.5 kV, FWHM is 4 ns, repetition rate is 500 kHz, and the bias is 500 V.) (c) Instantaneous force on neutral gas 0.5 μs after the pulse. The force is due to positive ions drifting to the dielectric. (Pulse voltage: amplitude −1.5 kV, FWHM is 4 ns, repetition rate is 500 kHz, and the bias is 500 V.)

velocity is similar to that commonly observed in conventional asymmetric DBD actuators, but it is achieved with a considerably lower voltage amplitude and an order of magnitude smaller plasma size compared with those in conventional DBD systems.[30–34]

V. DIFFERENT DBD REGIMES

As noted earlier in this paper, the voltage waveform consisting of repetitive short negative pulses and positive dc bias makes the best use of the dielectric surface charging and eliminates the inefficiencies present in sine-voltage cases. Despite the clear physics in low-voltage cases, the scaling predictions do not work for higher voltages, as the physics of the discharge dramatically changes with scaling. In the case of repetitive negative nanosecond pulses the proposed model works for 1.5–2 kV applied voltages. However, if the voltage is increased, the effects are unclear. On one hand, the positive ion cloud is increased, leading to a stronger pushing force on the gas downstream[52,53] But, on the other hand, the back breakdown occurs, causing the backward-directed force near the edge of the electrode. At high voltages another mechanism of gas pushing can be produced: repetitive positive nanosecond pulses with positive bias.[52,53] If the high-voltage positive pulses are applied to the exposed electrode, one can get the streamerlike solution, Fig. 16. These cases are discussed in detail in Refs. 52 and 53.

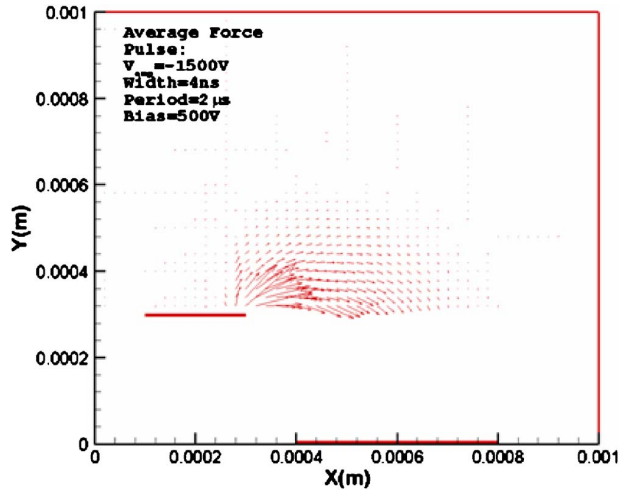

FIG. 14. (Color online) Average force acting on neutral gas during one cycle. (Pulse voltage: amplitude −1.5 kV, FWHM is 4 ns, repetition rate is 500 kHz, and the bias is 500 V.)

VI. CONCLUSIONS

A consistent, comprehensive, and physically based model for an asymmetric dielectric barrier discharge plasma

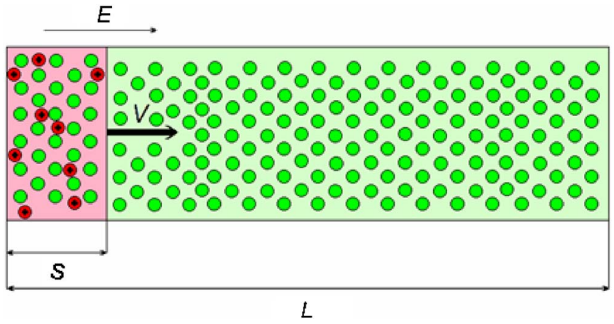

FIG. 15. (Color online) Simplified physical model (multiple sweeps by a "porous piston") describing the momentum transfer to the neutral gas in repetitive-pulse cases.

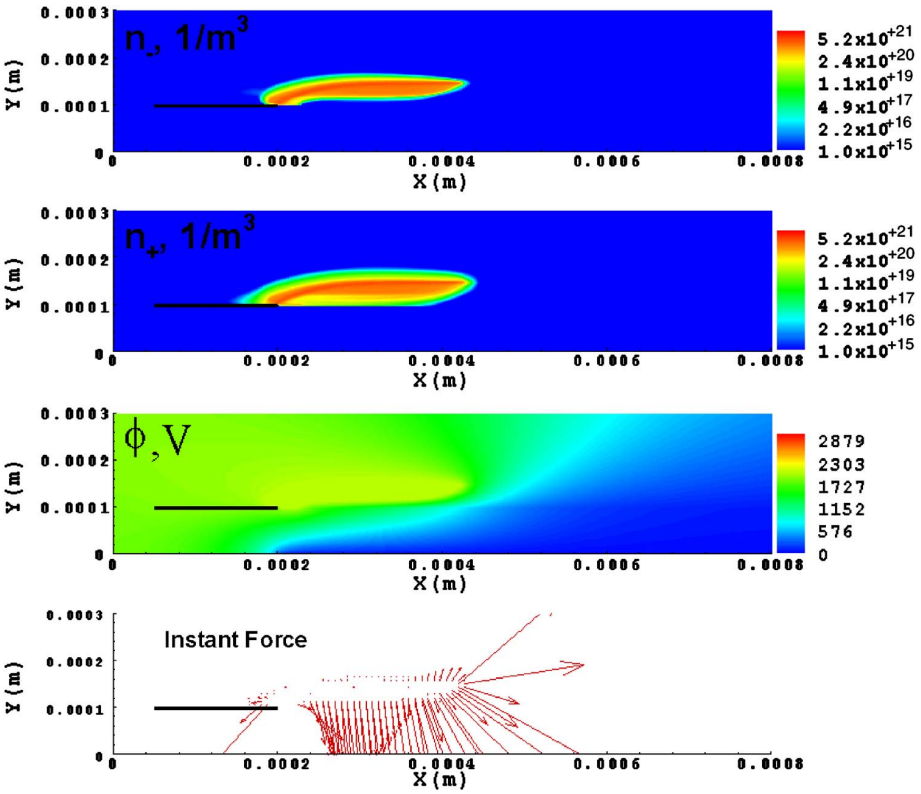

FIG. 16. (Color online) Streamer propagation in the case of repetitive positive nanosecond pulse with bias. Pictures shows the instant electron, positive ion densities, electric potential distribution, and force on the gas distribution right after the pulse. (Pulse voltage: amplitude 3 kV, FWHM is 4 ns, repetition rate is 500 kHz, and the bias is 1000 V.)

actuator in air has been developed, and the modeling has revealed the essential physics of DBD actuators. The charging of dielectric by electrons during the avalanche ionization process lasts only a small fraction of the negative (cathode) half-cycle, but plays a crucial role in DBD operation and gas acceleration. The tangential force on the gas is directed downstream in both cathode and anode half-cycles, and is created by the downstream motion of the negative ions in the cathode half-cycle and by the downstream motion of positive ions in the anode half-cycle. The motion of positive ions toward the exposed electrode in the cathode half-cycle was found to not only create a strong suction effect, but to also considerably decrease the integrated downstream-directed tangential force, thus resulting in a major inefficiency of the sine-voltage waveform. An additional inefficiency is due to the negative ion motion upstream in the anode half-cycle.

The understanding of the detailed mechanism of DBD actuator operation and the sources of inefficiency allowed us to propose a voltage waveform making the maximum use of dielectric charging and free from the above-mentioned inefficiencies. This optimal waveform consists of high repetition rate, extremely short (a few nanoseconds) pulses of negative voltage in combination with a positive dc bias applied to the exposed electrode. Computations and analytical estimates showed that a repetitive-pulse waveform can induce gas velocities similar to those in conventional sine-voltage DBD actuators at a considerably lower voltage and more than an order of magnitude shorter streamwise plasma size.

ACKNOWLEDGMENTS

This work was supported by Boeing and by the US-AFOSR Unsteady Aerodynamics and Hypersonics Program.

[1]S. O. Macheret, M. N. Shneider, and R. B. Miles, AIAA J. **42**, 1378 (2004).
[2]S. O. Macheret, M. N. Shneider, R. B. Miles, and R. J. Lipinski, AIAA J. **39**, 1127 (2001).
[3]S. O. Macheret, M. N. Shneider, and R. B. Miles, AIAA J. **40**, 74 (2002).
[4]S. O. Macheret, M. N. Shneider, and R. B. Miles, J. Propul. Power **18**, 424 (2002).
[5]M. N. Shneider, S. O. Macheret, and R. B. Miles, AIAA J. **42**, 2303 (2004).
[6]S. O. Macheret, M. N. Shneider, and R. B. Miles, "Optimum Performance of Electron Beam Driven MHD Generators for Scramjet Inlet Control," Paper AIAA 2003–3763, in 34th AIAA Plasmadynamics and Lasers Conference, Orlando, FL, 23–26 June 2003.
[7]R. C. Murray, L. Vasilyak, M. R. Carraro, S. H. Zaidi, S. O. Macheret, M. N. Shneider, and R. B. Miles, "Observation of MHD Effects With Nonequilibrium Ionization in Cold Supersonic Air Flows," Paper AIAA 2004–1025, in 42nd Aerospace Sciences Meeting and Exhibit, Reno, NV, 5–8 January 2004.
[8]S. O. Macheret, M. N. Shneider, and G. V. Candler, "Modeling of MHD Power Generation On Board Reentry Vehicles," Paper AIAA 2004–1024, in 42nd Aerospace Sciences Meeting and Exhibit, Reno, NV, 5–8 January 2004.
[9]M. N. Shneider and S. O. Macheret, "Modeling of Plasma Virtual Shape Control of Ram/Scramjet Inlet and Isolator," Paper AIAA 2004–2662, in 35th AIAA Plasmadynamics and Lasers Conference, Portland, OR, 28 June–1 July 2004.
[10]M. N. Shneider and S. O. Macheret, "Hypersonic Aerodynamic Control and Thrust Vectoring by Nonequilibrium Cold-Air MHD Devices," Paper AIAA-2005–0979, in 43rd AIAA Aerospace Sciences Meeting and Exhibit, Reno, NV, 10–13 January 2005.
[11]R. B. Miles, S. O. Macheret, M. N. Shneider, C. Steeves, R. C. Murray, T. Smith, and S. H. Zaidi, "Plasma-Enhanced Hypersonic Performance Enabled by MHD Power Extraction," Paper AIAA 2005–0561, in 43rd AIAA Aerospace Sciences Meeting and Exhibit, Reno, NV, 10–13 January 2005.
[12]A. L. Kuranov and E. G. Sheikin, "MHD Control on Hypersonic Aircraft under AJAX Concept: Possibilities of MHD Generator," Paper AIAA 2002–0490, in 40th AIAA Aerospace Sciences Meeting and Exhibit, Reno, NV, 14–17 January 2002.
[13]A. Vatazhin, V. Kopchenov, and O. Gouskov, "Some Estimations of Possibility to Use the MHD Control for Hypersonic Flow Deceleration," Pa-

per AIAA 1999–4972, in 3rd AIAA Weakly Ionized Gases Workshop, Norfolk, VA, 1–5 November 1999.
[14]V. A. Bityurin, A. I. Klimov, S. B. Leonov, A. N. Bocharov, and J. T. Lineberry, "Assessment of a Concept of Advanced Flow/Flight Control for Hypersonic Flights in Atmosphere," Paper AIAA 1999–4820, in 3rd AIAA Weakly Ionized Gases Workshop, Norfolk, VA, 1–5 November 1999.
[15]M. Nishihara, N. Jiang, J. W. Rich, W. R. Lempert, I. V. Adamovich, and S. Gogineni, Phys. Fluids **17**, 106102 (2005).
[16]M. Nishihara, J. W. Rich, W. R. Lempert, I. V. Adamovich, and S. Gogineni, Phys. Fluids **18**, 086101 (2006).
[17]D. Gaitonde, "Simulations of Global and Local Flow Control with Magnetic Field," Paper AIAA 2005–560, in 43rd AIAA Aerospace Sciences Meeting and Exhibit, Reno, NV, 10–13 January 2005.
[18]S. T. Surzhikov and J. S. Shang, "Subsonic and Supersonic Flow Around Wing with Localized Surface Gas Discharge," Paper AIAA 2005–0406, in 43rd AIAA Aerospace Sciences Meeting and Exhibit, Reno, NV, 10–13 January 2005.
[19]S. T. Surzhikov and J. S. Shang, J. Comput. Phys. **199**, 437 (2004).
[20]S. T. Surzhikov and J. S. Shang, "Magneto-Fluid-Dynamic Interactions for Hypersonic Flow Control," Paper AIAA 2004–0508, in 42nd Aerospace Sciences Meeting and Exhibit, Reno, NV, January 5–8, 2004.
[21]S. T. Surzhikov and J. S. Shang, High Temp. **43**, 19 (2005).
[22]R. Kimmel, J. Hayes, J. Menart, and J. S. Shang, "Effect of Surface Plasma Discharge on Boundary Layer at Mach 5," Paper AIAA 2004–0509, in 42nd Aerospace Sciences Meeting and Exhibit, Reno, NV, 5–8 January 2004.
[23]J. Poggie, "Numerical Exploration of Flow Control with Glow Discharges," Paper AIAA 2004–2858, in 35th AIAA Plasmadynamics and Lasers Conference, Portland, OR, 28 1 June–1 July 2004.
[24]J. S. Shang, R. Kimmel, J. Hayes, C. Tyler, and J. Menart, J. Spacecr. Rockets **42**, 780 (2005).
[25]J. S. Shang and S. T. Surzhikov, AIAA J. **43**, 1633 (2005).
[26]J. Menart, J. Shang, C. Atzbach, S. Magoteaux, M. Slagel, and B. Bilheimer, "Total Drag and Lift Measurements in a Mach 5 Flow Affected by a Plasma Discharge and a Magnetic Field," Paper AIAA-2005–947, in 43rd AIAA Aerospace Sciences Meeting and Exhibit, Reno, NV, 10–13 January 2005.
[27]S. B. Leonov, D. A. Yarantsev, V. G. Gromov, and A. P. Kuriachy, "Mechanisms of Flow Control by Near-Surface Electric Discharge Generation," Paper AIAA 2005–0780, in 43rd AIAA Aerospace Sciences Meeting and Exhibit, Reno, NV, 10–13 January 2005.
[28]S. O. Macheret, "Physics of Magnetically Accelerated Nonequilibrium Surface Discharges in High-Speed Flow," Paper AIAA 2006–1005, in 44th AIAA Aerospace Sciences Meeting and Exhibit, Reno, NV, 9–12 January 2006.
[29]S. H. Zaidi, T. Smith, S. O. Macheret, and R. B. Miles, "Snowplow Surface Discharge in Magnetic Field for High Speed Boundary Layer Control," Paper AIAA 2006–1006, in 44th AIAA Aerospace Sciences Meeting and Exhibit, Reno, NV, 9–12 January 2006.
[30]C. L. Enloe, T. E. McLaughlin, R. D. VanDyken, K. D. Kachner, E. J. Jumper, and T. C. Corke, AIAA J. **42**, 589 (2004).
[31]C. L. Enloe, T. E. McLaughlin, R. D. VanDyken, K. D. Kachner, E. J. Jumper, T. C. Corke, M. Post, and O. Haddad, AIAA J. **42**, 595 (2004).
[32]M. Post and T. C. Corke, "Flow Control with Single Dielectric Barrier Plasma Actuator," Paper AIAA 2005–4630, in 35th AIAA Fluid Dynamics Conference and Exhibit, Toronto, Ontario, 6–9 June 2005.
[33]T. C. Corke, E. J. Jumper, M. L. Post, D. Orlov, and T. E. McLaughlin, "Application of Weakly-Ionized Plasmas as Wing Flow-Control Devices," Paper AIAA 2002–350, in 40th AIAA Aerospace Sciences Meeting and Exhibit, Reno, NV, 14–17 January 2002.
[34]M. L. Post and T. C. Corke, AIAA J. **42**, 2177 (2004).
[35]D. F. Opaits, D. V. Roupassov, S. M. Starikovskaia, A. Yu. Starikovskii, I. N. Zavialov, and S. G. Saddoughi, "Plasma Control of Boundary Layer Using Low-Temperature Non-Equilibrium Plasma of Gas Discharge," Paper AIAA 2005–1180, in 43rd AIAA Aerospace Sciences Meeting and Exhibit, Reno, NV, 10–13 January 2005.
[36]F. Massines, A. Rabehi, F. Decomps, R. Ben Gadri, P. Ségur, and C. Mayoux, J. Appl. Phys. **83**, 2950 (1998).
[37]J. R. Roth, D. M. Sherman, and S. P. Wilkinson, AIAA J. **38**, 1173 (2000).
[38]S. Roy and D. V. Gaitonde, "Modeling Surface Discharge Effects of Atmospheric RF on Gas Flow Control," Paper AIAA 2005–160, 43rd AIAA Aerospace Sciences Meeting and Exhibit, Reno, NV, 10–13 January 2005.
[39]S. Roy, Appl. Phys. Lett. **86**, 101502 (2005).
[40]K. P. Singh and S. Roy, J. Appl. Phys. **98**, 083303 (2005)
[41]J. P. Boeuf and L. C. Pitchford, J. Appl. Phys. **97**, 103307 (2005).
[42]D. M. Orlov and T. C. Corke, "Numerical Simulation of Aerodynamic Plasma Actuator Effects," Paper AIAA 2005–1083, in 43rd AIAA Aerospace Sciences Meeting and Exhibit, Reno, NV, 10–13 January 2005.
[43]S. O. Macheret, M. N. Shneider, and R. B. Miles, Phys. Plasmas **8**, 1518 (2001).
[44]S. O. Macheret, M. N. Shneider, and R. B. Miles, IEEE Trans. Plasma Sci. **30**, 1301 (2002).
[45]Yu. P. Raizer, *Gas Discharge Physics* (Springer-Verlag, Berlin, 1997).
[46]I. S. Grigoriev and E. Z. Meilikhov, *Handbook of Physical Quantities* (CRC Press, Boca Raton, FL, 1997), Chap. 20.
[47]D. A. Anderson, J. C. Tannehill, and R. H. Pletcher, *Computational Fluid Mechanics and Heat Transfer* (Hemisphere, New York, 1984).
[48]H. K. Gummel, IEEE Trans. Electron Devices **11**, 455 (1964).
[49]Y. P. Raizer and M. N. Shneider, Sov. J. Plasma Phys. **14**, 128 (1988).
[50]M. N. Shneider, S. O. Macheret, and R. B. Miles, "Electric Charge Build-Up in Hypersonic Wind Tunnels with Electron Beam Energy," Paper AIAA-2003–4035, in 34th AIAA Plasmadynamics and Lasers Conference, Orlando, FL, 23–26 June 2003.
[51]D. L. Scharfetter and H. K.Gummel, IEEE Trans. Electron Devices **16**, 64 (1969).
[52]A. V. Likhanskii, M. N. Shneider, S. O. Macheret, and R. B. Miles, Paper AIAA-2007–633, in 45th AIAA Aerospace Sciences Meeting and Exhibit, Reno, NV, 2007.
[53]A. V. Likhanskii, M. N. Shneider, S. O. Macheret, and R. B. Miles, Phys. Plasmas **14**, 073501 (2007).

PHYSICS OF PLASMAS **15**, 073505 (2008)

Surface charge in dielectric barrier discharge plasma actuators

D. F. Opaits,[1,a)] M. N. Shneider,[1] Richard B. Miles,[1] A. V. Likhanskii,[2] and S. O. Macheret[3]
[1]*Department of Mechanical and Aerospace Engineering, Princeton University, Princeton, New Jersey 08544, USA*
[2]*The Pennsylvania State University, University Park, Pennsylvania 16802, USA*
[3]*Lockheed Martin Aeronautics Company, Palmdale, California 93599, USA*

(Received 10 April 2008; accepted 17 June 2008; published online 21 July 2008)

Direct measurements of the dielectric surface potential and its dynamics in asymmetric dielectric barrier discharge (DBD) plasma actuators show that the charge builds up at the dielectric surface and extends far downstream of the plasma. The surface charge persists for a long time (tens of minutes) after the driving voltage has been turned off. For a sinusoidal voltage waveform, the dielectric surface charges positively. With the voltage waveform consisting of nanosecond pulses superimposed on a dc bias, the sign of the dielectric surface charge is the same as the sign (polarity) of the bias voltage. The surface charging significantly affects DBD plasma actuator performance. © *2008 American Institute of Physics*. [DOI: 10.1063/1.2955767]

I. INTRODUCTION

Asymmetric dielectric barrier discharge (DBD) plasma actuators have been reported in a number of works which have addressed their potential use for aerodynamic control.[1–22,24–29] This application relies on a DBD-induced wall jet with typical velocities of several meters per second. It is understood that electric charge deposition on the dielectric surface limits the current and thus allows operation of nonequilibrium discharges at atmospheric pressure. The important role of the surface charge and its finite relaxation time (the "memory voltage") in the discharge physics was pointed out by Massines *et al.*[30] and Gadri[31] for the parallel-plate DBD configuration, and by Roth *et al.*[32] for One Atmosphere Uniform Glow Discharge Plasma (OAUGDP™). Since the surface charge plays an important role in DBD physics, it warrants a special study. In the work of Font *et al.*,[21] the surface potential in a DBD driven by sinusoidal voltage was measured using a V-dot probe technique, and the voltage across the plasma was shown to be less than half of that which is applied across the electrodes. Recently the same group[22] presented the time evolution and the spatial extent of the surface potential. In this paper, we describe electrostatic voltmeter measurements of surface charge in DBD plasma actuators driven by various voltage profiles, most notably by pulses plus dc bias but also by sinusoidal voltages. The work reported here extends our previously reported work which also used the electrostatic probe.[24] The results for the sinusoidal profile recently reported by Enloe *et al.*[22] are consistent with the work reported here and with our previous results. For sinusoidal voltages the two approaches are mutually complementary since Enloe *et al.* measure the surface potential using a different method.

a)Electronic mail: dopaits@princeton.edu.

II. SURFACE POTENTIAL MEASUREMENTS

A. Experimental setup

For nonintrusive surface potential measurements we used the Trek Model 247-3 Electrostatic Voltmeter with Trek Model 6000B-13C Electrostatic Voltmeter Probe. It has high resolution (around 1 mm), fast response time (less than 3 ms for a 1 kV step), and an operating range from 0 to ±3 kV dc or peak ac.

The description of the asymmetric DBD plasma actuator (Fig. 1) can be found in our earlier paper.[24] The electrodes were made of copper foil. The width of the electrodes was equal to 25 mm and their spanwise dimension was 75 mm. A 100 micron thick kapton tape was used as the dielectric. The discharge was ignited by applying high voltage to one of the electrodes. The other electrode was grounded.

B. Sinusoidal voltage experiments

First, experiments were conducted for the 3 kHz 10 kV peak-to-peak sinusoidal voltage profile. Since the sinusoidal profile is widely used in DBD experiments,[1–6,13–15,17–20] it is interesting to compare its surface potential distribution with the one obtained in pulsed DBD.[16,24–29] The actuator was run for 15 s and then the surface potential was measured. The result is presented in Fig. 2, where the distance is measured from the edge of the exposed electrode. The plasma extends only a few millimeters downstream of the edge of the exposed electrode, whereas the dielectric charge extends centimeters away from it, *far downstream* of the plasma. The maximum surface potential (1.5 kV) *is comparable* to the applied peak voltage (5 kV). This means that the electric field of the surface charge can significantly distort the electric field produced by the voltage applied to the electrodes. Also, even though the applied voltage is symmetrical (sinusoidal with no bias voltage) the time-averaged surface charge has a positive polarity. This is possibly due to the much higher mobility of electrons compared to positive ions which

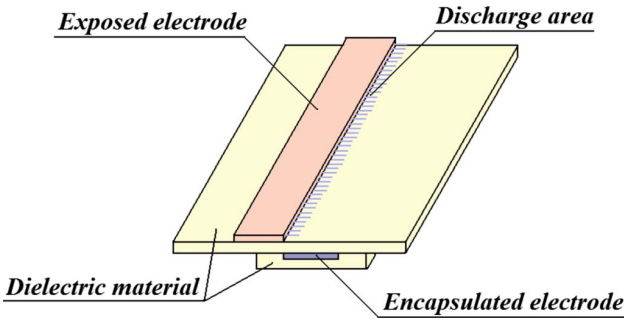

FIG. 1. (Color online) Asymmetric dielectric barrier discharge plasma actuator.

leads to a much higher electron current into the exposed electrode during the positive half-cycle of the sinusoidal voltage compared to the positive ion current into the exposed electrode during the negative half cycle. With this reasoning one might conclude that there is a net negative current into the exposed electrode and positive current flow from the DBD to infinity. This picture is consistent with results from other two experiments described in our earlier work.[24] Similar behavior is observed in asymmetric rf discharges, where there is a positive current flux to a virtual electrode at infinity.[23]

The persistence of surface charge far downstream of the plasma can be due either to surface mobility of the charges or to deposition of the charges onto the surface from the gas jet downstream of the plasma. Estimates show that while the dielectric surface charge mobility is too low, the deposition of ions from the DBD-generated tangential gas jet is likely to persist downstream of the plasma. Indeed, in the DBD generated jet downstream of the visible plasma, plasma electrons, no longer regenerated by ionization, rapidly (in tens of nanoseconds) recombine with positive ions and attach to oxygen molecules, which results in an ion-ion plasma jet with an estimated ion-ion recombination time on the order of several milliseconds. At a jet velocity of several m/s, this translates into several centimeters of ion-ion plasma and thus into several centimeters of dielectric surface charge.

C. Pulses plus dc bias experiments

In this set of experiments the voltage profile consisted of 3 kV 8-ns (FWHM) ionization pulses superimposed on 2 kV dc bias voltage. The pulse repetition rate was 10 kHz and the plasma was run for 10 s. The results of surface potential measurements are presented in Fig. 3. As in the case of a sinusoidal voltage, the charge builds up far downstream the plasma region. As can be seen from Fig. 3, the magnitude of the surface potential is quite close to that of the bias voltage, while the magnitude of the ionization pulse voltage has little effect.

We next examined how quickly the surface charge builds up. At a selected dc bias voltage, a predetermined number of pulses were sent to the actuator, and then the surface potential was measured. A typical result is shown at Fig. 4. Even though for a small number of pulses the accuracy of measurements is low, it can be seen that even a single pulse

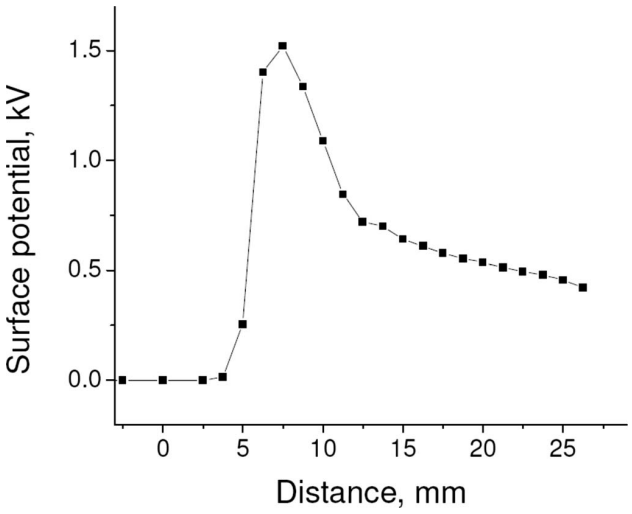

FIG. 2. Surface potential distribution. Applied voltage profile: Sinusoidal 3 kHz, 10 kV peak-to-peak. Electrodes edge at 0.

creates a noticeable surface charge. As the number of pulses increases, the surface charge builds up and moves farther away from the plasma. After thousands of pulses, the surface charge is close to its steady-state value. We have also found that 2 kV bias voltage itself builds up some surface charge at the dielectric. The charge is smaller then the one built by a single pulse but is still significant. We have also found that positive pulses added to positive bias are significantly more efficient in depositing the charge on the surface than other combinations of the pulse and bias polarities. This effect is illustrated in Fig. 5.

The purpose of the next set of experiments was to study the evolution of the surface charge with time after the discharge has been turned off. The results for positive polarity of the bias voltage are presented in Fig. 6. (In the case of negative polarity the potential distribution looks very similar.[24]) As seen in Fig. 6, the charge persists for a very long time. In 30 min it depletes by only 15%–20%. There is uniformly slow charge depletion from the surface in the region of low gradients of the charge concentration and a relatively fast depletion close to the exposed electrode in the region of high gradients. The fact that the depletion occurs at the same rate for both positive and negative charge is consistent with the charged particles at the dielectric surface being positive and negative ions from the gas rather than electrons.

An experiment was conducted with a plasma actuator in which a conventional Kapton tape was substituted by a low-static Kapton tape of the same thickness.[24] The results show that the depletion rate is faster for the low-static Kapton tape, but the characteristic time is still of the order of tens of minutes.

Note that Roth *et al.*[32] also observed the slow depletion of the residual surface charge on the dielectric after the driving voltage was turned off. The typical time periods were up to 30 s, which is much shorter than the times we observed. This difference may be associated with the difference in dielectric materials and configuration of the electrodes.

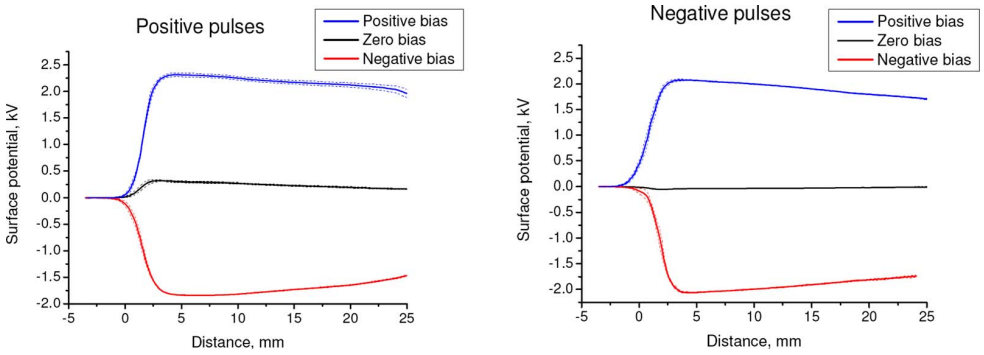

FIG. 3. (Color online) Surface potential distribution. Applied voltage profile: 2 kV dc bias, 3 kV pulses at 10 kHz PRR.

III. CALCULATION OF THE SURFACE CHARGE DENSITY

In order to interpret the experimental data and to infer the surface charge density from the measured surface potential, we used a numerical model based on the two-dimensional Poisson solver for the electric potential. We considered the DBD plasma actuator consisting of 2 electrodes of length 2.5 cm, separated by the 100 micron Kapton tape, i.e., the same configuration as in the experiments. The electrodes were assumed to be infinitely thin. The size of the computational domain was 25 mm by 1 mm. The computational domain included the entire lower (encapsulated) electrode and 5 mm of the upper (exposed) electrode. The reason for neglecting the remaining part of the upper electrode is its insignificant contribution to the electric potential on the surface. Since the electric potential distribution was measured experimentally after the DBD was turned off, and the recombination time of the plasma is of the order of microseconds, the gas above the dielectric was considered noncharged.

In the computations, the distribution of charge on the dielectric surface that would match the experimentally measured profile was obtained. Thus, having the experimentally measured potential, we reproduced the 2D electric potential distribution and the surface charge for each temporal measurement as the charge decayed. Figure 7 shows the calculated 2D electric potential distribution for the case of 3 kV negative pulses, 2 kV positive dc bias, right after the applied voltage was turned off. Figure 8 shows the calculated surface charge for the case of 3 kV negative pulses, 2 kV positive bias. As seen in Fig. 8, the surface charge is mainly located ~5–20 mm downstream of the exposed electrode. The peak surface charge density corresponds to ~1 ion per 5 ×5 (nm) (Ref. 2) site, which is a coverage of a few percent.

IV. THREE-ELECTRODE CONFIGURATION OF DBD PLASMA ACTUATORS

One of the results of our numerical simulations[7,28] of DBD actuators driven by repetitive nanosecond pulses superimposed on a dc bias was the prediction of a significant effect of the dc bias voltage on the plasma produced tangential gas velocity and thrust. However, the experiments[26] did not show such an effect. The reason was found to be the surface charge which builds up in tens or hundreds of pulses and which shields the applied bias field. Indeed, the DBD induced tangential flow velocity and thrust depend quite strongly on the voltage amplitude.[4–7,15,24–28] Thus, a reduction in the effective voltage on the plasma caused by the surface charge results in a significant decrease in the actuator performance. The numerical model[7,27] could not include large numbers of pulses and intervals between those due to

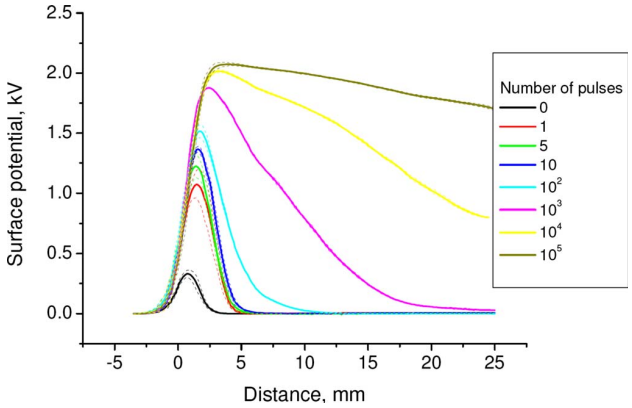

FIG. 4. (Color online) Surface potential for a fixed number of pulses. Applied voltage profile: Positive 2 kV dc bias, negative 3 kV pulses at 10 kHz PRR.

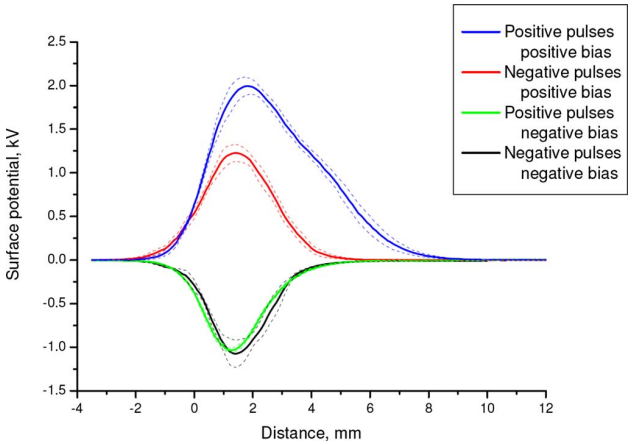

FIG. 5. (Color online) Surface potential after five ionizing pulses for different pulses and bias polarities.

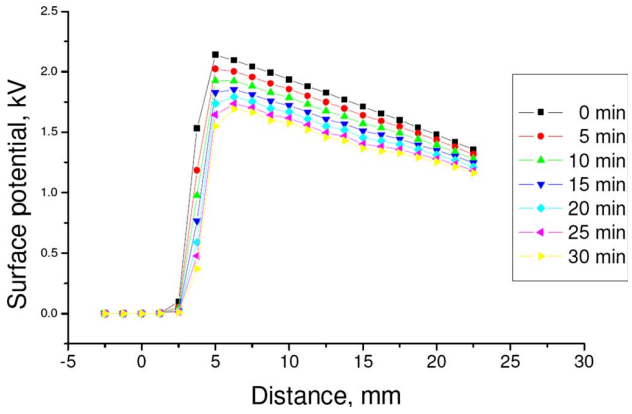

FIG. 6. (Color online) Surface potential vs time for positive surface charge. (Negative 3 kV pulses, positive 2 kV dc voltage.)

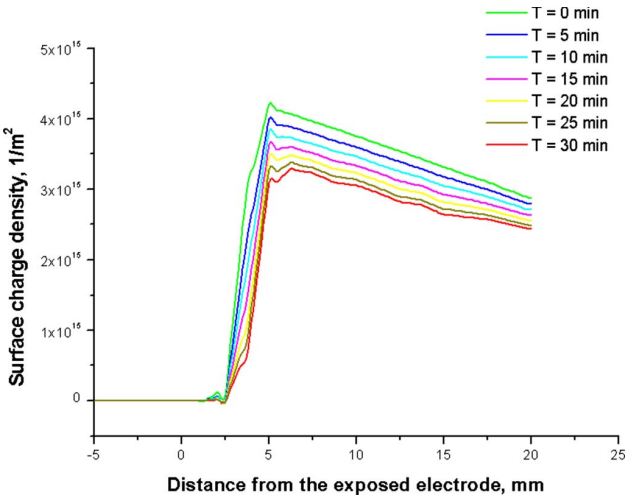

FIG. 8. (Color online) Calculated charge density on the dielectric surface at different moments of time after the DBD was turned off. (Negative 3 kV pulses, positive 2 kV dc voltage.)

numerical difficulties; the total number of pulses in the computations never exceeded 4–5. Since several pulses deposit only little charge on the surface, the modeling did not capture the potential shielding and the performance decrease that occur after hundreds and thousands of pulses.

As a solution to the surface charge build up problem, it was proposed[26] to switch the bias periodically. This improved the DBD actuator performance.[26] However, in this paper we found that the surface charge builds up far downstream from the plasma. It would therefore be desirable to remove the surface charge as it builds up downstream of the exposed electrode. We therefore proposed a modification to the actuator configuration. In the new configuration, the dielectric covers only part of the lower electrode, leaving the rest of the electrode exposed, as shown in Fig. 9. In such a case the surface charge cannot build up far downstream and the dc bias voltage is not shielded. Some preliminary results of thrust measurements can be found in Ref. 24. The surface potential profile for the configuration of Fig. 9 after 10 s of running the plasma is shown in Fig. 10. A comparison of Figs. 3 and 10 shows that the surface charge has indeed been substantially reduced by exposing the electrode downstream of the plasma. Although gas dynamic measurements are outside the scope of this paper, the surface charge reduction accomplished by exposing the electrode downstream of the plasma can be expected to result in enhanced induced gas velocity and thrust.

Note that if a relatively thick dielectric layer is used, then simply cutting the dielectric layer off over a part of the lower electrode would produce a "step" which can be detrimental to aerodynamic drag. A simple modification of the idea would then be to put a third electrode on the surface and to electrically connect this electrode with the encapsulated electrode, rather than cutting the dielectric off.

The three-electrode DBD configuration resembles that of the sliding discharge.[9–11] However, in sliding discharges the plasma actually reaches both exposed electrodes. In contrast, in the three-electrode DBD discharge proposed here, the electrons would not reach the auxiliary electrode whose purpose is simply to reduce or eliminate the charge accumulation on the dielectric surface.

V. CONCLUSIONS

In this work, surface charge dynamics in DBD plasma actuators were studied. Direct dielectric surface potential measurements showed that the electric field of the surface charge can dramatically distort the field produced by the voltage applied to the electrodes and thus reduce the actuator

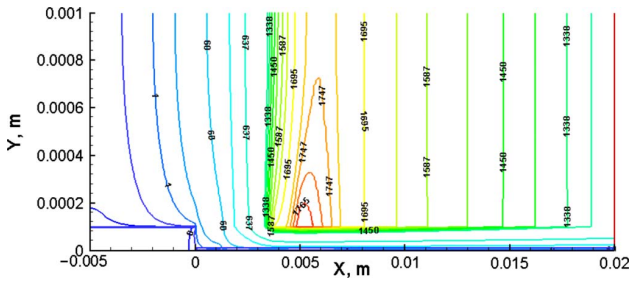

FIG. 7. (Color online) Calculated 2D electric potential distribution based on the experimental data for the electric potential on the dielectric surface right after the voltage applied to DBD was turned off. (Negative 3 kV pulses, positive 2 kV dc voltage.)

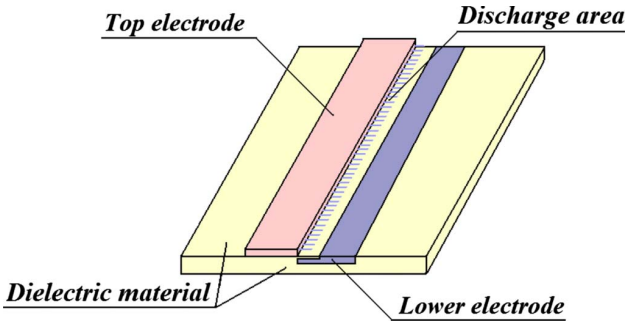

FIG. 9. (Color online) Modified DBD plasma actuator.

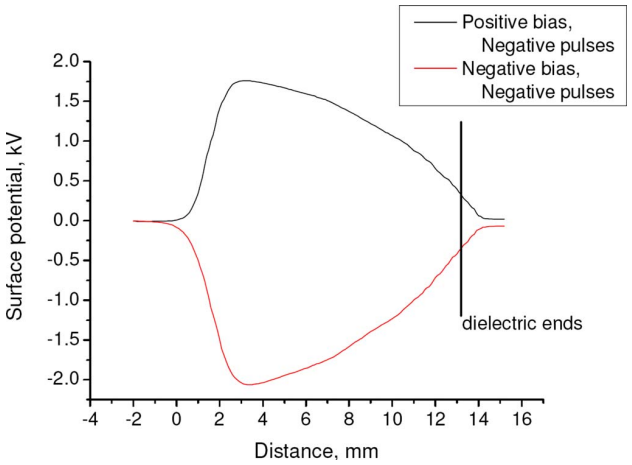

FIG. 10. (Color online) Surface potential distribution at modified DBD plasma actuator. Applied voltage profile: 2 kV dc bias, 3 kV pulses at 10 kHz PRR.

performance. For a sinusoidal voltage profile, significant positive charge builds up at the dielectric surface in the region *far downstream* of the plasma. For the "pulses plus dc bias" voltage waveform the dielectric surface potential depends primarily on the bias voltage. In particular, the sign of the surface potential coincides with the bias polarity. The surface charge builds up relatively quickly (in a few pulses) and depletes slowly (in tens of minutes). Based on the results of the surface potential measurements, a three-electrode configuration of DBD plasma actuators was proposed.

ACKNOWLEDGMENTS

This work was supported in part by NASA Glenn Research Center (Dr. David Ashpis), and in part by the Air Force Office of Scientific Research (Dr. John Schmisseur).

[1]E. Moreau, J. Phys. D **40**, 605 (2007).
[2]J. R. Roth, D. M. Sherman, and S. P. Wilkinson, *Proceedings of the 46th AIAA Aerospace Sciences Meeting and Exhibit, Reno, NV, 1998* (AIAA, Washington, D.C., 1998), Paper No. AIAA-1998-328.
[3]J. Pons, E. Moreau, and G. Touchard, J. Phys. D **38**, 3635 (2005).
[4]D. Orlov, T. Corke, and M. Patel, *Proceedings of the 46th AIAA Aerospace Sciences Meeting and Exhibit, Reno, NV, 2006* (AIAA, Washington, D.C., 2006), Paper No. AIAA-2006-1206.
[5]C. L. Enloe, T. E. McLaughlin, R. D. VanDyken, K. D. Kachner, E. J. Jumper, and T. C. Corke, AIAA J. **42**, 589 (2004).
[6]C. L. Enloe, T. E. McLaughlin, R. D. VanDyken, K. D. Kachner, E. J. Jumper, T. C. Corke, M. Post, and O. Haddad, AIAA J. **42**, 595 (2004).
[7]A. V. Likhanskii, M. N. Shneider, S. O. Macheret, and R. B. Miles, J. Appl. Phys. **103**, 053305 (2008).
[8]J. P. Boeuf and L. C. Pitchford, J. Appl. Phys. **97**, 103307 (2005).
[9]C. Louste, G. Artana, E. Moreau, and G. Touchard, J. Electrost. **63**, 615 (2005).
[10]C. Louste, E. Moreau, and G. Touchard, *Proceedings of the ESA-IAS-IEJ Joint Symposium, Berkeley* (Laplacian Press, Morgan Hills, CA, 2006).
[11]B. Arad, Y. Gazit, and A. Ludmirsky, J. Phys. D **20**, 360 (1987).
[12]D. Orlov, G. Font, and D. Edelstein, *Proceedings of the 46th AIAA Aerospace Sciences Meeting and Exhibit, Reno, NV, 2008* (AIAA, Washington, D.C., 2008), Paper No. AIAA-2008-1409.
[13]C. A. Borghi, A. Cristofolini, M. Carraro, and G. Neretti, *Proceedings of the 37th AIAA Plasma Dynamics and Lasers Conference, San Francisco, CA, 2006* (AIAA, Washington, D.C., 2006), Paper No. AIAA-2006-3380.
[14]Y. V. Shcherbakov, N. S. Isanov, N. D. Baryshev, V. S. Frolovskij, and V. S. Syssoev, *Proceedings of the 31st AIAA Plasma Dynamics and Lasers Conference, Denver, CO, 2000* (AIAA, Washington, D.C., 2000), Paper No. AIAA-2000-2670.
[15]M. L. Post and T. C. Corke, *Proceedings of the 43th AIAA Aerospace Sciences Meeting and Exhibit, Reno, NV, 2005* (AIAA, Washington, D.C., 2005), Paper No. AIAA-2005-563.
[16]D. F. Opaits, D. V. Roupassov, A. Yu. Starikovskii, I. N. Zavialov, and S. G. Saddoughi, *Proceedings of the 43th AIAA Aerospace Sciences Meeting and Exhibit, Reno, NV, 2005* (AIAA, Washington, D.C., 2005), Paper No. AIAA-2005-1180.
[17]L. S. Hultgren and D. E. Ashpis, *Proceedings of the 41th AIAA Aerospace Sciences Meeting and Exhibit, Reno, NV, 2003* (AIAA, Washington, D.C., 2003), Paper No. AIAA-2003-1025.
[18]J. R. Roth, Phys. Plasmas **10**, 2117 (2003).
[19]S. Grundmann and C. Tropea, *Proceedings of the 46th AIAA Aerospace Sciences Meeting and Exhibit, Reno, NV, 2008* (AIAA, Washington, D.C., 2008), Paper No. AIAA-2008-1369.
[20]A. Hoskinson and N. Hershkowitz, *Proceedings of the 46th AIAA Aerospace Sciences Meeting and Exhibit, Reno, NV, 2008* (AIAA, Washington, D.C., 2008), Paper No. AIAA-2008-1370.
[21]G. I. Font, C. L. Enloe, T. E. McLaughlin, and D. Orlov, *Proceedings of the 45th AIAA Aerospace Sciences Meeting and Exhibit, Reno, NV, 2007* (AIAA, Washington, D.C., 2007), Paper No. AIAA-2007-188.
[22]C. L. Enloe, T. E. McLaughlin, J. W. Gregory, R. A. Medina, and W. S. Miller, *Proceedings of the 46th AIAA Aerospace Sciences Meeting and Exhibit, Reno, NV, 2008* (AIAA, Washington, D.C., 2008), Paper No. AIAA-2008-1103.
[23]Yu. P. Raizer, M. N. Shneider, and N. A. Yatsenko, *Radio-Frequency Capacitive Discharges* (CRC, Boca Raton, 2006).
[24]D. Opaits, A. Likhanskii, M. Shneider, G. Neretti, S. Zaidi, S. Macheret, and R. Miles, *Proceedings of the 46th AIAA Aerospace Sciences Meeting and Exhibit, Reno, NV, 2008* (AIAA, Washington, D.C., 2008), Paper No. AIAA-2008-1372.
[25]A. Likhanskii, V. Semak, D. Opaits, M. Shneider, R. Miles, and S. Macheret, *Proceedings of the 46th AIAA Aerospace Sciences Meeting and Exhibit, Reno, NV, 2008* (AIAA, Washington, D.C., 2008), Paper No. AIAA-2008-1380.
[26]D. Opaits, A. Likhanskii, M. Shneider, G. Neretti, S. Zaidi, S. Macheret, and R. Miles, *Proceedings of the 38th Plasma Dynamics and Lasers Conference, Miami, FL, 2007* (AIAA, Washington, D.C., 2007), Paper No. AIAA-2007-4532.
[27]A. Likhanskii, M. Shneider, D. Opaits, S. Macheret, and R. Miles, *Proceedings of the 38th Plasma Dynamics and Lasers Conference, Miami, FL, 2007* (AIAA, Washington, D.C., 2007), Paper No. AIAA-2007-4533.
[28]A. Likhanskii, M. Shneider, S. Macheret, and R. Miles, *Proceedings of the 44th AIAA Aerospace Sciences Meeting and Exhibit, Reno, NV, 2006* (AIAA, Washington, D.C., 2006), Paper No. AIAA-2006-1204.
[29]A. Likhanskii, M. Shneider, S. Macheret, and R. Miles, *Proceedings of the 45th AIAA Aerospace Sciences Meeting and Exhibit, Reno, NV, 2007* (AIAA, Washington, D.C., 2007), Paper No. AIAA-2007-633.
[30]F. Massines, R. B. Gadri, A. Rabehi, Ph. Decomps, P. Segur, and Ch. Mayoux, J. Appl. Phys. **83**, 2950 (1998).
[31]R. Ben Gadri, IEEE Trans. Plasma Sci. **27**, 36 (1999).
[32]J. R. Roth, J. Rahel, X. Dai, and D. M. Sherman, J. Phys. D **38**, 555 (2005).

APPLIED PHYSICS LETTERS **94**, 061503 (2009)

Electrodynamic effects in nanosecond-pulse-sustained long dielectric-barrier-discharge plasma actuators

D. F. Opaits,[a] M. N. Shneider, and R. B. Miles
Applied Physics Group, Mechanical and Aerospace Engineering, Princeton University, Princeton, New Jersey 08540, USA

(Received 17 November 2008; accepted 19 January 2009; published online 10 February 2009)

Both numerical and experimental studies of the voltage distribution in a pulsed long dielectric barrier discharge plasma actuator have been performed. The results demonstrate the importance of electrodynamic effects in actuators for which the length is comparable with the length of the propagating pulses. These effects lead to a nonuniform voltage distribution along the electrodes, voltage doubling at the end of the actuator, nonoptimized power coupling to the actuator, and ringing. In addition to the direct voltage measurements, images of the discharge were taken which revealed its nonuniform structure. © *2009 American Institute of Physics*.
[DOI: 10.1063/1.3081027]

The most promising prospective application of the asymmetric dielectric barrier discharge (DBD) plasma actuator is flow control over an airfoil.[1–6] Recently, a number of both numerical[7] and experimental[8–10] works have demonstrated the effectiveness of nanosecond, high voltage pulse sustained DBDs in achieving improved performance for the generation of surface flow for control authority. While these pulse sustained devices have worked well for laboratory size models (tens of centimeters in spanwise direction) important issues arise when it comes to scaling the pulse sustained actuator to the practical airfoil sizes (several meters spanwise).

If the actuator is extended across a wing its size may become comparable with physical length of the high voltage pulse or to the wavelength of the applied rf voltage if the actuator discharge is sustained by a rf generator. In such case the electrodes cannot be considered equipotential anymore and the wave nature of the electromagnetic signal propagating along the long line (the actuator) must be taken into account. This effect can lead to variations in the voltage along the actuator, voltage doubling at the end, nonoptimized power coupling into the actuator, and ringing due to mismatched impedance of the cable and the actuator. The nonuniform voltage distribution across electrodes was observed for the first time in rf driven CO_2 lasers of slab geometry by Lapucci *et al.*[11] Theory of the phenomenon was later developed by Raizer and Shneider.[12] Later a similar problem was studied for large-area rf plasma chemical reactors by Lieberman *et al.*[13]

The plasma actuator used for this study was 2.4 m long and was connected to the pulse generator at one end, as shown in Fig. 1. The electrodes were made of copper foil. The width and thickness of the electrodes were 25 mm and 100 μm, respectively, which resulted in resistance $R=1.34\times10^{-2}$ $\Omega\,\mathrm{m}^{-1}$. A 100 μm thick kapton tape was used as the dielectric. The actuator's capacitance was measured experimentally using a Fluke 189 multimeter and found to be $C=127$ pF m^{-1}. Its inductance was found to be $L=0.178$ $\mu\mathrm{H}\,\mathrm{m}^{-1}$ by measuring the pulse propagation speed $v=2.1\times10^{8}$ $\mathrm{m\,s}^{-1}$ in the actuator and using the expression $v=1/\sqrt{LC}$. The impedance of the actuator can be found from the expression $Z_{\mathrm{actuator}}=\sqrt{L/C}=37$ Ω. The voltage was monitored with PP005A 500 MHz LeCroy voltage probe connected to WavePro 7300A 3GHz LeCroy oscilloscope.

The experiments were conducted for low and high voltage pulses. The low voltage pulses were used to measure the pulse propagation speed in the absence of the plasma, which may introduce significant dissipation. A Stanford Research Systems pulse generator was used as a source and the pulses were applied to one end of the actuator through a 50 Ω cable. High voltage pulses of negative polarity were used to ignite the plasma and observe the visible appearance of the discharge. These pulses were generated by FPG 25–200MC4 pulser by FID Technology. The pulse profiles are shown in Fig. 2.

The signal propagation in a long line is described by telegraph equations

$$C\frac{\partial u}{\partial t}+Gu+\frac{\partial i}{\partial x}=0, \tag{1}$$

$$L\frac{\partial i}{\partial t}+Ri+\frac{\partial u}{\partial x}=0, \tag{2}$$

where u and i are voltage and current; L, C, G, and R are the impedance parameters specified per unit length—inductance, capacitance, leakage conductance, and resistance correspondingly. The values of the impedance parameters were taken from the experiment and are specified above. The leakage conductance was considered to be negligibly low.

A numerical code has been developed to solve the set of telegraph [Eqs. (1) and (2)] using a second order Lax–Wendroff method coupled with Flux Corrected Transport

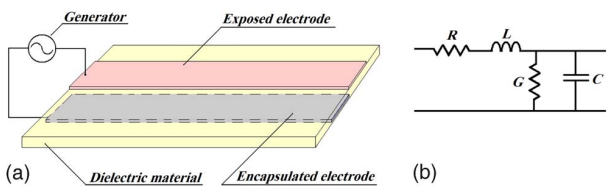

FIG. 1. (Color online) DBD plasma actuator (a) and schematic representation of its elementary components (b).

[a]Electronic mail: dopaits@princeton.edu.

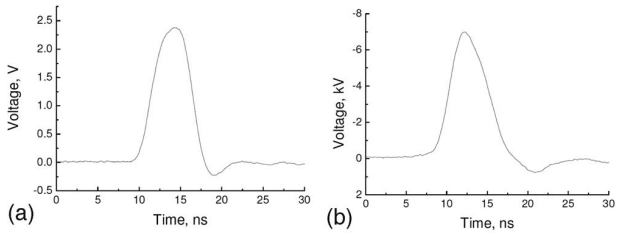

FIG. 2. Low (a) and high (b) voltage pulse profiles.

technique.[14–16] Proper boundary conditions for forward and reversed waves, see for instance,[17] were imposed at the cable/actuator connection point as well as at the end of actuator (open circuit). The code allows simulation of the actuator with an arbitrary active (noninductive resistor) or reactive (inductor, capacitor) load at the end.

Results of both numerical simulation and experimental measurements of the low voltage nanosecond pulse in the long plasma actuator are presented in Fig. 3. The diagrams show the time evolution of the voltage distribution along the actuator. Negative values of the distance correspond to the voltage in the connecting cable. The finite capacitance (11 pF) of the voltage probe caused the small amount of pulse broadening seen in the comparison of the modeled voltage (left) with the measured voltage (right).

Several phenomena characteristics of long lines can be recognized in these diagrams. First of all, the voltage distribution is not uniform along the electrodes. Second, the pulse doubles at the end of the actuator which we expect to happen with a high impedance load. This leads to nonuniform discharge parameters along the actuator.

Also the impedance matching of the connecting cable and the DBD actuator is important. The mismatch leads to poor power coupling from the cable to the actuator as can be seen from the modeling. In this particular case the impedances have values which are close ($Z_{cable}=50\ \Omega$ and $Z_{actuator}=37\ \Omega$) so the effect is not particularly strong, but it is still observable. Similarly, a part of the pulse reflects on its way back to the cable which creates a ringing effect, which can be seen most clearly in the model results. By choosing the proper dimensions and dielectric constant, the actuator could be designed in a way to match the cable impedance. It means that pulse would be transferred from the cable to the actuator and back without any distortion and losses, so there would not be any ringing effect or poor power coupling. The finite conductivity of the electrodes did not play a significant role in the pulse propagation.

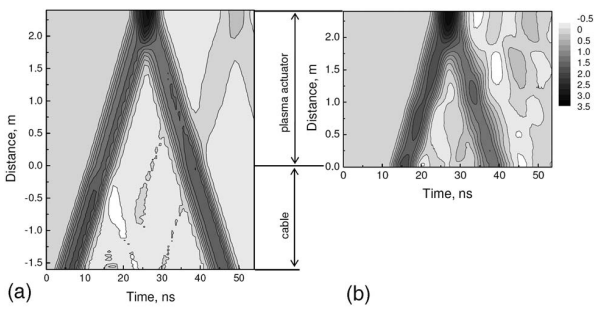

FIG. 3. Pulse propagation along the actuator. Numerical (a), experimental (b).

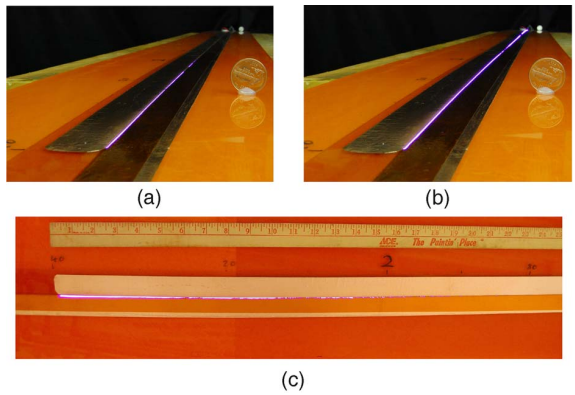

FIG. 4. (Color online) Images of DBD at different voltages. (a) low voltage, (b) high voltage, (c) low voltage seen from above.

Experiments with the high voltage nanosecond pulses were conducted in order to observe the plasma nonuniformity visually. The pictures of the discharge at different pulse voltages are shown in Fig. 4. The top left picture, Fig. 4(a), corresponds to the pulse voltage slightly below the breakdown value. The discharge ignites only at the far end where the pulse voltage doubles. In the second picture, Fig. 4(b), the pulse voltage is higher than the breakdown value and the discharge ignites along the whole length of the actuator. The image in Fig. 4(c), which is the top view of Fig. 4(a), shows the nonuniformity of the discharge, which becomes brighter and wider toward the end of the actuator. Gaps in the discharge are due to local variations in the electrode edges.

Experiments on the nonuniformity of the pulse voltage distribution in a long DBD plasma actuator have been conducted. Images of the discharge appearance have been taken and direct voltage distribution measurements have been made. The images demonstrate the discharge nonuniformity. Numerical modeling of short pulse propagation in long lines has also been performed and agreement between the experimental and the simulated voltage distribution was obtained. The results show the importance of the wave nature of pulse propagation. This results in a nonuniform potential distribution along the electrodes, a doubling of the pulse voltage, at the end of the actuator, nonoptimized power coupling, ringing effects, etc.

This work was supported in part by a grant from the Air Force Office of Scientific Research (Dr. John Schmisseur, Program Manager) and in part by NASA Glenn Research Center (Dr. David Ashpis, Program Manager).

[1]E. Moreau, J. Phys. D **40**, 605 (2007).
[2]C. L. Enloe, T. E. McLaughlin, R. D. VanDyken, K. D. Kachner, E. J. Jumper, and T. C. Corke, AIAA J. **42**, 589 (2004).
[3]C. L. Enloe, T. E. McLaughlin, R. D. VanDyken, K. D. Kachner, E. J. Jumper, T. C. Corke, M. Post, and O. Haddad, AIAA J. **42**, 595 (2004).
[4]J. R. Roth, J. Rahel, X. Dai, and D. M. Sherman, J. Phys. D **38**, 555 (2005).
[5]B. Jayaraman, Y.-C. Cho, and W. Shyy, Proceedings of the 38th AIAA Plasmadynamics and Lasers Conference, Miami, Florida, 2007 (unpublished).
[6]M. A. Huerta and L. D. Ludeking, Proceedings of the 38th AIAA Plasmadynamics and Lasers Conference, Seattle, Washington, 2008 (unpublished).
[7]A. V. Likhanskii, M. N. Shneider, S. O. Macheret, and R. B. Miles, J. Appl. Phys. **103**, 053305 (2008).
[8]D. F. Opaits, A. V. Likhanskii, G. Neretti, S. Zaidi, M. N. Shneider, R. B.

Miles, and S. O. Macheret, J. Appl. Phys. **104**, 043304 (2008).
[9]D. F. Opaits, D. V. Roupassov, A. Yu. Starikovskii, I. N. Zavialov, and S. G. Saddoughi, Proceedings of the 43th AIAA Aerospace Sciences Meeting and Exhibit, Reno, Nevada, 2005 (unpublished).
[10]D. V. Roupassov, I. N. Zavyalov, and A. Yu. Starikovskii, Proceedings of the 44th AIAA Aerospace Sciences Meeting and Exhibit, Reno, Nevada, 2006 (unpublished).
[11]A. Lapucci, F. Rossetti, M. Giofini, and G. Orlando, IEEE J. Quantum Electron. **31**, 1537 (1995).
[12]Y. P. Raizer and M. N. Shneider, IEEE Trans. Plasma Sci. **26**, 1017 (1998).
[13]M. A. Lieberman, J. P. Booth, P. Chabert, J. M. Rax, and M. M. Turner, Plasma Sources Sci. Technol. **11**, 283 (2002).
[14]P. D. Lax and B. Wendroff, Commun. Pure Appl. Math. **13**, 217 (1960).
[15]E. S. Oran and J. P. Boris, *Numerical Simulation of Reactive Flow* (Cambridge University Press, Cambridge, England, 2000).
[16]Y. N. Dnestrovskii and D. P. Kostomarov, *Numerical Simulation of Plasmas* (Springer, Berlin, 1985).
[17]P. N. Herbert, *Introductory Electromagnetics* (Wiley, New York, 1991).

Eur. Phys. J. Appl. Phys. **47**, 22802 (2009)
DOI: 10.1051/epjap/2009081

THE EUROPEAN PHYSICAL JOURNAL APPLIED PHYSICS

Regular Article

Non-thermal atmospheric pressure plasmas for aeronautic applications

R.B. Miles[1,a], D.F. Opaits[1], M.N. Shneider[1], S.H. Zaidi[1], and S.O. Macheret[2]

[1] Department of Mechanical and Aerospace Engineering, Princeton University, Princeton, NJ 08544, USA
[2] Lockheed Martin Aeronautics Company, Palmdale, CA 93599, USA

Received: 27 November 2008 / Accepted: 12 February 2009
Published online: 14 May 2009 – © EDP Sciences

Abstract. Dielectric barrier surface discharges (DBD) have the potential to act as flush mounted flow control devices for separation control and other aeronautic applications. A pulse-sustained plasma with the ions driven by a DC bias voltage is proposed for optimum performance. While characterizing these devices, it was found that their performance is severely limited by surface charge build-up. That charge builds up rapidly and remains for as long as hours. Work in this paper shows that the surface charge can be mitigated by using a reversing DC bias potential or by using a constant DC bias potential with a partially covered electrode.

PACS. 52.40.Hf Plasma-material interactions; boundary layer effects – 47.85.L- Flow control – 52.80.-S Electric discharges

1 Introduction

Many recent studies have demonstrated the utility of dielectric barrier discharge (DBD) plasma actuators with offset electrodes (Fig. 1a) for aerodynamic control [1–5]. In particular, they have been shown to suppress boundary layer separation in low-speed flow on airfoils, so there has been great practical interest in developing this technology further. Typically, these DBD discharges are driven by high peak-to-peak sinusoidal voltages (tens of kilovolts), and they produce surface jets that are in the direction of the offset covered electrode, as shown by the arrow in Figure 1a. Understanding the physics of the process is still proceeding, with the current picture being that charge separation and attachment of electrons to the surface play a critical role. Modeling in our laboratory captured that process [6], and, with that insight, we predicted that a voltage waveform consisting of high-voltage nanosecond repetitive pulses superimposed on a DC bias voltage would produce significantly enhanced wall jet velocities compared with those generated with the conventional sinusoidal voltage. In this case, the plasma is generated and the charge separation formed by the repetitive short ionization pulses, and the momentum transfer to the neutral gas occurs due to the ions that are driven by the charge separation enhanced by the DC bias voltage. The advantage of this non-self-sustained discharge is that the parameters of ionizing pulses and the driving bias voltage can be varied independently, which adds efficiency and flexibility to control and optimization of the actuator performance. The nanosecond pulses accelerate electrons to high velocity between collisions, so the ionization process is more efficient, and the timing and repetition rate of the pulses can be optimized to minimize power and maximize thrust. The DC bias avoids the intermittent generation of thrust characteristic of AC driven systems, and thus can have a 100% duty cycle.

However, laboratory measurements with this pulse plus DC waveform did not yield the increased performance predicted. Upon closer inspection we observed that the jet velocity was high for a few pulses when the DC was turned on, but slowed significantly thereafter [7]. From this observation we determined that surface charge, which built up over a number of pulses, was limiting the performance [8,9]. This charge opposes the applied DC potential. This build-up process is not captured in the model because subnanosecond time steps are necessary, and the long build-up time exceeds the few microsecond single CPU computational limit. Further experiments [8–10] have shown that the same surface charge builds up in the conventional sinusoidal-driven DBD configuration, so it is important to develop approaches that will minimize its effect.

We have taken two approaches to overcome this charge build up. Both still rely on the high voltage nanosecond pulses to form the discharge. The first approach applies an alternating bias, which sweeps the charge off the dielectric,

[a] e-mail: miles@Princeton.EDU

Article published by EDP Sciences

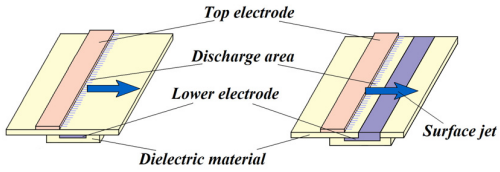

Fig. 1. (Color online) Dielectric barrier discharge configurations. (left) The standard configuration with an exposed upper electrode and a lower electrode, offset from the upper and covered with a think dielectric material. (right) The new configuration designed to suppress charge build up. Here the lower electrode is uncovered downstream to allow charge that builds up on the dielectric to bleed-off.

and the second approach is a change in the electrode geometry, with the buried electrode uncovered a few millimeters downstream (Fig. 1b). Both of these have shown some success in alleviating the problem [8,9].

2 Measurement of surface charge

The series of experiments we undertook to quantify the charge build-up used a non-contacting Trek Model 247-3 Electrostatic Voltmeter with Trek Model 6000B-13C Electrostatic Voltmeter Probe [8,9]. This probe has high resolution, fast response time (less then 3 ms for a 1 kV step), and an operating range from 0 to +/− 3 kV DC or peak AC. The spatial resolution of the probe is around 1 mm. Initial experiments were conducted for 3 kHz 10 kV peak-to-peak sinusoidal voltage profile. Since the sinusoidal profile is widely used in DBD experiments, the initial experiments were conducted with a sinusoidal voltage driven discharge (no pulses). The actuator was run for 15 s and then the surface potential was measured. The result is presented in Figure 2. As can be seen in the figure, there is a significant charge build-up on the dielectric in the region far downstream of the plasma. The plasma extends only a few millimeters downstream of the edge of the exposed electrode whereas the dielectric charges up to centimeters away from it. The maximum surface potential (1.5 kV) is comparable with the applied peak voltage (5 kV). This means that the electric field of the surface charge can dramatically distort the electric field produced by the voltage applied to the electrodes. Also, even though the applied voltage is symmetrical (sinusoidal with no bias voltage) the surface charge has a positive polarity.

We then conducted experiments with the pulse-sustained plasma using a DC bias. This was the configuration our modeling suggested would produce the highest thrust. Four kilovolt (4 kV) nanosecond pulses were applied at a rate of 10 kHz along with a DC bias of + or −2 kV. The plasma was run for 15 s. Results of surface potential measurements are presented in Figure 3. As in the case of a sinusoidal voltage, the charge builds up far downstream the plasma region, and the magnitude of the surface potential is primarily determined by the bias voltage. The ionization pulse voltage has little effect on it. In order to determine how quickly the surface charge builds up at a selected DC bias voltage, a pre-determined number of pulses were sent to the actuator and then the surface potential was measured. The results are shown in Figure 4. Even though this was for a small number of pulses and the accuracy of measurements is low, it can be seen that a single pulse creates a noticeable surface charge. As the number of pulses increases, the surface charge builds up and moves farther away from the plasma. After it builds up, the surface charge remains for a very long time. Measurements shown in Figure 5 indicate that in 30 min it depletes only by 15–20 per cent. Since the depletion occurs at the same rate for both positive and negative charge, we can assume that the charged particles at the dielectric surface are positive and negative ions from the gas, not electrons or holes.

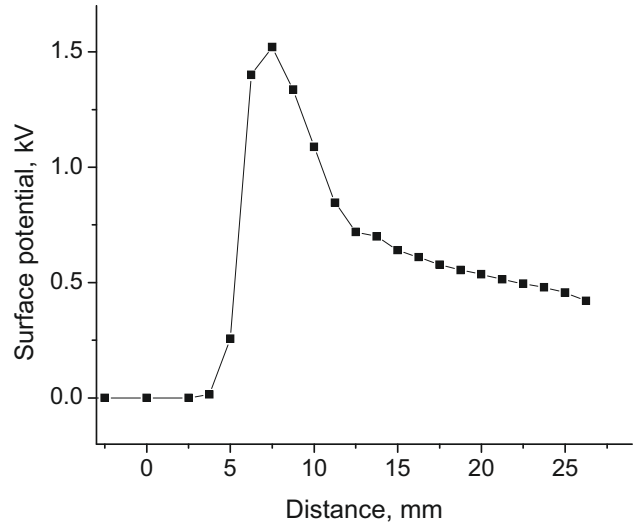

Fig. 2. Surface potential distribution. Applied voltage profile − sinusoidal 3 kHz, 10 kV peak-to-peak. Electrodes edge at 0.

In order to interpret the experimental data a numerical model, based on the described above Poisson solver, was developed [11]. The DBD plasma actuator consisted of 2 electrodes of length 2.5 cm, separated by the 100 micron Kapton tape. The electrodes were assumed to be infinitely thin. The computational model [11] was able to provide the distribution of charge on the dielectric surface, as shown in Figure 6. It is important to note that numerical results shown in Figure 6 correspond to potential distribution shown in Figure 5.

3 Periodically reversing bias for charge build up suppression

Our first approach to the minimization of the surface charge build-up has been to use a time-varying bias together with the high repetition rate pulses. We observed that, as long as the bias reverses, the build-up is of the

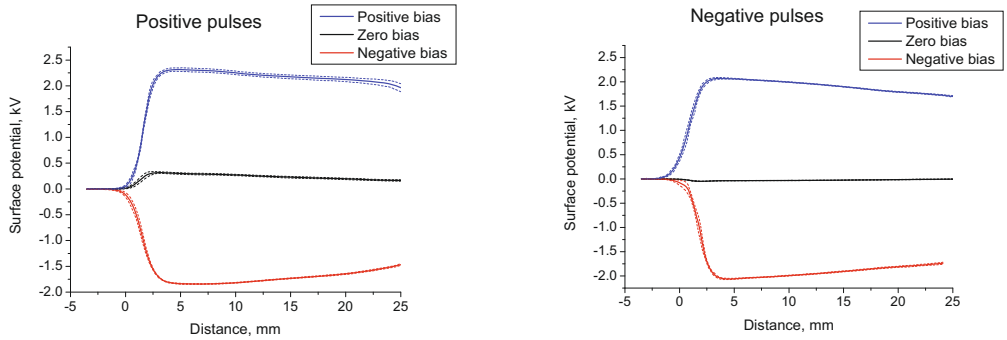

Fig. 3. (Color online) Surface potential distribution. Applied voltage profile +/− 2 kV DC bias, 3 kV pulses at 10 kHz PRR.

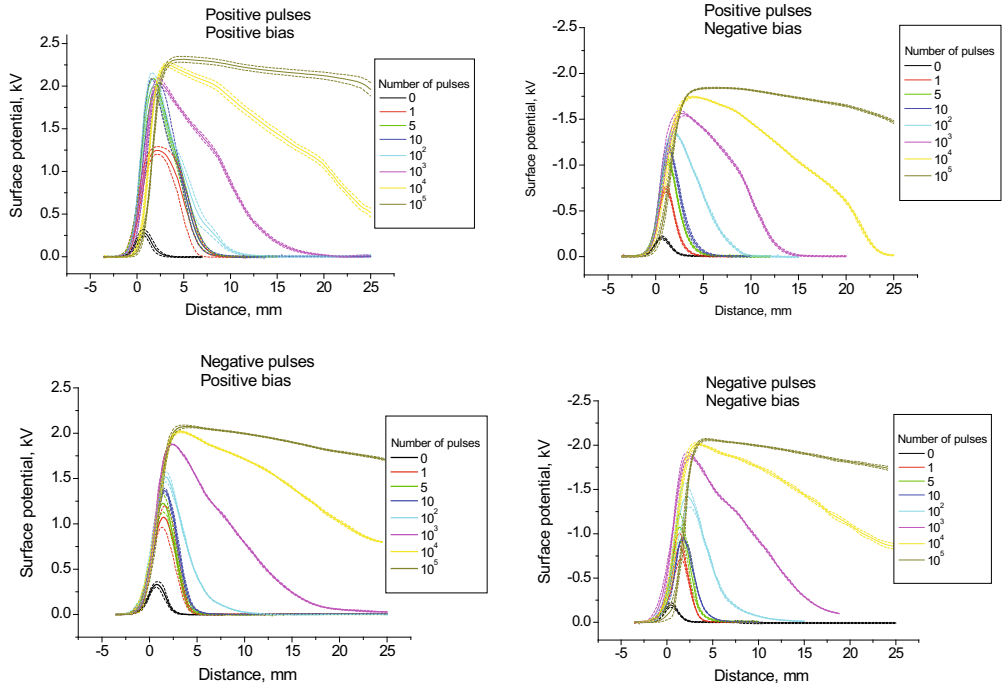

Fig. 4. (Color online) Surface potential for a fixed number of pulses. Applied voltage profile +/− 2 kV DC bias, 3 kV pulses at 10 kHz PRR.

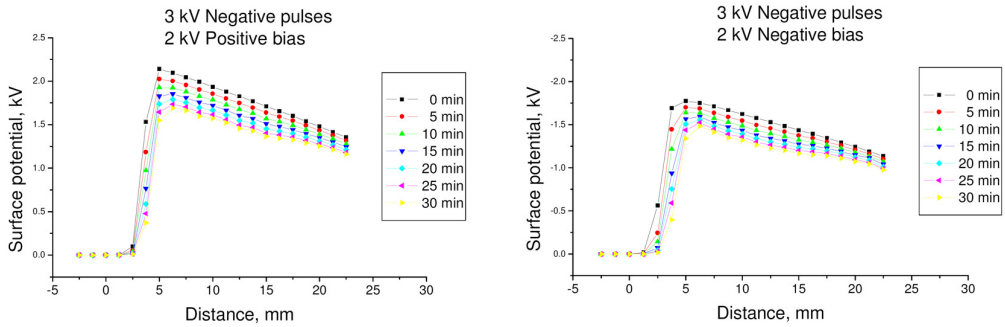

Fig. 5. (Color online) Surface potential versus time for positive (left) and negative (right) surface charges.

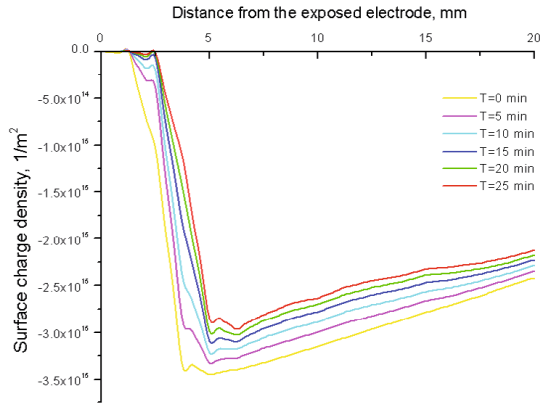

Fig. 6. (Color online) Calculated charge density on the dielectric surface at different moments of time after the DBD was turned off (negative 3 kV pulses, negative 2 kV DC voltage).

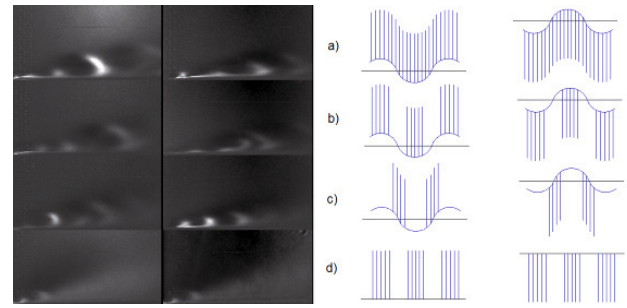

Fig. 7. (Color online) Images of surface vortexes taken at the same time relative to the sinusoidal wave form showing the variation is vortex speed for different pulse and bias configurations. Each full cycle of the bias voltage generates two vortexes, one during the positive half cycle and one during the negative half cycle.

opposite sign, so the overall performance of the device recovers each half cycle. Our experiments have used a schlieren technique and a thrust stand to evaluate the plasma actuator performance. The schlieren approach is totally non-intrusive and permits studies of the induced flow structure. The schlieren system illuminates the actuator from the side and images the induced surface jet. In order to obtain good visibility, the nanosecond pulser is run in a burst mode, synchronous with the time-varying bias voltage. This produces sequential surface jets that generate vortexes that propagate downstream. We have also undertaken computational modeling of the effects of these jets on the flow so that we can infer from the speed of the vortex the original speed of the surface jet [11]. These schlieren measurements allow us to determine the deleterious effects of long-time charge build-up on the surface and permit us to explore different pulse sequences, different bias waveforms and polarizations, and different geometries. Figure 7 shows a series of such measurements where the images on the left correspond to the pulse timing relative to sinusoidal bias sequences shown on the right. The sign of the applied pulses and the bias is defined as positive if the exposed top electrode is positive relative to the encapsulated bottom electrode. The bottom two images are for positive and negative nanosecond pulses without bias.

The measurement of the velocity of the vortex as it propagates downstream gives a relative measure of the speed of the surface jet. Computations indicate that the surface jet at the electrode is about ten times the speed of the propagating vortex [12]. The vortex speed is measured as a function of distance downstream from the edge of the upper electrode, and variations in the voltage, waveform, and pulse repetition rate show that the highest speed occurs with negative nanosecond pulses. In that case, the most important parameter controlling the speed of the jet is the bias voltage. In the experiments, the vortexes originating from the positive half cycle and the negative half cycle are separately recorded. Figure 8a shows the variation of the jet speed as a function of bias voltage for a sinusoidal bias with negative pulses applied at the peak of the positive half cycle, and Figure 8b shows the vortex speed for negative pulses applied at the peak of the negative half cycle. Both must be running at the same time to avoid significant charge build up, so these data were taken in sequence. Note that the peak vortex speed occurs for negative pulses during the positive bias half cycle and is around 3 m/s at 12 kV, corresponding to surface jet speeds of around 30 m/s.

Experiments on induced thrust measurements were conducted using a PL303 Mettler Toledo balance [8]. A Faraday cage was constructed to shield the balance from electronic noise. The actuator was mounted on a dielectric post and was operated with thrust either up or down so buoyancy effects were determined to be negligible. Parametric studies were made of the thrust and Figure 9 shows some of the results of those studies, indicating that the thrust increase is most dramatic with increasing bias voltage, as previously expected from Schlieren images. What is most interesting is that the thrust measured is much higher than achieved elsewhere at low bias voltages, as shown by the orange and blue lines on the left of Figures 10a and 10b. The same thrust is measured for 20 kV peak-to-peak bias as for 40 kV in the more conventional configuration. Note that the high bias voltages require much thicker dielectrics to avoid breakdown. These results indicate that the pulse plus bias approach has great promise for improved performance of DBD control devices. In our experiments the peak bias voltage was limited by the isolation circuit elements between the bias and the pulse forming electronics.

4 Partially covered electrode configuration for charge bleed off

Our second approach to the solution of the surface charge problem is a new electrode configuration that is intended to take advantage of the fact that the surface charge builds up far downstream from the plasma. In this new configuration, the dielectric covers only part of the lower electrode,

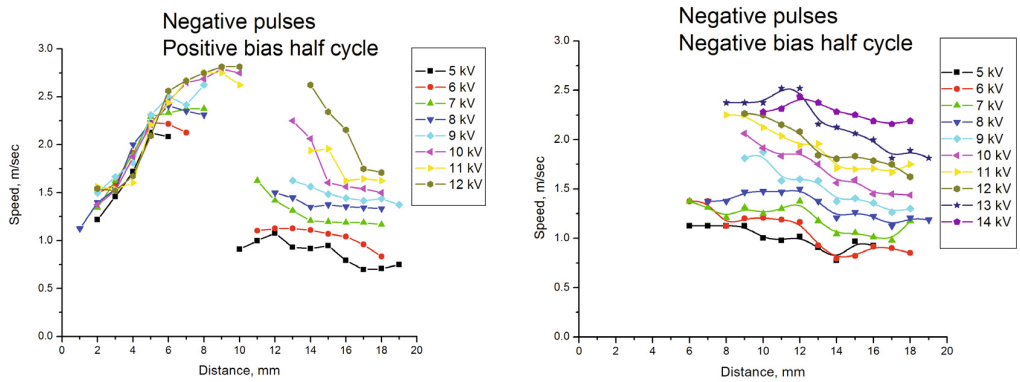

Fig. 8. (Color online) Vortex speed as a function of distance downstream of the upper electrode edge for negative high voltage pulses and sinusoidal bias voltages ranging from 5 to 12 kV. (right) Vortexes generated during the positive half cycle of the bias and (left) vortex generated during the negative half cycle of the bias.

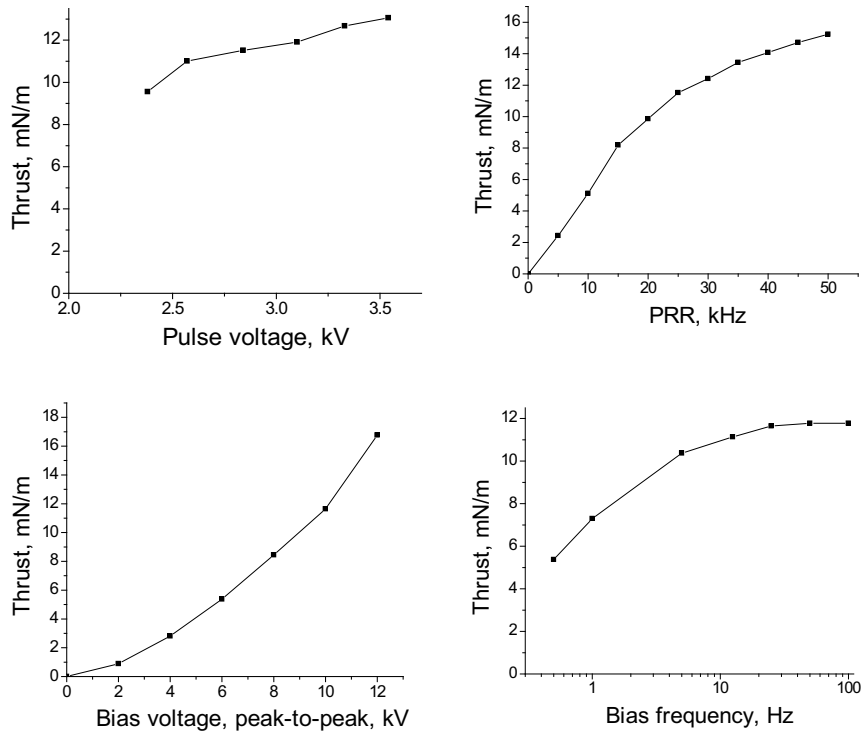

Fig. 9. Thrust dependence on applied voltage parameters. Negative pulses. Bias: square, 10 kV peak-to-peak, 100 Hz. Pulses: 3 kV, 25 kHz.

leaving the rest of the electrode exposed, as shown in Figure 1b. This configuration allows a return to the more effective repetitive nanosecond pulses plus DC bias concept. In such a case, the surface charge cannot build up far downstream and the shielding of the DC bias voltage is reduced. Some preliminary results are shown in green (far left curve) in Figures 10a and 10b. The induced thrust is greater than the DBD plasma actuator driven by repetitive pulses with an alternating sign 100 Hz square wave low frequency bias. The thrust for this new electrode configuration scales linearly with the bias voltage and nanosecond pulse repetition rate, at least in the low voltage regime that we have so far been able to explore. This actuator has a simpler bias voltage profile (DC but not AC) and there is 100% duty cycle because the bias voltage does not have to reverse.

5 Summary

Our work indicates that sustaining the plasma with repetitive high voltage nanosecond pulses and driving the ions with a bias leads to significantly improved performance of the flush mounted DBD surface control jet as compared

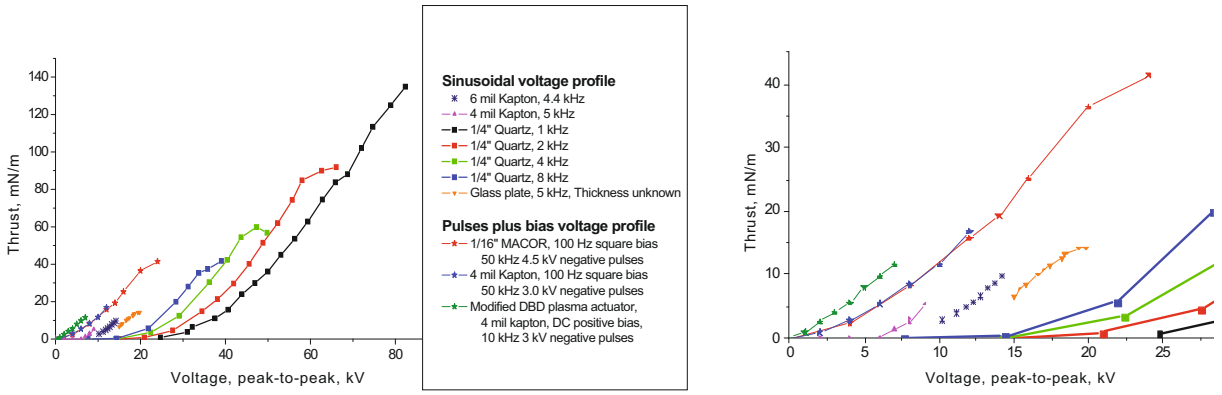

Fig. 10. (Color online) Thrust per unit length of the DBD electrode as a function of sinusoidal bias voltage for different configurations at Princeton and in the literature. (Right) is a close up of the left side of (left). The three curves on the left are with the Princeton pulse sustained plasma system operating at 50 kHz with a 100 Hz square wave bias a DC bias and the lower electrode partially covered with 4 mil kapton (green – farthest to the left).

to the conventional configuration driven with a sinusoidal high voltage. Ion charge build up on the dielectric surface inhibits the performance both for the conventional DBD configuration and for the pulse sustained concept. In order to suppress the charge build up, we show that either a reversing bias or a new electrode configuration can be used. The new electrode configuration exposes the lower electrode downstream of the dielectric coating, and thus provides a route for charge bleed off. Using this configuration, a DC bias can be applied leading to 100% duty cycle and high performance at low bias voltage. Scaling suggests that higher DC biases will lead to much improved performance compared to both the pulse sustained reversing bias configuration and the conventional sinusoidal configuration.

This work was supported in part by NASA Glenn Research Center (Dr. David Ashpis, contract Number NNX07AC02A), in part by the Air Force Office of Scientific Research (Dr. John Schmisseur).

References

1. J. Reece Roth, J. Phys. D: Appl. Phys. **40** (2007)
2. E. Moreau, J. Phys. D: Appl. Phys. **40**, 605 (2007)
3. R. Van Dyken, T. McLaughlin, C. Enloe, 42nd AIAA Aerospace Sciences Meeting and Exhibit, Reno, NV, 2004 (US Air Force Academy, Colorado Springs, CO AIAA-2004-846)
4. T. Corke, 44th AIAA Aerospace Sciences Meeting and Exhibit, Reno, NV, 2006 (University of Notre Dame, Notre Dame, IN, AIAA-2006-1208)
5. T.C. Corke, E.J. Jumper, M.L. Post, D. Orlov, T.E. Mclaughlin, 40th AIAA Aerospace Sciences Meeting & Exhibit, Reno, NV, 2002
6. A.V. Likhanskii, M.N. Shneider, S.O. Macheret et al., J. Appl. Phys. **103**, 053305 (2008)
7. D.F. Opaits, G. Neretti, A.V. Likhanskii, S. Zaidi, M.N. Shneider, R.B. Miles, S.O. Macheret, 38th Plasma Dynamics and Lasers Conference, Miami, FL, 2007 (AIAA-2007-4532)
8. D. Opaits, G. Neretti, S. Zaidi M. Shneider, R.B. Miles, A. Likhanskii, S. Macheret, 46th AIAA Aerospace Sciences Meeting, Reno, NV, 2008 (AIAA-2008-1372)
9. D.F. Opaits, M.N. Shneider, R.B. Miles, A.V. Likhanskii, S.O. Macheret, Phys. Plasmas **15**, 073505 (2008), doi:10.1063/1.2955767
10. C. Enloe, T. McLaughlin, J. Gregory, R. Medina, W. Miller, 46th AIAA Aerospace Sciences Meeting and Exhibit, Reno, NV, 2008 (AIAA-2008-1103)
11. A.V. Likhanskii, V.V. Semak, M.N. Shneider, D.F. Opaits, R.B. Miles, S.O. Macheret, 46th AIAA Aerospace Sciences Meeting, Reno, NV, 2008 (AIAA-2008-1380), p. 604
12. A. Likhanskii, D. Opaits, M. Shneider, S. Macheret, R. Miles, 38th AIAA Plasmadynamics and Lasers Conference, Miami, FL, 2007 (AIAA-2007-4533)

REPORT DOCUMENTATION PAGE		Form Approved OMB No. 0704-0188

1. REPORT DATE *(DD-MM-YYYY)*	2. REPORT TYPE	3. DATES COVERED *(From - To)*
01-09-2012	Final Contractor Report	January 1, 2007 to December 31, 2010

4. TITLE AND SUBTITLE
Plasma Actuators for Turbomachinery Flow Control
Final Report

5a. CONTRACT NUMBER
NNX07AC02A

5b. GRANT NUMBER

5c. PROGRAM ELEMENT NUMBER

6. AUTHOR(S)
Miles, Richard, B.; Shneider, Mikhail, N.

5d. PROJECT NUMBER

5e. TASK NUMBER

5f. WORK UNIT NUMBER
WBS 561581.02.08.03.21.66

7. PERFORMING ORGANIZATION NAME(S) AND ADDRESS(ES)
Princeton University
Princeton, New Jersey 08544

8. PERFORMING ORGANIZATION REPORT NUMBER
E-18231

9. SPONSORING/MONITORING AGENCY NAME(S) AND ADDRESS(ES)
National Aeronautics and Space Administration
Washington, DC 20546-0001

10. SPONSORING/MONITOR'S ACRONYM(S)
NASA

11. SPONSORING/MONITORING REPORT NUMBER
NASA/CR-2012-217654

12. DISTRIBUTION/AVAILABILITY STATEMENT
Unclassified-Unlimited
Subject Categories: 02, 07, 34, and 75
Available electronically at http://www.sti.nasa.gov
This publication is available from the NASA Center for AeroSpace Information, 443-757-5802

13. SUPPLEMENTARY NOTES
Grant technical monitor, David E. Ashpis, Aeropropulsion Division, Glenn Research Center, organization code RTTO, ashpis@nasa.gov

14. ABSTRACT
This report is Part I of the final report of NASA Cooperative Agreement contract no. NNX07AC02A. The period of performance was January 1, 2007 to December 31, 2010. This report includes the project summary, a list of publications and reprints of the publications that appeared in archival journals. Part II of the final report includes a Ph.D. dissertation and is published separately as NASA/CR-2012-2172655. The research performed under this project was focused on the operation of surface dielectric barrier discharge (DBD) devices driven by high voltage, nanosecond scale pulses plus constant or time varying bias voltages. The main interest was in momentum production and the range of voltages applied eliminated significant heating effects. The approach was experimental supplemented by computational modeling. All the experiments were conducted at Princeton University. The project provided comprehensive understanding of the associated physical phenomena. Limitations on the performance of the devices for the generation of high velocity surface jets were established and various means for overcoming those limitations were proposed and tested. The major limitations included the maximum velocity limit of the jet due to electrical breakdown in air and across the dielectric, the occurrence of backward breakdown during the short pulse causing reverse thrust, the buildup of surface charge in the dielectric offsetting the forward driving potential of the bias voltage, and the interaction of the surface jet with the surface through viscous losses. It was also noted that the best performance occurred when the nanosecond pulse and the bias voltage were of opposite sign. Solutions include the development of partially conducting surface coatings, the development of a semiconductor diode inlaid surface material to suppress the backward breakdown. Extension to long discharge channels was studied and a new ozone imaging method developed for more quantitative determination of surface jet properties.

15. SUBJECT TERMS
Flow control; Tubomachinery; Low pressure turbine; Turbulence; Wall jet; Separation; Dielectric barrier discharge plasma; DBD; Electric field; Dielectric; Electrode; Glow discharge nanosecond pulsing

16. SECURITY CLASSIFICATION OF:			17. LIMITATION OF ABSTRACT	18. NUMBER OF PAGES	19a. NAME OF RESPONSIBLE PERSON
a. REPORT	b. ABSTRACT	c. THIS PAGE			STI Help Desk (email:help@sti.nasa.gov)
U	U	U	UU	62	19b. TELEPHONE NUMBER *(include area code)* 443-757-5802